

Computer-Aided Design And Management Of Wine Grapes For Adaptation To
Climate Warming

By

MARÍA ALEJANDRA PONCE DE LEÓN JARA
DISSERTATION

Submitted in partial satisfaction of the requirements for the degree of

DOCTOR OF PHILOSOPHY

in

Horticulture and Agronomy

in the

OFFICE OF GRADUATE STUDIES

of the

UNIVERSITY OF CALIFORNIA

DAVIS

Approved:

Brian N. Bailey, Chair

Elisabeth J. Forrestel

S. Kaan Kurtural

Committee in Charge

2021

Copyright © 2021 by
María Alejandra Ponce de León Jara
All rights reserved.

To my family and friends for their love and support.

CONTENTS

List of Figures	vi
List of Tables	xi
Abstract	xiii
1 Introduction	1
2 Evaluating the use of Beer's law for estimating light interception in canopy architectures with varying heterogeneity and anisotropy	4
2.1 Introduction	5
2.2 Materials and methods	7
2.2.1 Plant geometry	7
2.2.2 Canopy structure	8
2.2.3 One-dimensional model of light interception	9
2.2.4 Three-dimensional model of light interception	12
2.2.5 Radiation input data	13
2.3 Results	14
2.3.1 Daily total light interception	14
2.3.2 Hourly light interception	14
2.3.3 Vertical profiles of hourly absorbed radiation	16
2.3.4 Impact of scattering	17
2.4 Discussion	22
2.4.1 Effect of leaf angle distribution (anisotropy)	22
2.4.2 Effect of plant spacing (horizontal heterogeneity)	23
2.4.3 Effect of row orientation	25
2.4.4 Effect of light scattering	26
2.5 Conclusion	26
3 A 3D model for simulating spatial and temporal fluctuations in grape berry temperature	28

3.1	Introduction	29
3.2	Model description	30
3.2.1	Model of 3D vineyard geometry	30
3.2.2	Surface energy balance equation	31
3.2.3	Berry model parameters	33
3.2.4	Leaf model parameters	34
3.2.5	Ground model parameters	35
3.2.6	Numerical solution	35
3.3	Field experiment materials and methods	36
3.3.1	Evaluation of model performance	38
3.4	Results	39
3.4.1	Ambient berry microclimate	39
3.4.2	Spatial and temporal variation in berry temperature	41
3.4.3	Modeled berry energy balance	41
3.4.4	Validation of modeled berry temperature	43
3.5	Discussion	45
3.5.1	Canopy architecture and berry microclimate	45
3.5.2	Implications for modeling of berry temperature	48
3.5.3	Limitations and future work	49
3.6	Conclusion	50
4	Fruit Zone Shading to Control Grape Berry Temperature: A Modeling Study	51
4.1	Introduction	52
4.2	Materials and methods	54
4.2.1	3D model of grape berry temperature	54
4.2.2	Validation and simulation experiments	56
4.3	Results	63
4.3.1	Ambient berry microclimate	63
4.3.2	Effect of shade cloth on grape berry temperature	65
4.3.3	Model validation	66

4.3.4	Simulation study	68
4.4	Discussion	72
4.4.1	Model performance	72
4.4.2	Vineyard design on flat terrain	74
4.4.3	Vineyard design on sloped terrain	76
4.5	Conclusion	76
5	Conclusion	78
A	Appendix	80
A.1	Berry thermal time constant	80

LIST OF FIGURES

2.1	Probability density function of leaf inclination for: (a) Grape N-S/E-W, (b) Almond, (c) Corn, and (d) Potato-Uniform and Potato-Row canopies.	10
2.2	Probability density function of leaf azimuthal angle for Grape (a) N-S and (b) E-W.	10
2.3	Fraction of leaf area projected in the direction of the sun, G , as a function of time for the virtual canopies.	11
2.4	3D visualization of absorbed radiation flux (W m^{-2}) at 12:00 hours ($I_0=928 \text{ W m}^{-2}$, $\theta_s = 21.5^\circ$) on Julian day 153 from: (a) Grape N-S, (b) Almond, (c) Corn, and (d) Potato-Row canopy.	13
2.5	Scatter plot of results for daily total light interception listed in Table 2.2 for homogeneous and isotropic (red), and for homogeneous but anisotropic (blue) canopies. Dotted line is 1:1.	15
2.6	Comparisons of the 1D model and 3D model for hourly flux of light interception on Julian day 153 from: (a) Grape N-S, (b) Grape E-W, (c) Almond, (d) Corn, (e) Potato-Uniform, (f) Potato-Row, and (g) homogeneous canopies with three different L values. Both homogeneous and isotropic and homogeneous and anisotropic refer to the 1D model.	17
2.7	Comparisons of the 1D model and 3D model of hourly light interception, expressed as a fraction of direct-beam radiation, on Julian day 153 for: (a) Grape N-S, (b) Grape E-W, (c) Almond, (d) Corn, (e) Potato-Uniform, (f) Potato-Row, and (g) homogeneous canopies with three different L values. Both homogeneous and isotropic and homogeneous and anisotropic refer to the 1D model.	18
2.8	Same as Fig. 2.7 except for Julian day 232.	19
2.9	Same as Fig. 2.7 except for Julian day 305.	20
2.10	Vertical profile of absorbed radiation from Grape N-S (a, b, c); Grape E-W (d, e, f); Almond (g, h, i); and Corn, (j, k, l) on Julian day 153. Columns correspond to 8:00 ($\theta_s=66^\circ$), 10:00 ($\theta_s=43^\circ$), and 12:00 ($\theta_s=21^\circ$) hours for each crop.	22

2.11	Scatter plot of results for daily total light interception for homogeneous and isotropic canopies in the PAR band (red) and NIR (blue) for different assumptions regarding radiation scattering based on a) Eq. 2.1; leaf absorb all incoming radiation, b) Eq. 2.5, and c) Eq. 2.6. Dotted line is 1:1.	23
3.1	3D Visualization of the vine and air temperature difference ($^{\circ}\text{C}$) in the East side of the vine at 11:00 hours on Sept 19 th from: (a) VSP-2018, (b) Wye-2019, (c) Goblet-2019, (d) Unilateral-2019. Simulations depicted in (a) and (b) utilized periodic horizontal boundary conditions, whereas (c) and (d) utilized periodic conditions only in the row-parallel direction.	32
3.2	Measured ambient meteorological values used for model inputs: air temperature (T_{air}), relative humidity (RH), specific humidity (q) and wind speed (U) for VSP (a,e,i,m), Wye (b,f,j,n), Goblet (c,g,k,o) and Unilateral (d,h,l,p).	40
3.3	Daily course of each measured grape berry temperature in the east and west side of the vine for (a) VSP, (b) Wye, (c) Goblet and (d) Unilateral. Each line corresponds to a different berry measurement. The ambient air temperature is denoted by the black dotted line for reference.	42
3.4	Simulated berry temperatures of (a) VSP, (b) Wye, (c) Goblet and (d) Unilateral. The dark blue line shows temperatures of an east-facing berry, the red dashed line of a west-facing berry, the light blue lines of all berry temperatures, and the black dashed line of air temperature.	43
3.5	Simulated average berry surface heat fluxes for the four different vineyard designs: (a) VSP, (b) Wye (c) Goblet and (d) Unilateral. The adopted sign convention is that fluxes are positive for energy transfer into the berry surface.	44
3.6	Daily course of the simulated and average measured grape berry temperature in the east and west side of the vine for (a) VSP, (b) Wye, (c) Goblet and (d) Unilateral.	45
3.7	Effect of heat storage on average modeled temperature of a berry in the east and west side of the vine for (a-b) VSP, (c-d) Wye, (e-f) Goblet and (g-h) Unilateral.	47

4.1	3D Visualization of the surface temperature (°C) in the east side of the vine at 10:00 on 19 Sept. 2019 for (A) Goblet, (B) Unilateral and (C) VSP trellises.	62
4.2	Meteorological data for Goblet vineyard. Daily course of measured air temperature (A,B,C), wind speed (D,E,F), wind direction (G,H,I) and relative humidity (J,K,L) data during three different days (columns). Data is plotted every 5 min., except for wind direction which was plotted every 40 min.	64
4.3	Same as Fig. 4.2 except for Unilateral vineyard.	65
4.4	Measured berry temperature increase over air temperature for Goblet (A,B,C) and Unilateral (D,E,F) vineyard. Daily course of average measured grape berry temperature in the west side of the vine for three days with different ranges in air temperature. Data plotted every 5 min.	66
4.5	Daily course of measured and simulated grape berry temperature increase over air temperature for berries under 40% shade cloths in the west side of the vine for (A) Goblet and (B) Unilateral, and of exposed berries with no shade cloth (control) for (C) Goblet and (D) Unilateral. Each black or brown line corresponds to a different berry measurement.	67
4.6	Simulated total canopy and berry daily light interception (PAR+NIR) in the VSP trellis system with different row spacing (1 m, 2 m, and 3 m), row orientation (N-S, NE-SW, E-W, NW-SE), and topography (flat and sloped vineyards facing N, NE, E, SE, S, SW, W, and NW). Each point represents a single value for each vineyard design.	69
4.7	Number of hours with berry temperatures >35°C in the VSP trellis system with 3 m row spacing with different shade cloth densities (control, 30%, 50% and 70%), row orientation (N-S, NE-SW, E-W, NW-SE) and topography (flat and sloped vineyards facing N, NE, E, SE, S, SW, W, and NW). Maximum air temperature was 31.9 °C.	71

4.8	Growing degree hours from 7:00 to 19:00 hours in the VSP trellis system with 3 m row spacing with different shade cloth densities (control, 30%, 50% and 70%), row orientation (N-S, NE-SW, E-W, NW-SE) and topography (flat and sloped vineyards facing N, NE, E, SE, S, SW, W, and NW).	72
4.9	Conditional inference tree for berry temperature difference between both sides of the vine from 7:00 to 19:00 hours. Categories for each split are shown below the variable name box. For instance, for node 1 (Slope) the split was into berry temperature data in the Flat, E, NW, S and SE facing slopes vs those in the N, NE, SW and W slopes. The p-value in the nodes of denotes the significance level used for a split to take place. Box plots include the medians (solid black line), upper and lower quartiles (grey box) and 1.5x the inner quartiles (error bars). Sample sizes at each terminal node show number of values in that boxplot. The complete data set is plotted in Fig. S1.	73
A.1	(a) Measured, 3D simulated and fitted (Eq. A.1) temperature response of an isolated berry. (b) Normalized temperature response for data shown in (a).	81
S.1	Simulated canopy light interception in the VSP trellis system with different row spacing (1 m, 2 m, and 3 m), row orientation (N-S, NE-SW, E-W, NW-SE), and topography (flat and sloped vineyards facing N, NE, E, SE, S, SW, W, and NW).	95
S.2	Simulated berry daily interception in the VSP trellis system with 3 m row spacing with different shade cloth densities (control, 30%, 50% and 70%), row orientation (N-S, NE-SW, E-W, NW-SE) and topography (flat and sloped vineyards facing N, NE, E, SE, S, SW, W, and NW).	96
S.3	Simulated temperature of berries exposed berries and berries under shade cloths with three different densities: 30%, 50%, and 70% positioned on both sides of the VSP trellis system in rows oriented N-S, NE-SW, E-W, and NW-SE, in three different row spacings 1 m, 2 m and 3 m and in different topographies. The topographies included a flat surface and 30° slopes facing: N, NE, E, SE, S, SW, W, and NW. The dashed lines correspond to berries on the right side of the vine and the solid lines to berries on the left side of the vine.	97

S.4 Simulated temperature difference of berries under shade cloths between both sides of the vine with three different densities: 30%, 50%, and 70% positioned on both sides of the VSP trellis system in rows oriented N-S, NE-SW, E-W, and NW-SE, in three different row spacing's 1 m, 2 m and 3 m and in different topographies. The topographies included a flat surface and 30° slopes facing: N, NE, E, SE, S, SW, W, and NW. 98

S.5 Simulated berry temperature response to shade cloths with three different densities: 30%, 50%, and 70% positioned on both sides of the VSP trellis system in rows oriented N-S, NE-SW, E-W, and NW-SE, in three different row spacing's 1 m, 2 m and 3 m and in different topographies. The topographies included a flat surface and 30° slopes facing: N, NE, E, SE, S, SW, W, and NW. The dashed lines correspond to berries on the right side of the vine and the solid lines to berries on the left side of the vine. 99

LIST OF TABLES

2.1	Parameters used to quantify the structure of the virtually-generated crop canopies.	9
2.2	Daily total light interception ($\text{MJ m}^{-2} \text{d}^{-1}$) for the canopies in study	15
2.3	Model performance measures comparing results from the 1D and the 3D model for hourly light interception for the virtually-generated canopies based on data for hourly light interception on Julian Day 153 plotted in Fig. 6.	21
3.1	Averaged measured surface radiative properties used for model inputs	38
3.2	Parameters used to quantify the structure of the virtually-generated vineyards.	38
3.3	Measured daily average, average of the daily maximum and minimum air temperature and air relative humidity, and maximum wind speed data for the different experimental vineyard designs from Sept 19 th to Oct 10 th of 2018 and 2019.	40
3.4	Model performance measures for the four different vineyard designs comparing modeled with measured berry temperature for 288 data points from exposed berries in the east and west side of the vine. Berry temperature data was calculated with and without the heat storage term. Berry temperature data calculated including the heat storage term is plotted in Fig. 3.6].	46
4.1	Parameter description and source of the values associated with the energy budget equation in the 3D model for the different vineyard designs.	57
4.2	Variables assessed in simulations that included vineyard designs with different shade cloth density, row spacing, row orientation, and topography.	62
4.3	Characterization of differences in average microclimate between treatments for the entire experimental period spanning 19 Sep to 10 Oct 2019: Daily average of berry temperature; average of daily maximum and minimum temperature of berries in the west side of the vine; average of the daily maximum and minimum temperature difference between the berries and air temperature.	66

4.4	Model performance metrics for Goblet and Unilateral comparing modeled and measured berry temperature under shade cloth in the west side of the vine for three days with different ranges in air temperature. A graphical comparison of the data on 19 Sept 2019 only is shown in Fig. 4.5.	67
A.1	Time constant τ determined from fitting of Eq. A.1 to measured and simulated data, and associated error metrics.	81
S.1	Summary statistics for 1 m, 2 m, and 3 m row spacing treatments and N-S, NE-SW, E-W, and NW-SE row orientations in a flat and sloped terrain for the VSP	100

ABSTRACT

Computer-Aided Design And Management Of Wine Grapes For Adaptation To Climate Warming

Increasing temperatures and heat wave intensity have become a major concern for wine grape farmers due to their effect on grape production and quality. As a result, growers are exploring approaches to protect berries while maintaining grape quality and optimum yield. Some approaches include reducing grape exposure by natural shading through management of pruning, using row orientation, or changing the trellis type and row spacing. However, given the extremely large number of interacting variables that determine berry temperature (e.g., radiation load, bunch exposure, topography, latitude, climate), it is not feasible to independently vary all of these parameters in field experiments, thus making it difficult to determine optimal strategies at a given location. Crop models have the potential to complement experimental efforts by allowing for controlled study of the interactions between these numerous variables in order to determine optimal strategies for reducing the effect of excess temperature on crop productivity.

Given the significant rise of berry temperature when exposed to direct sunlight, this research first evaluated widely used assumptions for modeling solar radiation interception in plant canopies, namely assumptions of vegetation homogeneity and isotropy. Because of their simple, tractable form, 1D models of light interception that assume homogeneity or isotropy are used across a broad range of disciplines. However, it is relatively well-known that with varying levels of vegetation sparseness and preferential leaf orientations, the implicit assumptions of vegetation homogeneity and isotropy in simple 1D models are frequently violated. Yet, it is not well understood at what point this leads to high model errors. Results of this work provided quantitative guidance as to when a simple 1D model can be appropriately used to estimate light interception. For canopies in which plant spacing was much smaller than the canopy height, the 1D homogeneous and isotropic model produced small errors. However, for discontinuous and anisotropic canopies, errors significantly increased with increasing the sparseness of the canopy.

Results of this initial study suggested that a 3D model was needed to accurately quantify grapevine light interception and to predict the complex interactions between vine architecture

and microclimate at the berry level. In doing so, strategies for mitigating unfavorable grape berry temperatures could be identified and evaluated. This research developed and validated a 3D model for grape berry temperature, supported by field and laboratory experiments. The model accurately simulated the spatial and temporal fluctuations of grape berries in vineyards with different climates, topographies, and trellises. Furthermore, the effects of shade cloth on berry temperature were incorporated in the model and validated against experimental data. By using this modeling approach, different vineyard designs and their effect on berry temperature were simulated. The results provided quantitative guidance on the effect of different vineyard designs and management strategies that have the potential to reduce the effect of excess temperature in a warming climate. For instance, on flat terrain, NE-SW row orientation provided the best compromise of berry light and temperature balance between opposing sides of the vine while avoiding excessive berry temperatures, while N-S rows provided good daily symmetry but had a risk of fruit overexposure and high temperatures in the afternoon. Slopes with southern or western exposure increased imbalance and risk of high berry temperatures, which in some cases could not be well-managed by shade cloth.

Chapter 1

Introduction

Increasing temperatures and temperature variability associated with a changing climate have become a major concern for many wine grape growing regions due to their effect on grape and wine composition. As is true for other crops, adequate sun exposure is vital because grapevines need sunlight for photosynthesis, growth, and development, and absorbed radiation by the berries is crucial for the biochemical and physiological processes that determine grape berry quality [30, 32, 70, 79, 95]. Regrettably, excess sunlight and elevated temperatures are negatively affecting grape productivity in many growing regions [16, 33, 64, 65, 78, 88]. In California, minimum and maximum annual temperatures have increased from 1985 to 2011 by 2.34°C and 1.77°C, respectively, and in the summers by 3.88°C and 3.31°C, respectively [81]. In Oakville, CA, Martínez-Lüscher et al. [64] reported that elevated temperatures for grape clusters resulted in unbalanced wines with higher pH and lower levels of anthocyanins. Other research in Murrumbidgee, Australia reported that temperatures exceeding 40°C result in delaying ripening and causing berry sunburn [33]. Thus, strategies to minimize harmful berry temperatures are needed to sustain production in warm climates.

It is challenging to manage the grapevine canopy to reduce the effect of excess temperature because of the complex interactions between plant architecture and the environment. Traditionally, it has been recommended to time canopy management to maintain sun-exposure for young fruits, but also to allow some shading of mature grape clusters to prevent excess sun exposure [24]. Although increasing the shade in vineyards palliates the effect of elevated temperature, trade-offs need to be evaluated as well. For instance, shaded clusters can cause delay in fruit

ripening, reduce wine quality [101], and increase disease prevalence due to pathogens such as bunch rot (*Botrytis cinerea* Pers.) [82] and powdery mildew (*Erysiphe necator*) [1].

The negative effects of elevated temperature on grape berries could likely be mitigated in many cases if the complex interactions between canopy architecture and microclimate were better understood and predicted at the berry level. Developing and evaluating proposed mitigation strategies experimentally based on field trials is costly and time-consuming [125], which can limit their breadth and generalizability. Crop models can have the potential to extrapolate the results of a limited set of experiments through systematic variation of relevant variables, however, there are currently no models available that can represent varying grapevine architectures and their effect on spatial and temporal fluctuations in grape berry temperature. Through three different studies, this dissertation aims to 1) investigate the impact of the heterogeneous and anisotropic vegetation structure characteristic of grapevines on light interception, 2) develop a 3D model to simulate grape berry temperature in response to varying vineyard architecture and topography, and 3) identify strategies that have the potential to mitigate unfavorable temperatures in grape berries.

Chapter 2 evaluates widely used assumptions when modeling solar radiation interception in plant canopies. The solar radiation intercepted by plant canopies is a fundamental driver of biophysical processes on Earth, and thus, quantifying such interception is a critical part of understanding and predicting a wide range of processes occurring at the land-atmosphere interface. The study showed that using a 1D model to simulate light interception for discontinuous canopies (e.g., grapevines) resulted in overestimation of light interception by up to 115% for the cases considered. These results highlighted the need to use a 3D radiation model to account for complex canopies because these models can represent the vertical and horizontal variability in the canopy and its effect on light interception accurately.

Chapter 3 develops a 3D model that can accurately resolve spatial and temporal heterogeneity in berry temperature. The spatially-explicit nature of the model allows for robust representation of varying canopy architectures and their effect on berry temperature. The high model complexity is afforded by performing calculations in parallel on the computer's graphic processing unit (GPU). This ability to resolve the geometry of the vineyard is critical in this particular study

because it means the model is robust to changes in row spacing, trellis system, row height, etc. To generate data for validation of the 3D grape berry temperature model, field and laboratory experiments were conducted. Validation results demonstrated that by accurately representing the 3D vine structure, the model was able to closely replicate measured spatial and temporal fluctuations in berry temperature.

Chapter 4 aims to explore whether elevated berry temperature can be mitigated by designing and managing vineyards in a way that effectively creates a favorable microclimate for berry development. Identifying strategies that have the potential to reduce elevated temperatures in a warming climate is of great interest to grape growers. However, given the extremely large number of interacting variables that determine berry temperature (e.g., row spacing, row orientation, trellis type, topography, latitude, climate) it is not feasible to independently vary all of these parameters in field experiments. Thus, to study the interactions between these variables that might yield favorable results, Chapter 4 expands the model developed and validated in Chapter 3 by incorporating the effects of shade cloth on berry temperature. The model was used to ultimately predict the efficacy of potential mitigation strategies for high berry temperature. The results of this study provided new insights into the effect of fruit zone shading to control berry temperature for the establishment of new vineyards and targeting the management of existing vineyards.

Chapter 2

Evaluating the use of Beer's law for estimating light interception in canopy architectures with varying heterogeneity and anisotropy

▮

Light interception in plant canopies is most commonly estimated using a simple one-dimensional turbid medium model (i.e., Beer's law). Inherent in this class of models are assumptions that vegetation is uniformly distributed in space (homogeneous) and in many cases that vegetation orientation is uniformly distributed (isotropic). It is known that these assumptions are violated in a wide range of canopies, as real canopies commonly have heterogeneity at multiple scales and almost always have highly anisotropic leaf angle distributions. However, it is not quantitatively known under what conditions these assumptions become problematic given the difficulty of robustly evaluating model results for a range of canopy architectures. In this study, assumptions of vegetation homogeneity and isotropy were evaluated under clear sky conditions for a range of virtually-generated crop canopies with the aid of a detailed three-dimensional, leaf-resolving radiation model. Results showed that Beer's law consistently over predicted light interception for all canopy configurations. For canopies where the plant spacing was comparable

The material contained in this chapter is taken from the published journal article: Ponce de León, M. A. and Bailey, B. N. (2019). Evaluating the use of Beer's law for estimating light interception in canopy architectures with varying heterogeneity and anisotropy. *Ecological Modelling*. 406, 133-143.

to the plant height, Beer’s law performed poorly, and over predicted daily intercepted sunlight by up to $\sim 115\%$. For vegetation with a highly anisotropic leaf inclination distribution but a relatively isotropic leaf azimuth distribution, the assumption of canopy isotropy (i.e., $G=0.5$) resulted in relatively small errors. However, if leaf elevation and azimuth were both highly anisotropic, the assumption of canopy isotropy could introduce significant errors depending on the orientation of the azimuthal anisotropy with respect to the sun’s path.

2.1 Introduction

Solar radiation is a primary driver of most plant biophysical processes, including energy transfer, turbulent transport, evapotranspiration, photosynthesis, and phenology. Fluxes of absorbed radiation in plant canopies have strong gradients in the vertical direction, and potentially in horizontal directions in the case of heterogeneous canopies [93]. Capturing these high gradients through direct measurement is often challenging, and therefore models are frequently used to predict absorbed radiative flux distributions.

For practical purposes, relatively simple models are frequently used to estimate light interception in plant canopies. For example, crop models have become important tools for studying agricultural systems [49], yet they commonly utilize relatively simple models for light interception given the frequent lack of detailed architectural inputs.

The most commonly used approach for estimating light interception treats the canopy as a homogeneous medium of unresolved vegetation (i.e., a “turbid” medium), which allows for the use of a simple exponential model for radiation attenuation commonly known as Beer’s law, Beer-Lambert law, or Beer-Lambert-Bouguer law [10, 48, 57, 60, 63, 69, 84, 96]. Beer’s law calculates the probability of radiation interception as an exponentially increasing function of the leaf area projected in the direction of radiation propagation and the distance travelled through the canopy. Using this approach, light interception can be calculated as

$$I = I_0 \left[1 - \exp \left(- \frac{GL}{\cos \theta_s} \right) \right], \quad (2.1)$$

where I is the radiation flux intercepted over the depth of the canopy, I_0 is the direct-beam radiation flux on a horizontal surface at the top of the canopy, L is the leaf area index ($\text{m}^2 \text{m}^{-2}$),

and θ_s is the solar zenith angle. G is the fraction of leaf area projected in the direction of the sun, and is defined mathematically as [93]

$$G = \frac{1}{2\pi} \int_{2\pi} g_L(\Omega_L) |\Omega_s \cdot \Omega_L| d\Omega_L, \quad (2.2)$$

where Ω_s is a unit vector pointing in the direction of the sun, Ω_L is a unit vector in the direction of the leaf normal, and $g_L(\Omega_L)$ is the probability that a leaf normal is oriented in the direction Ω_L . If g_L is constant for all Ω_L (i.e., leaves have no preferred orientation and are thus isotropic), integration of Eq. 2.2 yields a value of $G = 0.5$ [93].

The form of Beer's law given in Eq. 2.1 functions under two main assumptions. The first assumption is that leaves are randomly distributed both vertically and horizontally (i.e., homogeneous) in a continuous medium where leaves are relatively small. The second assumption is that leaves absorb all incident radiation (i.e., no scattering or transmission) [55, 57], which may be reasonable for photosynthetically active radiation bands where leaves absorb roughly 90% of incident radiation, but is likely a poor assumption in other bands such as the near-infrared where absorption is low. Equation 2.1 also requires specification of G , which is most commonly set to be equal to 0.5 based on the assumption that leaves are isotropic [28, 46, 93, 100, 106].

The assumptions of vegetation homogeneity and isotropy are usually violated in actual plant canopies. Leaf area density typically varies sharply in the vertical direction [4, 38, 73]. Many natural plant canopies have considerable horizontal heterogeneity such as savannas [17], or heterogeneity due to natural or man-made disturbances [59]. Crop canopies also commonly have a sparse, row-oriented configuration that creates high heterogeneity in light interception. Furthermore, it is rare to find canopies with isotropic leaf angle distributions, as this is typically not the most efficient configuration for light interception [5, 87].

Despite the known limitations of Beer's law in the above cases, it is still frequently applied in these systems due to its simple, tractable form. However, there is a general lack of quantitative understanding of the errors resulting from the application of these simplified models in various canopy architectures, primarily because it is difficult to quantify light interception from field measurements for a range of architectures [92]. The objective of this study is to better understand and quantify errors in modeled radiation absorption under assumptions of vegetation heterogene-

ity or isotropy for various canopy configurations. The authors' hypothesis is that Beer's law will perform well for relatively dense, closed canopies provided that G is specified appropriately. For sparse canopies, it is hypothesized that assumptions of vegetation homogeneity will result in significant model errors, thus necessitating a more complicated model.

Since accurately measuring the distribution of absorbed radiation in space and time is often unfeasible using traditional experimental approaches, we used a sophisticated 3D radiation model [2] along with virtually-generated canopies to evaluate Beer's law under different simplifying assumptions. Virtual canopies with varying levels of heterogeneity, sparseness, and leaf orientation distributions were generated to evaluate assumptions of vegetation homogeneity or isotropy in terms of absorption of direct solar radiation. A considerable advantage of using virtually-generated canopies is that the input parameters in Eq. 2.1 (i.e., G and L) can be calculated exactly from the virtual canopies. When combined with a detailed 3D radiation model, this resulted in a robust means for evaluating the performance of simplified models for a range of canopy architectures.

2.2 Materials and methods

2.2.1 Plant geometry

For simulating plant light interactions, detailed 3D geometric models were used to describe the architecture of the canopy. Agricultural crops were chosen for the plant types because: (1) many 3D models are readily available, (2) they have sufficient yet regular heterogeneity that limited the degrees of freedom when generating the canopies, and (3) they represent an economically important practical application of the use of Beer's law. The chosen crop canopies were grape, almond, potato, and corn, which were represented in the 3D model using a mesh of rectangular and triangular elements. To minimize the number of elements needed to describe their complex geometries, images with a transparency channel could be overlaid on these basic elements, where the transparency channel is used to remove a portion of the element's surface [see 2, 110]. Virtually-generated plants were either read from a polygon file (corn and potato), or created using the procedural plant generator described by Weber and Penn [121] (grape and almond).

2.2.2 Canopy structure

Parameters used to quantify canopy architecture are given in Table 2.1. The procedural model used to generate the grape and almond plants had a random component to each architectural parameter, making each plant unique. Each corn and potato plant was identical, therefore a random azimuthal rotation was applied to each plant to decrease regularity of the canopy. Plants were placed in a marked row structure to form a canopy. Two grape canopy cases were considered: one with a North-South row orientation (Grape N-S) and one with an East-West row orientation (Grape E-W). Two potato canopies were considered in which plants were arranged in either a East-West row-oriented pattern (Potato-Row), or a uniformly spaced planting pattern (Potato-Uniform). In all cases, the size of the 3D scene was chosen such that further increasing the total number of plants did not have an impact on results.

To test the model in the case of homogeneous and isotropic vegetation, a set of canopies were created with uniformly distributed leaves in space with three different leaf area index values: $L = 1.5$, which consisted of 100,000 leaves; $L = 3.1$, which consisted of 200,000 leaves; and $L = 6.2$, which consisted of 400,000 leaves. The surface area of each leaf was 0.006 m^2 . Each leaf angle was set by randomly drawing from a spherical distribution.

To characterize the plant geometry, L and the leaf inclination angle probability density function (PDF) were calculated for all five generated canopies, and the leaf azimuthal angle PDF was calculated for the Grape N-S and Grape E-W cases (all other cases had azimuthal distributions that were close to uniform). The L was calculated by summing the one-sided area of all leaves in the canopy and dividing by the total canopy footprint area. The leaf inclination angle and leaf azimuthal angle were calculated for each of the elements from the surface normal of the leaf, and a PDF was formed by weighting each element's contribution to the PDF by its surface area, then normalizing such that the PDF integrates to unity.

The corn model had predominantly vertically oriented leaves, while the almond and potato models had leaves closer to horizontal on average (Fig. 2.1). Grape leaf inclination skewed toward vertical, and leaf azimuth tended to be oriented parallel with the row (Fig. 2.2), which is supported by previous manual and LiDAR measurements [5, 6].

The gap fraction was calculated from the 3D models by computing the fraction of direct

Table 2.1. Parameters used to quantify the structure of the virtually-generated crop canopies.

Case	Plant height (m)	Plant spacing (m)	Row spacing (m)	L ($\text{m}^2 \text{m}^{-2}$)	Gap fraction
Grape N-S/E-W	2.3	2	2.4	0.9	0.8
Almond	7.6	4.8	6.4	5.1	0.49
Corn	2.4	0.4	1	4.2	0.21
Potato-Uniform	0.8	0.6	0.6	6.5	0.22
Potato-Row	0.8	0.4	0.9	6.5	0.36

sunlight not intercepted when $\theta_s = 0$ (Table 2.1). Gap fraction values ranged from 80% in the grape canopy cases down to 21% for the corn canopy case. Although both potato canopy cases had the same L , their gap fractions were 22% for uniformly spaced plants and 36% for row-oriented plants.

2.2.3 One-dimensional model of light interception

A simple 1D model (Eq. 2.1) was used to calculate hourly light interception, which utilized two different assumptions of canopy structure. The first approach assumed that canopy vegetation is both homogeneous and isotropic. The homogeneous assumption implies that vegetation is randomly distributed in space, which is already inherent in Eq. 2.1. The isotropic assumption implies that leaves have no preferred orientation, or that the leaf angle PDF is “spherical”.

The second approach assumed that leaves are homogeneous but anisotropic. Rather than calculating the leaf angle PDF and integrating according to Eq. 2.2, the canopy-level $G(\theta_s)$ was calculated directly from the 3D models using a weighted average of the projected area fraction for each leaf according to

$$G(\theta_s) = \frac{\sum_{i=1}^m A_i |\vec{n}_i \cdot \vec{v}|}{\sum_{i=1}^m A_i}, \quad (2.3)$$

where m is the total number of geometric elements in the virtual canopy, \vec{n}_i is a unit vector normal to the surface of the i^{th} geometric element, \vec{v} is a unit vector pointing towards the sun,

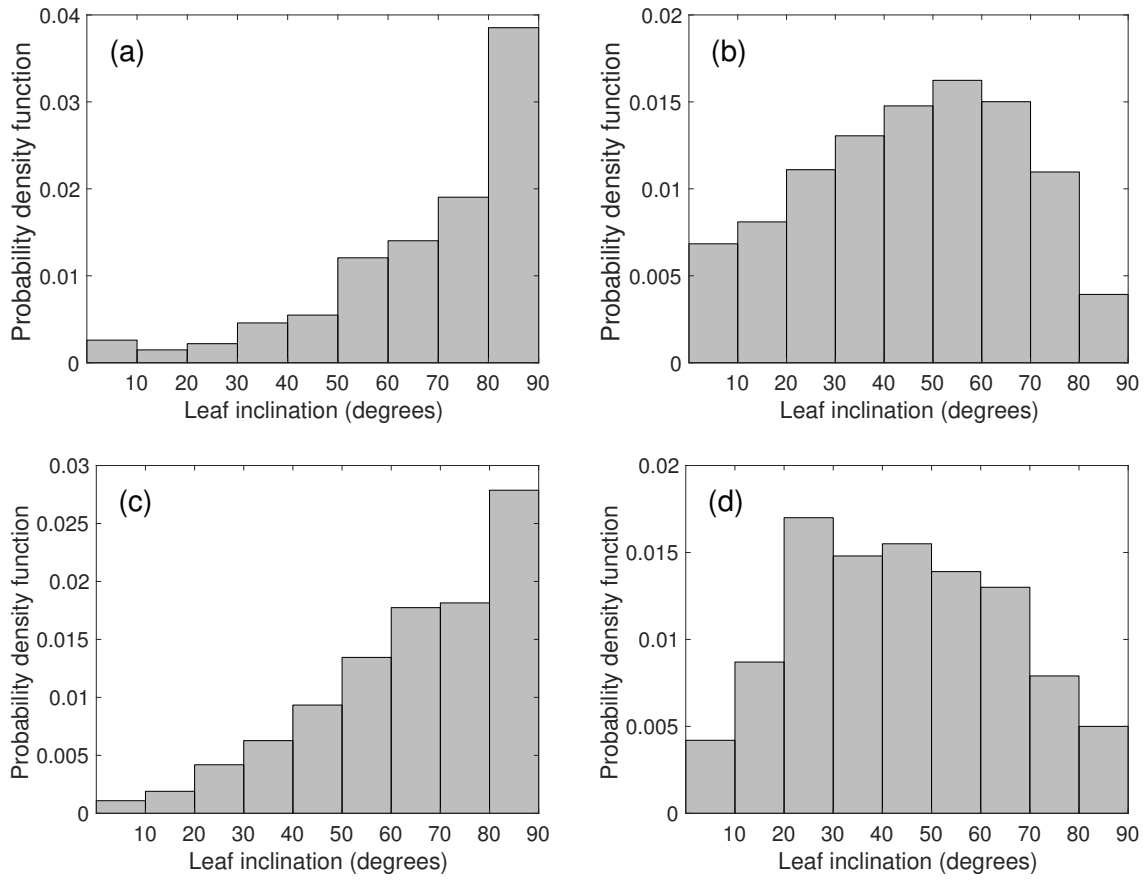


Figure 2.1. ty density function of leaf inclination for: (a) Grape N-S/E-W, (b) Almond, (c) Corn, and (d) Potato-Uniform and Potato-Row canopies.

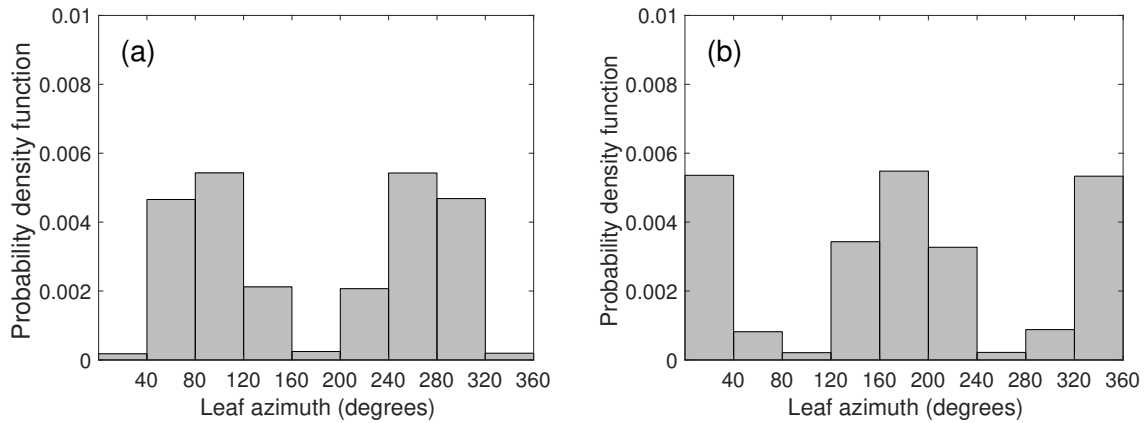


Figure 2.2. Probability density function of leaf azimuthal angle for Grape (a) N-S and (b) E-W.

and A_i is the one-sided surface area of the i^{th} geometric element.

G values for each hour of a diurnal cycle on Julian days 153, 232, and 305 are shown in

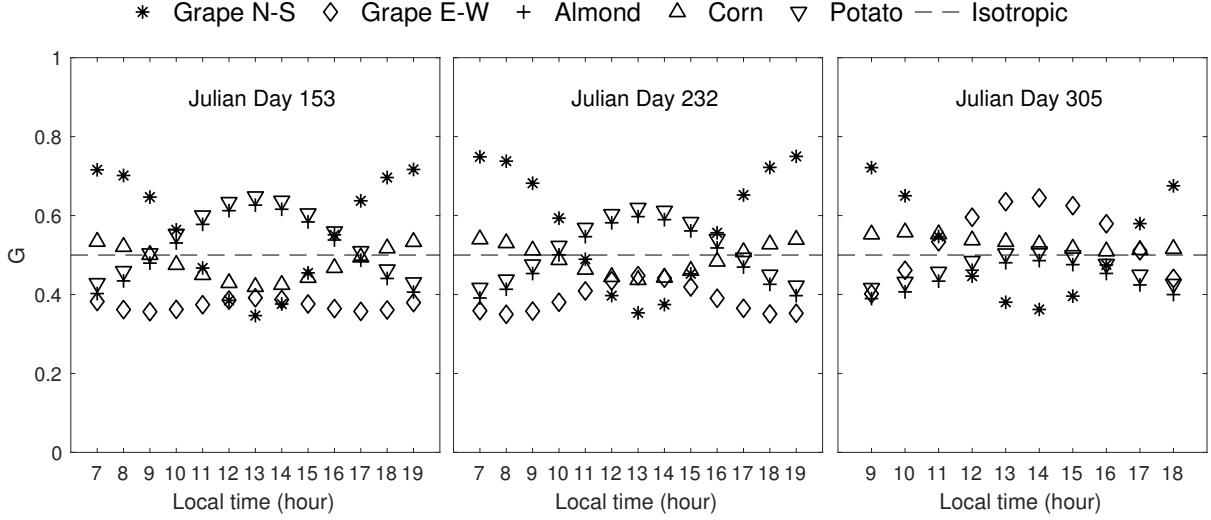


Figure 2.3. Fraction of leaf area projected in the direction of the sun, G , as a function of time for the virtual canopies.

Fig. 2.3. For Corn, G does not vary considerably with the position of the sun, whereas the potato and almond cases, have high diurnal variation in G . As Warren Wilson [120] pointed out, G values intersect at a solar elevation of about 32.5° for azimuthally symmetric vegetation, which corresponds to roughly 8:45 and 17:25 hours on Julian day 153 and 9:20 and 17:00 hours on Julian day 232 in Fig 2.3. This intersection occurs for the almond, corn, and potato cases, however, because of the highly anisotropic azimuthal leaf distribution of the grape canopies, they do not follow this rule.

In addition to Eq. 2.1, which assumes vertical homogeneity within the canopy, vertical profiles of hourly absorbed radiation were also calculated by explicitly representing variation of leaf area with height and its corresponding effect on light interception. The radiation flux intercepted over a horizontal layer of thickness Δz at height z within the canopy was calculated according to

$$I(z) = I_0 \left[1 - \exp\left(-\frac{Ga\Delta z}{\cos \theta_s}\right) \right] \exp\left(-\frac{GL_z}{\cos \theta_s}\right), \quad (2.4)$$

where L_z is the leaf area index between z and the canopy top, and a ($\text{m}^2 \text{m}^{-3}$) is the one-sided leaf area density of the layer.

The 1D model inherently assumes that leaves absorb all incoming radiation. There is no

theoretically consistent means of accounting for reflection and transmission using Eq. 2.1, as the derivation of Beer’s law requires removal of the scattering terms from the radiative transfer equation [68]. Several *ad hoc* approaches have been used in previous work to account for transmission and reflection using some function of the leaf reflectivity (ρ) and transmissivity (τ), of which two are considered here. The first is to multiply the incoming radiation by $1-\rho$

$$I = I_0(1 - \rho) \left[1 - \exp\left(-\frac{GL}{\cos \theta_s}\right) \right], \quad (2.5)$$

which assumes that all reflected radiation either exits the canopy or reaches the ground without being re-absorbed and that there is no transmission. The second is to multiply by $1-\rho-\tau$

$$I = I_0(1 - \rho - \tau) \left[1 - \exp\left(-\frac{GL}{\cos \theta_s}\right) \right], \quad (2.6)$$

which assumes that all reflected and transmitted radiation either exits the canopy or reaches the ground without being re-absorbed.

2.2.4 Three-dimensional model of light interception

It was assumed that the reference or “true” light interception values were given by the detailed 3D model of Bailey [2], which explicitly represents radiation absorption by each element in the virtual canopy. The model uses a backward ray-tracing approach that ensures each canopy element adequately samples the sun, and was shown to converge exponentially towards the exact answer as the number of rays was increased (assuming model inputs are specified exactly). The 3D model software and documentation is available through the public GitHub repository <https://www.github.com/PlantSimulationLab/Helios>.

Inputs to the radiation model are the total hemispherical radiative flux (W m^{-2}) of the sun over an arbitrary wavelength band, as well as the reflectivity and transmissivity of each element in the virtual canopy. To test the assumptions of vegetation homogeneity and isotropy, reflectivity and transmissivity were set to 0, which is an assumption implicit in Eq. 2.1. Separate tests were then performed to examine the effect of reflection and transmission using either Eq. 2.5 or 2.6.

For all simulations, the diffuse solar radiation flux was set to 0, which is also implicit in Eq. 2.1. The number of rays that were sampled on each element was set to 1000 rays. It was

verified that further increasing the number of rays had a negligible impact on results. A sample visualization of the 3D distribution of absorbed radiation for the virtual canopy cases is shown in Fig. 2.4.

Total daily light interception was calculated by linear interpolation of the hourly light interception fluxes. Agreement between the 3D model and simplified 1D models was quantified using the index of agreement [IA; 124], normalized root mean square error (NRMSE), and the coefficient of determination (R^2).

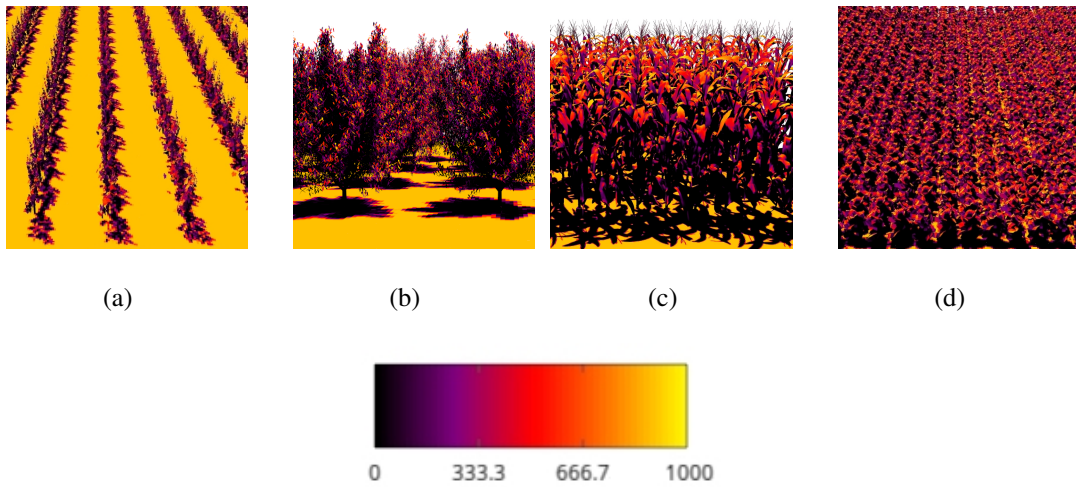


Figure 2.4. 3D visualization of absorbed radiation flux (W m^{-2}) at 12:00 hours ($I_0=928 \text{ W m}^{-2}$, $\theta_s = 21.5^\circ$) on Julian day 153 from: (a) Grape N-S, (b) Almond, (c) Corn, and (d) Potato-Row canopy.

2.2.5 Radiation input data

The incoming radiation data used to drive the radiation absorption simulations in this study was generated following the REST-2 model of Gueymard [35]. The hourly incoming radiation was calculated based on the assumed virtual site longitude (121.7405° W), latitude (38.5449° N), offset from UTC (7 hours), atmospheric pressure (101,325 Pa), air temperature near ground level (25° C), atmospheric turbidity coefficient (0.05), relative humidity (50%), and Julian day of the year (153, 232, and 305). It is noted that the precipitable water in the REST-2 model was specified using the model of Viswanadham [118]. The direction of the sun for any time of day at the virtual site was calculated following the approach outlined by Iqbal [45].

In cases where scattering was included, two radiative bands were considered - one character-

istic of efficient absorption by leaves such as the photosynthetically active band (PAR; 400-700 nm), and another characteristic of high scattering such as the solar near-infrared band (NIR; >700 nm). The total incoming solar flux was partitioned as 47% in the PAR band and 53% in the NIR band. In the PAR band, ρ was set to 0.056 and τ to 0.042, while in the NIR band, ρ was set to 0.425 and τ to 0.334 [6].

2.3 Results

2.3.1 Daily total light interception

Results for the daily total light interception on Julian days 153, 232, and 305 are listed in Table 2.2, and shown graphically in Fig. 2.5. For the homogeneous canopy cases, very close agreement was found between the 1D and 3D models regardless of L , which indicated that the approach used to compare the 1D and 3D models was consistent and that leaf-scale heterogeneity created by discrete leaf surfaces did not create significant errors.

Cases with relatively high ground cover fractions and uniformly arranged plants showed good agreement between the 1D and 3D models regardless of whether the assumption of leaf isotropy was made. As the canopies became more heterogeneous in space, agreement between the models generally declined. Although Potato-Uniform and Potato-Row had identical leaf area indices and leaf angle distributions, the regular distribution of plants within the canopy in Potato-Uniform resulted in better agreement between the 1D and 3D models compared to Potato-Row. Despite all cases having highly anisotropic leaf inclination distributions, the assumption of leaf anisotropy had relatively small impact for all cases except for the Grape E-W case. Any effects of heterogeneity or anisotropy tended to decrease as the day of year became further away from the summer solstice. Toward the end of the year (day 305), the 1D and 3D models were in fairly good agreement for all canopy cases.

2.3.2 Hourly light interception

The diurnal flux of radiation intercepted by the canopy for an hourly time step on Julian day 153 is shown in Fig. 2.6, with corresponding fractions of total radiation intercepted by the canopy shown in Fig. 2.7. The fraction of total radiation intercepted on Julian day 253 and 305 are shown in Figs. 2.8 and 2.9, respectively. For the homogeneous canopy cases, the assumptions of

Table 2.2. Daily total light interception ($\text{MJ m}^{-2} \text{d}^{-1}$) for the canopies in study

Canopy	Homogeneous and isotropic			Homogeneous and anisotropic			3D model			
	Julian day									
	153	232	305	153	232	305	153	232	305	
Grape N-S	296	267	157	293	264	147	229	203	108	
Grape E-W	292	264	155	236	227	171	136	150	162	
Almond	607	529	256	618	535	255	380	348	225	
Corn	588	514	253	574	505	254	485	475	250	
Potato-Uniform	622	539	257	628	544	257	544	499	250	
Potato-Row	622	539	257	628	544	257	422	404	257	
Homogeneous canopy										
$L=1.5$	406	362	203	406	362	203	408	360	203	
$L=3.1$	545	480	245	545	479	245	550	482	245	
$L=6.2$	619	538	257	619	538	257	619	537	257	

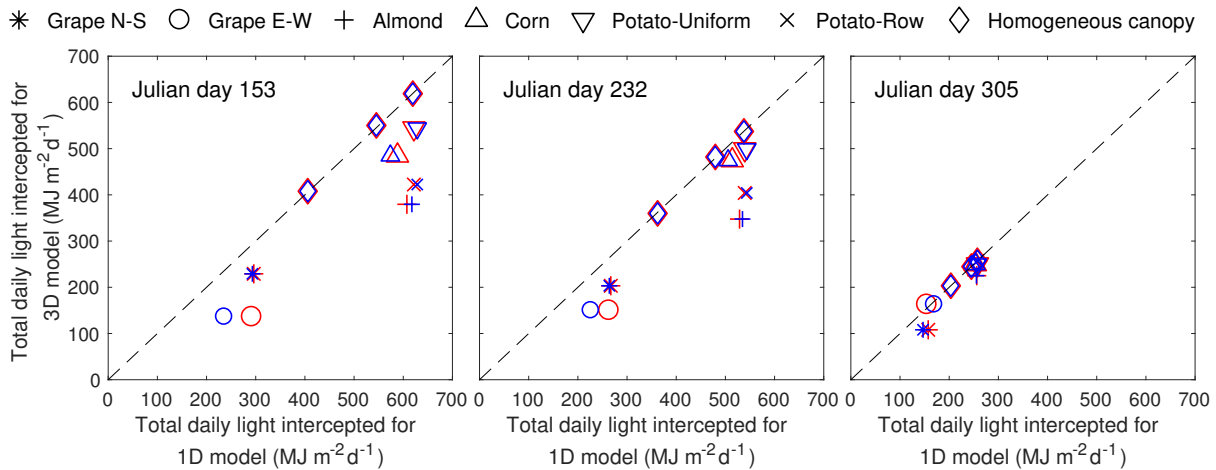


Figure 2.5. Scatter plot of results for daily total light interception listed in Table 2.2 for homogeneous and isotropic (red), and for homogeneous but anisotropic (blue) canopies. Dotted line is 1:1.

vegetation homogeneity and isotropy were closely satisfied, and therefore, the 1D model was in very good agreement with the 3D model regardless of leaf density (Table 2.3).

For the crop canopy cases, the 1D model consistently over estimated light interception as compared to the 3D model, except for Grape E-W and Potato-Row on Julian day 305. For all but the grape cases, eliminating the isotropic assumption resulted in little improvement of agreement between the 1D and 3D models, indicating that errors arose primarily from heterogeneity in these cases. For the Grape N-S, Almond, and Potato cases, errors between the 1D and 3D models were largest near midday when sunlight could most readily reach the ground by penetrating through gaps in vegetation. For Grape E-W, the largest discrepancies occurred at early and late times of the day. The effect of row orientation on diurnal interception patterns for the grape cases was dramatic, as this completely changed the character of interception at different times of the year (see Figs. 2.6, 2.7, 2.8, 2.9). The potato cases also illustrated the pronounced effect of heterogeneity in planting pattern on diurnal interception patterns.

2.3.3 Vertical profiles of hourly absorbed radiation

Figure 2.10 depicts vertical profiles of the absorbed radiation flux at 8:00, 10:00, and 12:00 hours on Julian day 153 for Grape N-S, Grape E-W, Almond, and Corn. Errors in absorbed fluxes for Grape N-S were relatively consistent with height, where errors at a given height were most closely related to the magnitude of the absorbed flux at that height. This was also roughly the case for Almond, except that there was the potential for some under estimation of absorption in the lower canopy when the 1D model was used, which was most pronounced for larger solar zenith angles. For Grape E-W, the 1D model tended to shift the peak in the absorbed flux deeper into the canopy, which was most pronounced for larger solar zenith angles.

In the corn canopy, the vertical pattern in radiation interception differed significantly between the 1D and 3D models. There were up to 50% differences between 1D and 3D fluxes at a given vertical level, with irregular patterns of over or under estimation. In the lower canopy, there was a peak in absorption in the 3D model, which was largely absent in the 1D model, leading to under prediction of absorption by the 1D model in the lower canopy. This is likely due to the substantial over prediction of absorption by the 1D model in the upper canopy, which removes the necessary energy needed to produce a secondary peak in absorption in the lower canopy.

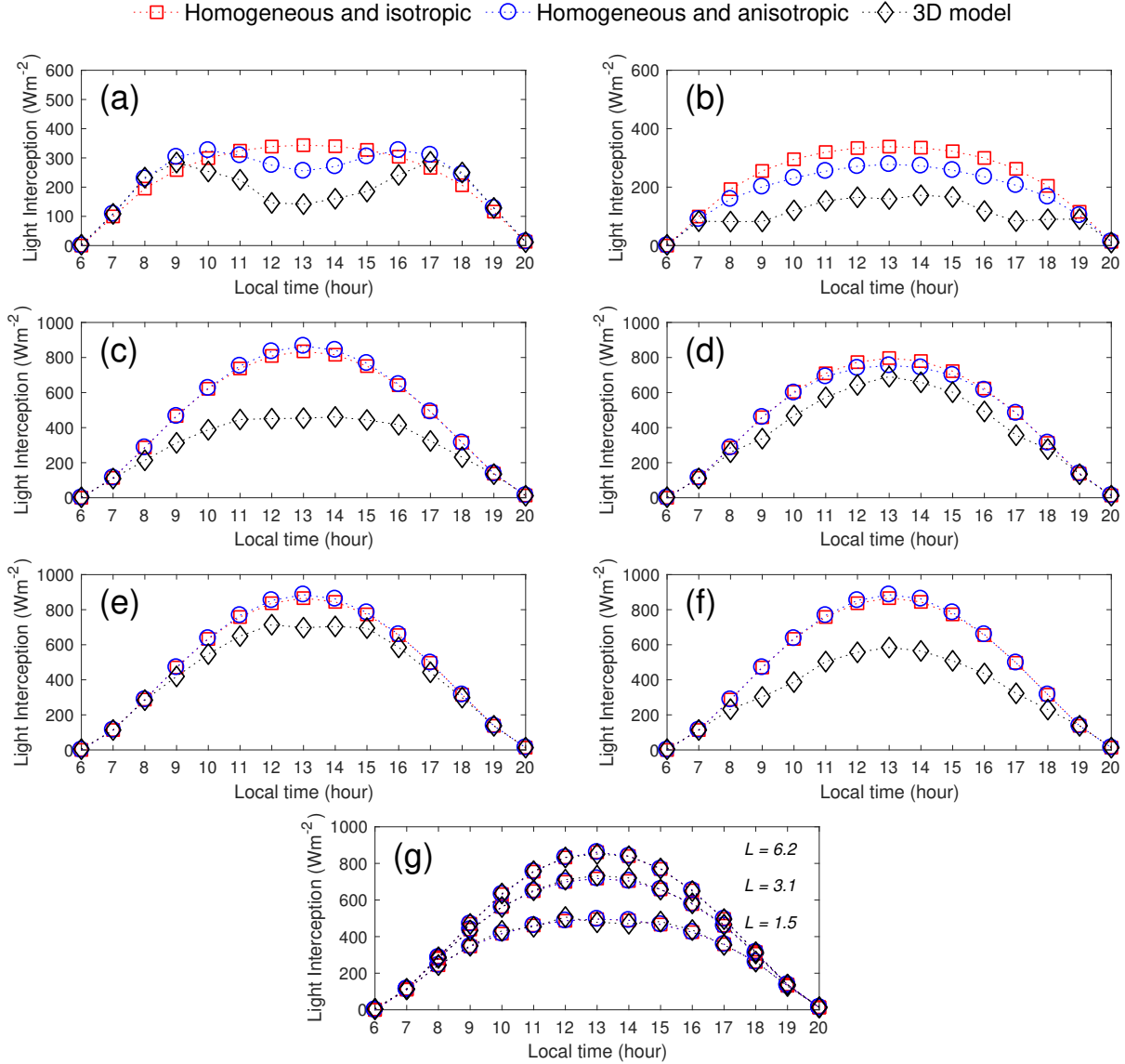


Figure 2.6. Comparisons of the 1D model and 3D model for hourly flux of light interception on Julian day 153 from: (a) Grape N-S, (b) Grape E-W, (c) Almond, (d) Corn, (e) Potato-Uniform, (f) Potato-Row, and (g) homogeneous canopies with three different L values. Both homogeneous and isotropic and homogeneous and anisotropic refer to the 1D model.

2.3.4 Impact of scattering

Total daily light interception for Julian day 153 is shown in Fig. 2.11 for different assumptions regarding radiation scattering, which is given by either Eq. 2.1 (Fig. 2.11a; no scattering), Eq. 2.5 (Fig. 2.11b; only reflection), or Eq. 2.6 (Fig. 2.11c; reflection and transmission). It is important to note that for the homogeneous canopy cases, errors in Fig. 2.11 are due only to effects of scattering, as it was shown in Fig. 2.5 that agreement between the 1D and 3D models was

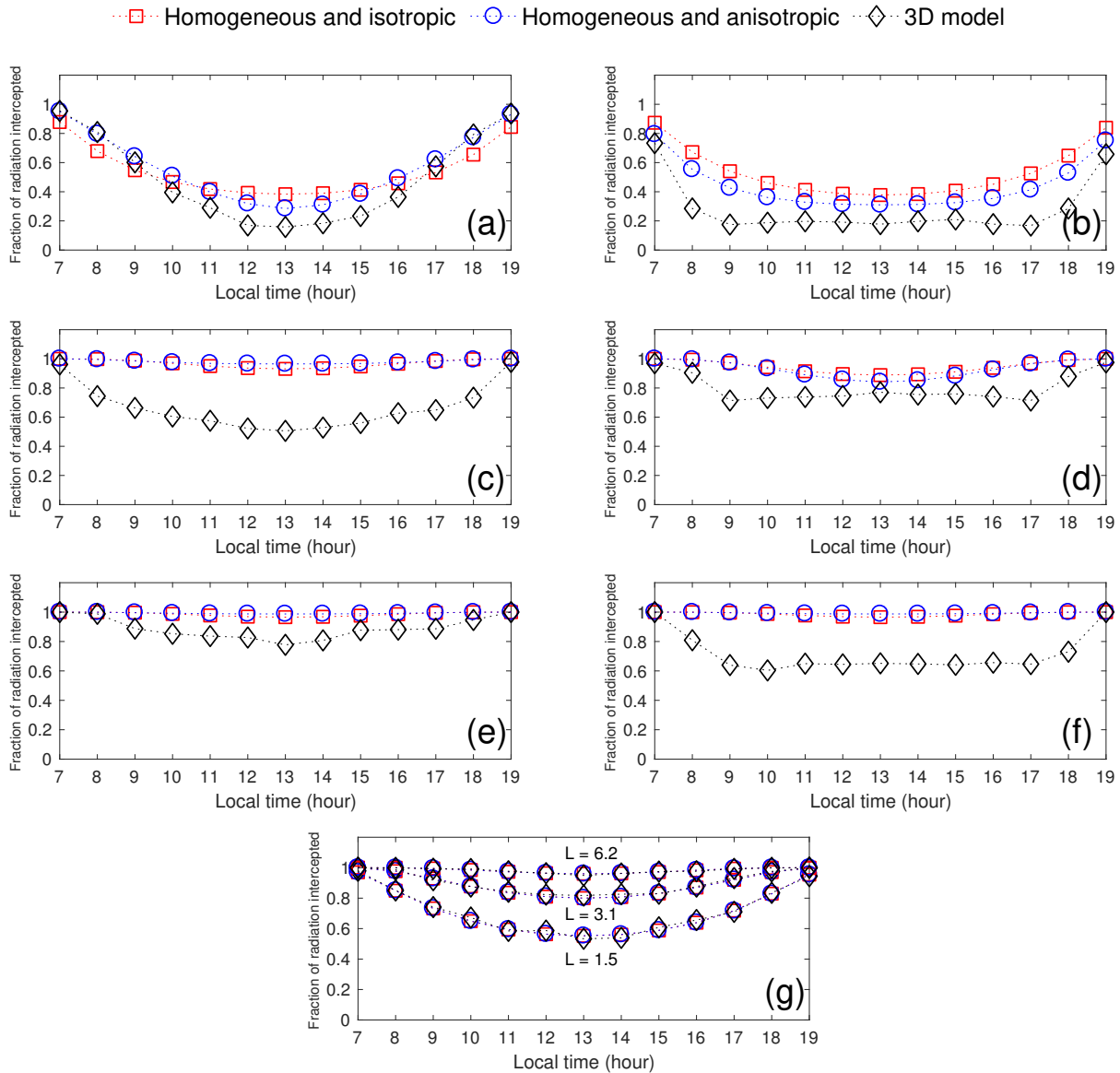


Figure 2.7. Comparisons of the 1D model and 3D model of hourly light interception, expressed as a fraction of direct-beam radiation, on Julian day 153 for: (a) Grape N-S, (b) Grape E-W, (c) Almond, (d) Corn, (e) Potato-Uniform, (f) Potato-Row, and (g) homogeneous canopies with three different L values. Both homogeneous and isotropic and homogeneous and anisotropic refer to the 1D model.

excellent when leaves were black. For the crop canopy cases, errors in Fig. 2.11 are due to the combined effect of scattering and heterogeneity, which makes these results somewhat difficult to interpret.

As evidenced by the homogeneous canopy cases, the impact of scattering was minimal for the PAR band, and thus most of the errors in the heterogeneous crop canopy cases are

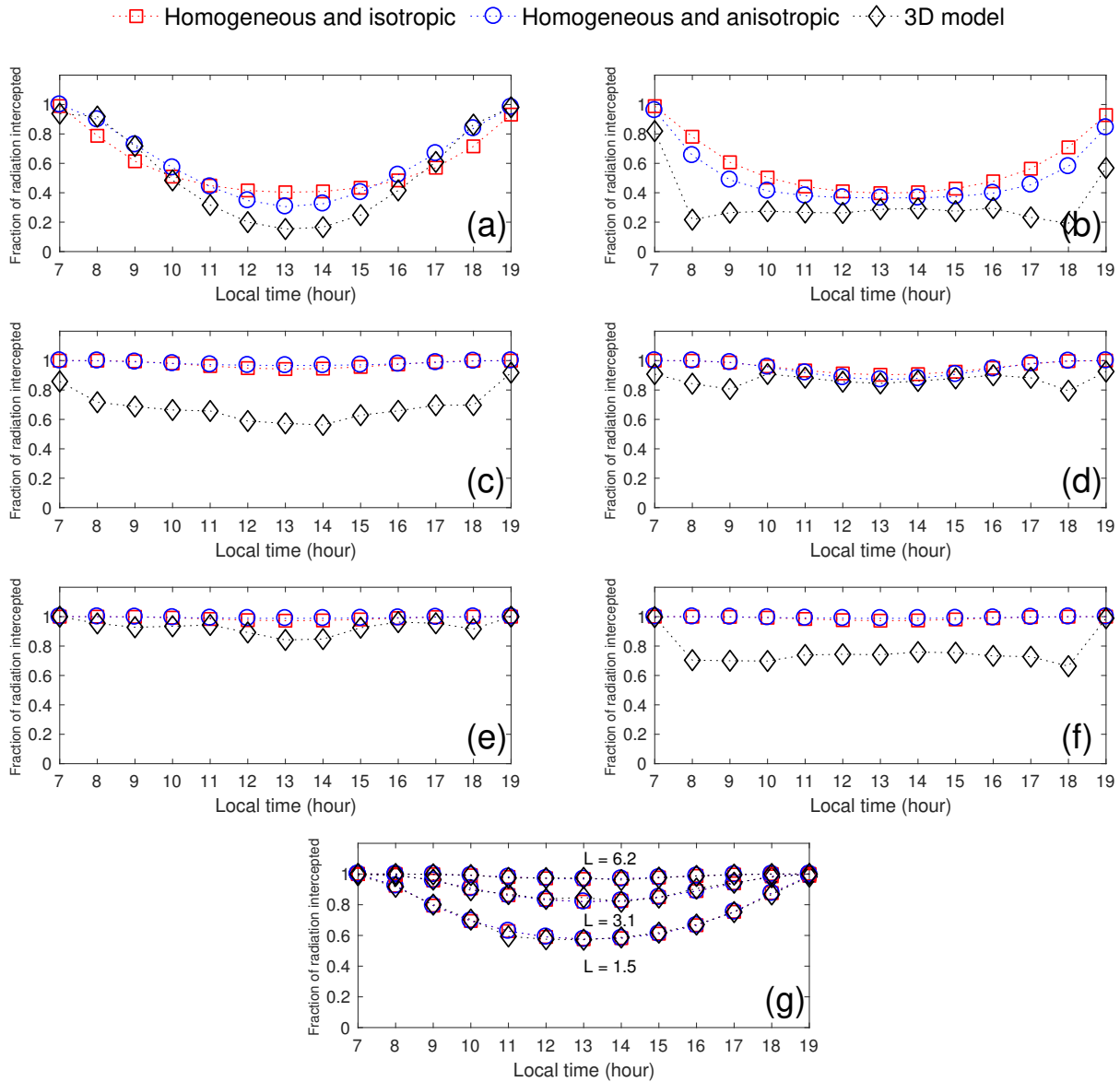


Figure 2.8. Same as Fig. 2.7 except for Julian day 232.

due to heterogeneity and not scattering. In the NIR band, scattering caused very large errors when the standard 1D model was used, with all cases over estimating absorption by more than 100%. Accounting for reflection using Eq. 2.5 removed much of this energy, but still resulted in significant over estimation of absorbed radiation. This approach creates offsetting errors in which absorption is over estimated because transmission is not accounted for, but there is simultaneous over estimation due to the assumption that all reflected radiation either reaches the ground or is reflected back to the sky (but the net result is over estimation). Accounting for both reflection

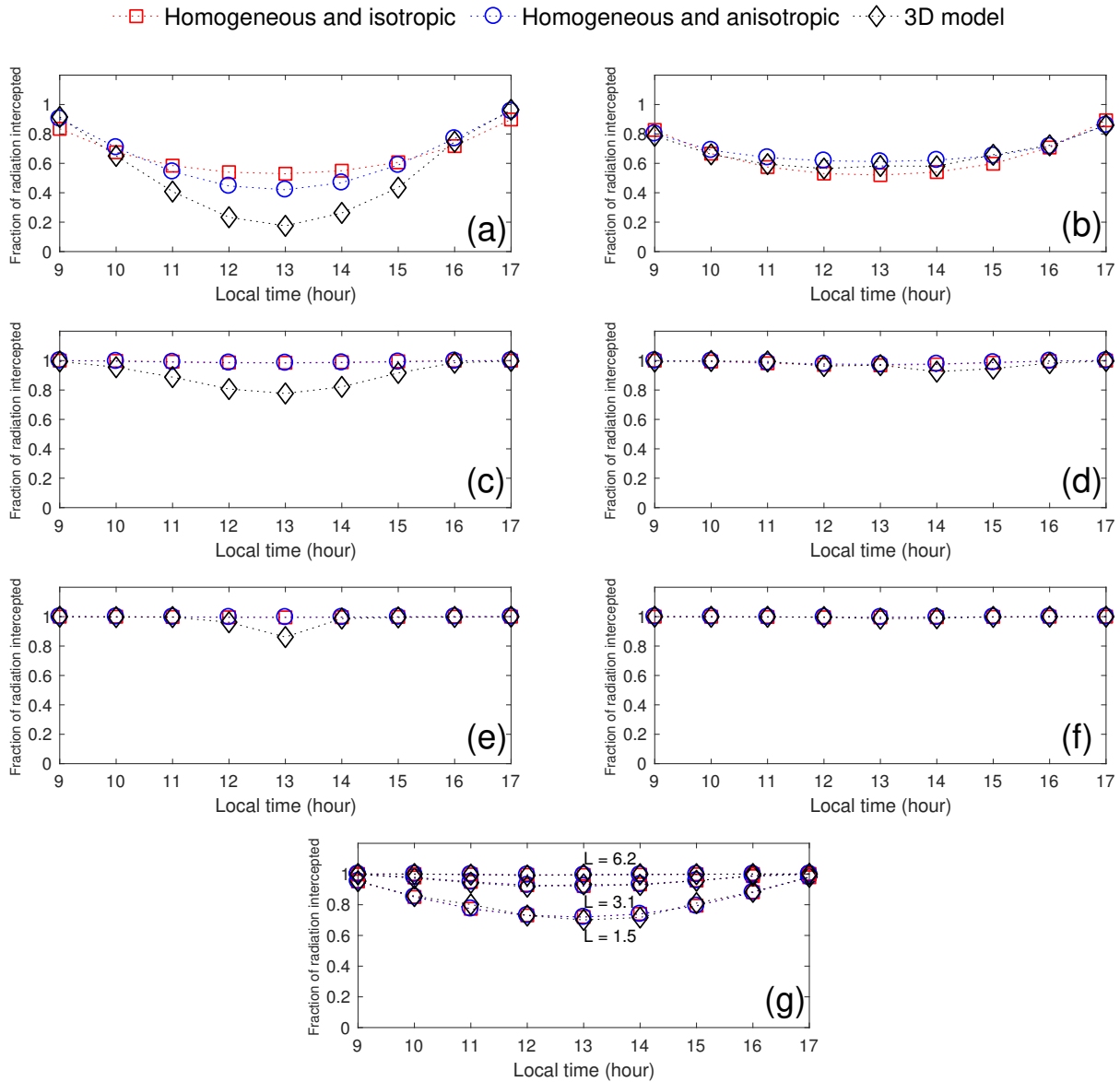


Figure 2.9. Same as Fig. 2.7 except for Julian day 305.

and transmission using Eq. 2.6 caused net under estimation of the total absorbed flux. This is because Eq. 2.6 assumes that all reflected and transmitted radiation either reaches the ground or is reflected back to the sky, thus overall absorption is under estimated.

Table 2.3. Model performance measures comparing results from the 1D and the 3D model for hourly light interception for the virtually-generated canopies based on data for hourly light interception on Julian Day 153 plotted in Fig. 6.

3D vs.1D (Homogeneous and isotropic)									
Canopy	Julian Day 153			Julian Day 232			Julian Day 305		
	R ²	IA	NRMSE	R ²	IA	NRMSE	R ²	IA	NRMSE
Grape N-S	-0.35	0.78	0.29	-0.14	0.81	0.29	-0.59	0.79	0.30
Grape E-W	-6.39	0.65	0.41	-0.32	0.81	0.31	0.98	0.99	0.5
Almond	-0.95	0.8	0.27	0.02	0.87	0.23	0.9	0.98	0.1
Corn	0.82	0.96	0.12	0.98	1.00	0.05	1.00	1.00	0.02
Potato-Uniform	0.90	0.98	0.09	0.97	0.99	0.06	0.99	1.00	0.04
Potato-Row	0.02	0.87	0.22	0.68	0.94	0.16	1.00	1.00	0.00
Homogeneous canopy									
<i>L</i> =1.5	1.00	1.00	0.02	1.00	1.00	0.02	1.00	1.00	0.02
<i>L</i> =3.1	1.00	1.00	0.01	1.00	1.00	0.01	1.00	1.00	0.01
<i>L</i> =6.2	1.00	1.00	0.00	1.00	1.00	0.00	1.00	1.00	0.00
3D vs.1D (Homogeneous and anisotropic)									
Canopy	R ²	IA	NRMSE	R ²	IA	NRMSE	R ²	IA	NRMSE
Grape N-S	0.32	0.88	0.22	0.42	0.89	0.22	0.19	0.87	0.27
Grape E-W	-2.08	0.73	0.32	0.40	0.89	0.22	0.99	1.00	0.04
Almond	-1.17	0.79	0.27	-0.07	0.86	0.23	0.90	0.98	0.1
Corn	0.86	0.97	0.11	0.99	1.00	0.04	1.00	1.00	0.02
Potato-Uniform	0.87	0.98	0.10	0.96	0.99	0.06	0.99	1.00	0.04
Potato-Row	-0.06	0.86	0.22	0.66	0.94	0.16	1.00	1.00	0.00
Homogeneous canopy									
<i>L</i> =1.5	1.00	1.00	0.02	1.00	1.00	0.02	1.00	1.00	0.02
<i>L</i> =3.1	1.00	1.00	0.01	1.00	1.00	0.01	1.00	1.00	0.01
<i>L</i> =6.2	1.00	1.00	0.00	1.00	1.00	0.00	1.00	1.00	0.00

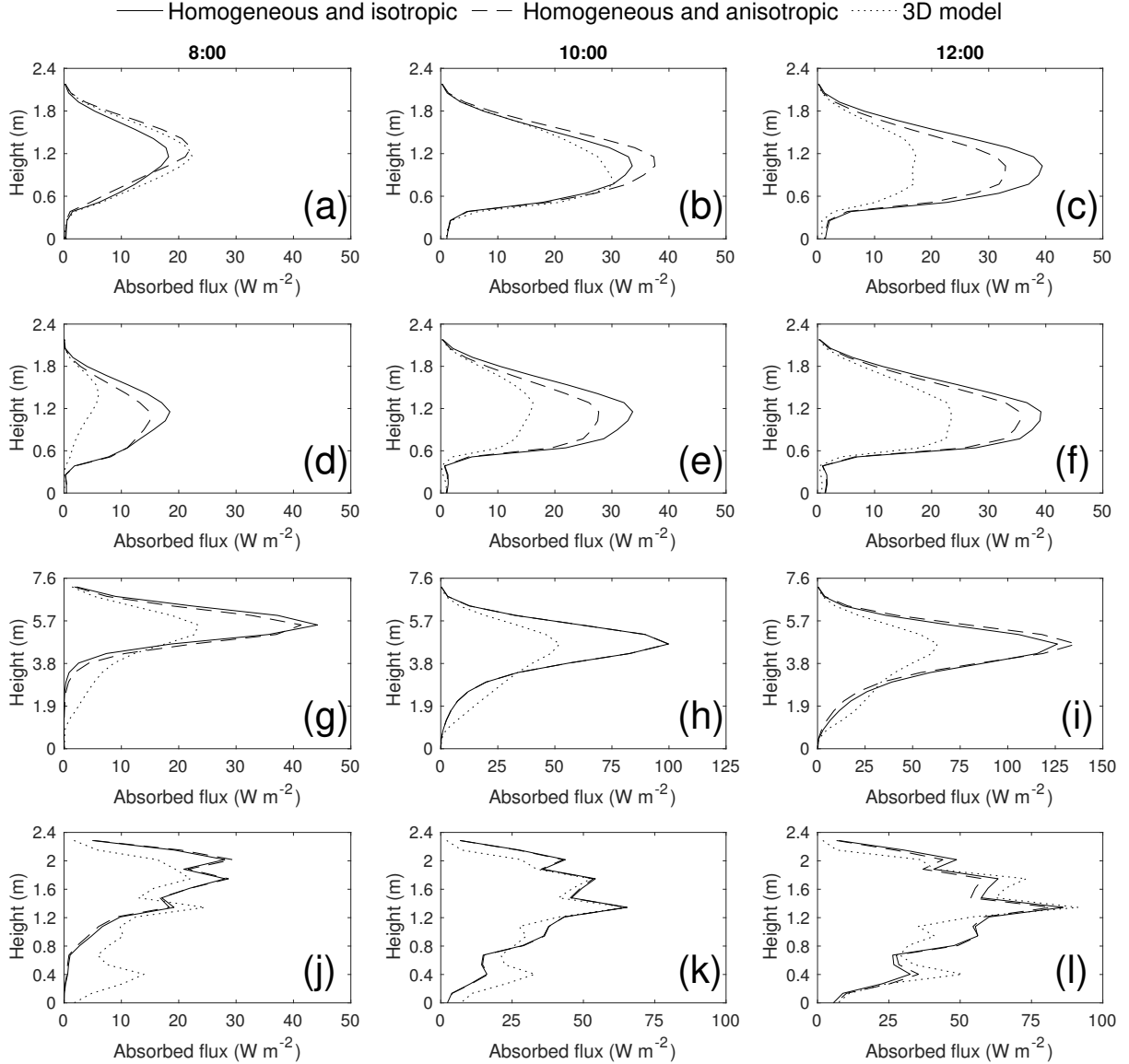


Figure 2.10. Vertical profile of absorbed radiation from Grape N-S (a, b, c); Grape E-W (d, e, f); Almond (g, h, i); and Corn, (j, k, l) on Julian day 153. Columns correspond to 8:00 ($\theta_s=66^\circ$), 10:00 ($\theta_s=43^\circ$), and 12:00 ($\theta_s=21^\circ$) hours for each crop.

2.4 Discussion

2.4.1 Effect of leaf angle distribution (anisotropy)

Overall, anisotropy in leaf inclination had a relatively small effect on errors resulting from the application of Beer's law in cases when leaf azimuth was uniformly distributed (Almond, Corn, and Potato). The grape cases, which had high anisotropy in both the leaf inclination and azimuth

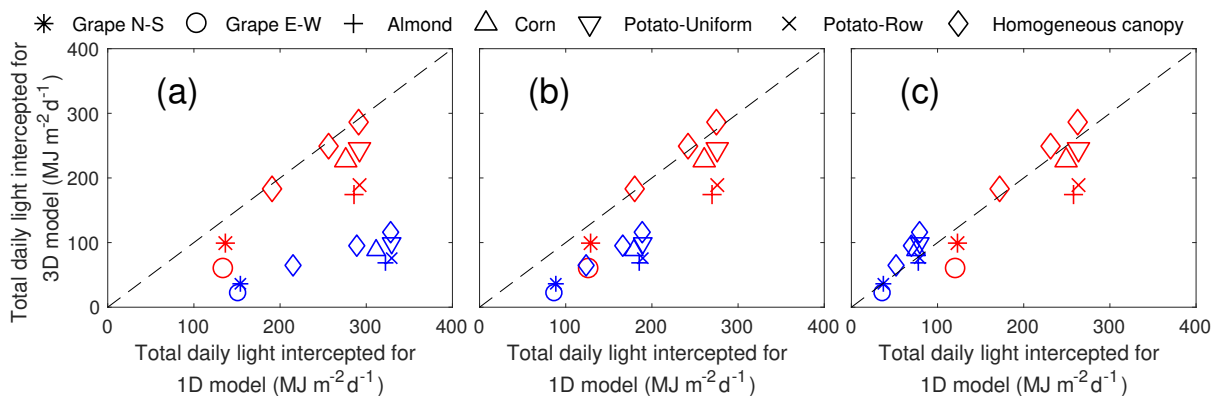


Figure 2.11. Scatter plot of results for daily total light interception for homogeneous and isotropic canopies in the PAR band (red) and NIR (blue) for different assumptions regarding radiation scattering based on a) Eq. 2.1; leaf absorb all incoming radiation, b) Eq. 2.5 and c) Eq. 2.6. Dotted line is 1:1.

distributions, did incur significant errors due leaf anisotropy for the 1D model.

If leaf azimuth is uniformly distributed, this effectively reduces the impact of anisotropy in leaf inclination on the projected area fraction G . Since a leaf with a certain elevation angle could be parallel to the sun at one azimuth and perpendicular to the sun at another, an integration over all azimuths can smear out the effects of leaf inclination alone.

As in the virtual canopies of this study, field measurements have shown that leaf inclination distributions are usually highly anisotropic [5, 72, 73, 87]. The azimuthal distribution of leaves may be strongly anisotropic within a single plant [5], but for relatively dense canopies, the azimuthal distribution is often fairly isotropic [93]. In these cases, the assumption of leaf isotropy is likely to result in minimal errors. However, sparse, row-oriented crops such as vineyards may have highly anisotropic azimuthal distributions [5], in which case it may be necessary to explicitly calculate G based on measurements. These types of canopies are becoming increasingly prevalent in agricultural applications [e.g., apples, olives; 22, 56], due in part to the improved access to mechanical harvesters that a trellised or hedgerow canopy provides.

2.4.2 Effect of plant spacing (horizontal heterogeneity)

Plant spacing and the resulting heterogeneity had the most pronounced effect on errors resulting from the use of Beer's law. For the Grape N-S case, the assumption of heterogeneity resulted in an overestimation of the total daily absorbed radiation by 28%, 30%, and 36% on Julian days

153, 232, and 305, respectively, with larger instantaneous over estimation near midday. For the Grape E-W case, the assumption of heterogeneity also resulted in overestimating the total daily absorbed radiation by 74%, 51%, and 5% on Julian days 153, 232, and 305, respectively. This was not simply an effect related to L , as was illustrated by the two potato cases. By simply rearranging the potato plants from a uniformly spaced into a row-oriented configuration, errors in the 1D model increased substantially.

It is possible that the effect of horizontal heterogeneity can vary in the vertical direction, which appeared to be the case with the Corn canopy. This significantly altered the performance of the 1D model at any given height, although the canopy was dense enough overall that the 1D model performed well when predicting whole-canopy radiation absorption. This could have important implications if the radiation model is coupled with other biophysical models such as a photosynthesis model. The response of photosynthesis to light is nonlinear and asymptotic [112], so although whole-canopy absorption may be well-represented in some cases by a 1D horizontally homogeneous model, it is unclear if that will result in significant errors in total photosynthetic production given the nonlinearity of its response to light.

A limitation of this study is that results are only applicable under clear sky conditions. However, results can provide some insight regarding diffuse sky conditions by simultaneously considering all canopy geometries and simulated sun angles. Under a uniformly overcast sky, equal energy originates from all directions. A particular combination of sun angle and leaf orientation bias was required in order to observe a pronounced effect of leaf anisotropy. Thus, for diffuse solar conditions, it is speculated that the impact of leaf anisotropy will be decreased. Sun angle had an important effect on the instantaneous impact of leaf heterogeneity, and most commonly it was observed that low sun angles resulted in a decreased impact of heterogeneity. Therefore, it is likely that highly diffuse conditions will reduce the impact of heterogeneity near midday because a significant fraction of incoming radiation will originate from directions nearer to the horizon.

Estimating light interception with Beer's law is based on the assumption that canopies are homogeneous. This inherently means that the rate of radiation attenuation along a given path is linearly related to the flux at that location. As the canopy becomes sparse, there are pathways for

radiation propagation that allow radiation to penetrate the entire canopy without any probability of interception, which fundamentally violates the assumptions behind Beer’s law or a turbid medium. Therefore, the non-random leaf dispersion in canopies limits the ability of Beer’s law to link light interception to simple bulk measures of plant architecture.

It is well-known that this heterogeneity or “clumping” of vegetation usually results in decreased radiation interception as compared with an equivalent homogeneous canopy. A common means of dealing with this problem without significantly increasing model complexity is to add a “clumping coefficient” Ω to the argument of the exponential function in Beer’s law [52, 74, 104]. While this is a simple and practical means of reducing the amount of radiation attenuation predicted by Beer’s law, the challenge in applying the clumping coefficient approach is that Ω is a complex function of nearly every applicable variable [17], and thus it is difficult to mechanistically specify. Another approach is to use a model that explicitly resolves plant-level heterogeneity [e.g., 6, 76, 77], as it may not be necessary to explicitly resolve every leaf if within-plant heterogeneity is small.

2.4.3 Effect of row orientation

Row orientation played an important role when estimating light interception from Beer’s law, particularly when the rows were widely spaced. For sparse, row-oriented canopies, the effective path length of the sun’s rays through vegetation can change dramatically with changes in sun azimuth. For East-West rows, absorption is significantly reduced early and late in the day because the rows are close to parallel with the sun’s rays, whereas North-South rows are perpendicular to the sun at this time. As the day of year progresses further from the summer solstice, the sun spends more time closer to the horizon and thus the impact of heterogeneity in an East-West row orientation increased. For the East-West row configuration, $G(\theta_s)$ and light interception were surprisingly constant throughout much of the day, which resulted in 41% and 36% less absorption on Julian days 153 and 232, respectively, compared to North-South rows. This has important practical implications for agricultural design applications. In some climates, it may be desirable to maximize sunlight interception, whereas in others it may be desirable to mitigate effects of excess sunlight to reduce temperatures and water use.

2.4.4 Effect of light scattering

Despite the simplified assumptions in Beer's law regarding scattering, there was good agreement between predicted radiation interception using the 1D and 3D models in the PAR band. Scattering did not significantly influence light interception in this band because most of the incident radiation received by individual leaves was absorbed. However, in the NIR band, scattering introduced significant over estimation of absorption using the standard 1D model, since leaves are poor absorbers in this band. Using an *ad hoc* correction to account for reflection only reduced this over estimation of absorption. An additional correction to account for both reflection and transmission resulted in over correction, and a net under prediction of total radiation absorption.

2.5 Conclusion

The objective of this work was to evaluate common assumptions used in estimating radiation absorption in plant canopies, namely assumptions of homogeneity or isotropy of vegetation. Our results demonstrated that for relatively dense canopies with azimuthally symmetric leaves, a 1D model that assumes homogeneity and isotropy of vegetation generally produced relatively small errors. As plant spacing became large, the assumptions of homogeneity break down and model errors became large. In the case of a vineyard with rows oriented in the East-West direction, errors in daily intercepted radiation were up to $\sim 70\%$ due to heterogeneity alone, with much larger instantaneous errors occurring during the day. If leaves were highly anisotropic in the azimuthal direction, there was also the potential for large errors resulting from the assumption of vegetation isotropy which had the potential to increase errors above 100%. Day of year had an impact on model errors, which was that overall errors tended to decline with time from the summer solstice.

In cases of canopies where the plant spacing starts to approach the plant height, it is likely necessary to use a plant-resolving radiation model in order to avoid substantial over prediction of absorbed radiative fluxes. Additionally, if vegetation is highly anisotropic in terms of both elevation and azimuthal angle distributions, it is also likely necessary to explicitly calculate the projected area fraction $G(\theta_s)$ based on measurements and the instantaneous position of the sun.

Acknowledgements

Financial support of this work was provided by the American Vineyard Foundation grants 2016-1825/2017-1825, and the USDA National Institute of Food and Agriculture Hatch project 1013396.

Chapter 3

A 3D model for simulating spatial and temporal fluctuations in grape berry temperature

▮

Recent shifts in climatic patterns have influenced the frequency, timing, and severity of heat waves in many wine grape growing regions, which has introduced challenges for viticulturists. Growing the same varieties under these altered climatic conditions often requires mitigation strategies, but quantitative, generalized understanding of the impacts of such strategies can be difficult or time consuming to determine through field trials. This work developed and validated a detailed three-dimensional (3D) model of grape berry temperature that could fully resolve spatial and temporal heterogeneity in berry temperature, and ultimately predict the impacts of potential high berry temperature mitigation strategies such as the use of alternative trellis systems. A novel experimental data set was generated in which the temperature of exposed grape berry clusters was measured with thermocouples at four field sites with different trellis systems, topography, and climate. Experimental measurements indicated that the temperature of shaded berries closely followed the ambient air temperature, but intermittent periods of direct solar radiation could generate berry temperatures in excess of 10°C above ambient. Validation results indicated that

The material contained in this chapter is taken from the published journal article: Ponce de León, M. A. and Bailey, B. N. (2021). A 3D model for simulating spatial and temporal fluctuations in grape berry temperature. *Agricultural and Forest Meteorology*. 306, 108431

by accurately representing the 3D vine structure, the model was able to closely replicate rapid spatial and temporal fluctuations in berry temperature. Including berry heat storage in the model reduced the errors by dampening extreme temporal swings in berry temperature.

3.1 Introduction

Increasing temperatures and temperature variability associated with a changing climate have become a major concern for grape producers due to the sensitivity of grape quality to climate, particularly in wine grape production [47, 79, 81, 117, 123]. Short-term temperature extremes associated with heat waves, along with longer-term shifts in seasonal temperature patterns are known to create significant challenges in managing grape quality. Diurnal fluctuations in solar irradiance and air temperature have been shown to affect amino acid and phenylpropanoid berry metabolism at hourly time scales [89]. Elevated temperatures during daily or weekly time periods have been shown to decrease anthocyanin concentration around véraison [31]. Furthermore, the duration of the elevated temperatures not only has an effect on berry composition but also on berry skin appearance. Exposed berries can be damaged by sunburn, and even a few minutes of high temperature exposure can result in cellular damage [41, 51, 119]. Moderate temperatures can also result in berry injury or death after long-term exposure [119].

Grape producers have begun to implement a number of canopy design and management strategies in an attempt to mitigate the negative effects of elevated berry temperatures, including the use of shade cloth [34, 64], trellis design [50, 71], and cluster height [90, 91]. However, grape berry microclimate is complex and highly heterogeneous due to interactions between the vine architecture and the environment, making it difficult to understand and predict the integrated effects of mitigation efforts. Experimental field trials are complicated by the fact that measurement of light and temperature at the berry level is labor-intensive and expensive [125]. Furthermore, the relatively slow development of grapevine systems means that field trials are costly and may require many years of data collection.

Because it is not feasible to independently vary every parameter that determines berry temperature in field experiments (e.g., radiation load, bunch exposure, climate, topography, latitude, trellis system), crop models provide a means for understanding, and ultimately optimizing, how

grapevine design and management practices can be used to mitigate elevated berry temperatures. Previous process-based models have been developed to predict berry radiative fluxes [83, 125] and berry temperatures from environmental parameters [21]. However, in these models the calculation of absorbed radiation and the parameters to represent specific geometrical canopy structure are often simplified. Therefore, the models cannot account for the vertical and horizontal variability within the cluster or canopy, making it difficult to represent different design or management choices such as using altered trellis designs or pruning practices. Previous work has developed models for individual grape [103] and apple fruits [98, 115], and the work of Saudreau et al. [97] successfully developed a 3D model of apple fruit temperature. However, to the authors' knowledge, previously developed 3D grapevine structural models [e.g., 44, 62] have yet to be coupled with a physically-based berry temperature model.

This work develops and tests a new 3D model for grape berry temperature based on the Helios modeling framework [3]. The berry temperature model was validated using a unique data set that spans four different canopy geometries. The spatially-explicit nature of the model allows for robust representation of varying canopy architectures and their effect on berry temperature. The objective of this study was to accurately simulate the spatial and temporal grape berry temperature fluctuations from different vineyard designs, such that model predictions are robust to changes in vineyard configuration such as row spacing, trellis system, and row orientation.

3.2 Model description

3.2.1 Model of 3D vineyard geometry

The 3D geometry of the ground, woody tissues, leaves, and grape berries were represented using a mesh of triangular and rectangular elements within the Helios 3D modeling framework [3]. The procedural plant model generator in Helios allows the user to specify average and random geometric parameter values in order to create a given canopy geometry. Grape berries were represented in 3D as tessellated spheres composed of triangular elements, the ground surface was represented as a planar grid of rectangular elements, woody tissues were represented as a cylindrical mesh of triangular elements, and leaves were represented as a planar rectangle that is masked to the shape of a leaf using the transparency channel of a PNG image [3].

When the terrain was flat, only one grapevine plant geometry was represented in the model, but with periodic boundary conditions applied in the horizontal directions which effectively yielded a horizontally infinite canopy. For inclined terrain, 7 rows of grapevine plants were represented in the slope-normal direction, and periodic boundary conditions were enforced in the slope-parallel direction (see Fig. 3.1).

3.2.2 Surface energy balance equation

The surface temperature for every rectangular or triangular geometric element in the simulated domain was modeled by solving the surface energy budget equation, which consists of a balance between radiative, sensible, latent, and storage heat fluxes:

$$R_n^\downarrow - \varepsilon\sigma T_s^4 = h(T_s - T_{air}) + \lambda g_w \frac{e_s(T_s) - e_a RH}{P_{atm}} + C_p \rho_A \frac{dT_s}{dt}. \quad (3.1)$$

Radiation Terms: R_n^\downarrow (W m^{-2}) is the net absorbed all-wave radiation flux (sum of shortwave and longwave components), ε is the surface emissivity, σ is the Stefan–Boltzmann constant ($5.67 \times 10^{-8} \text{ W K}^{-4} \text{ m}^{-2}$), and T_s (K) is the element surface temperature. Sensible Heat Term: T_{air} (K) is the ambient air temperature immediately outside of the element boundary-layer, and h ($\text{W m}^{-2} \text{ K}^{-1}$) is the convective heat transfer coefficient between the surface and ambient air. Latent Heat Term: $\lambda = 44,000 \text{ J mol}^{-1}$ is the latent heat of vaporization for water, g_w ($\text{mol m}^{-2} \text{ s}^{-1}$) is the conductance to water vapor diffusion between the inter-surface air spaces and ambient air, $e_s(T_s)$ (kPa) is the saturated water vapor pressure evaluated at the element surface temperature, e_a (kPa) is the ambient air saturation vapor pressure, RH is the ambient air humidity immediately outside of the element boundary-layer, and $P_{atm} = 101 \text{ kPa}$ is the assumed ambient air pressure. Heat Storage Term: C_p ($\text{J kg}^{-1} \text{ K}^{-1}$) is the heat capacity of the object, ρ_A (kg m^{-2}) is the object area density (i.e., mass per surface area), and t (sec.) is time.

The radiation terms are calculated using the model of Bailey [2] as implemented in the Helios 3D modeling framework [3]. Three radiative bands were represented in the model: PAR which corresponded to solar wavelengths less than 700 nm, NIR which corresponded to solar wavelengths greater than 700 nm, and longwave radiation which corresponded to all terrestrial radiation. The incoming above-canopy solar radiation flux was calculated using the model of Gueymard [35], which was calibrated for atmospheric turbidity using a radiometer located at

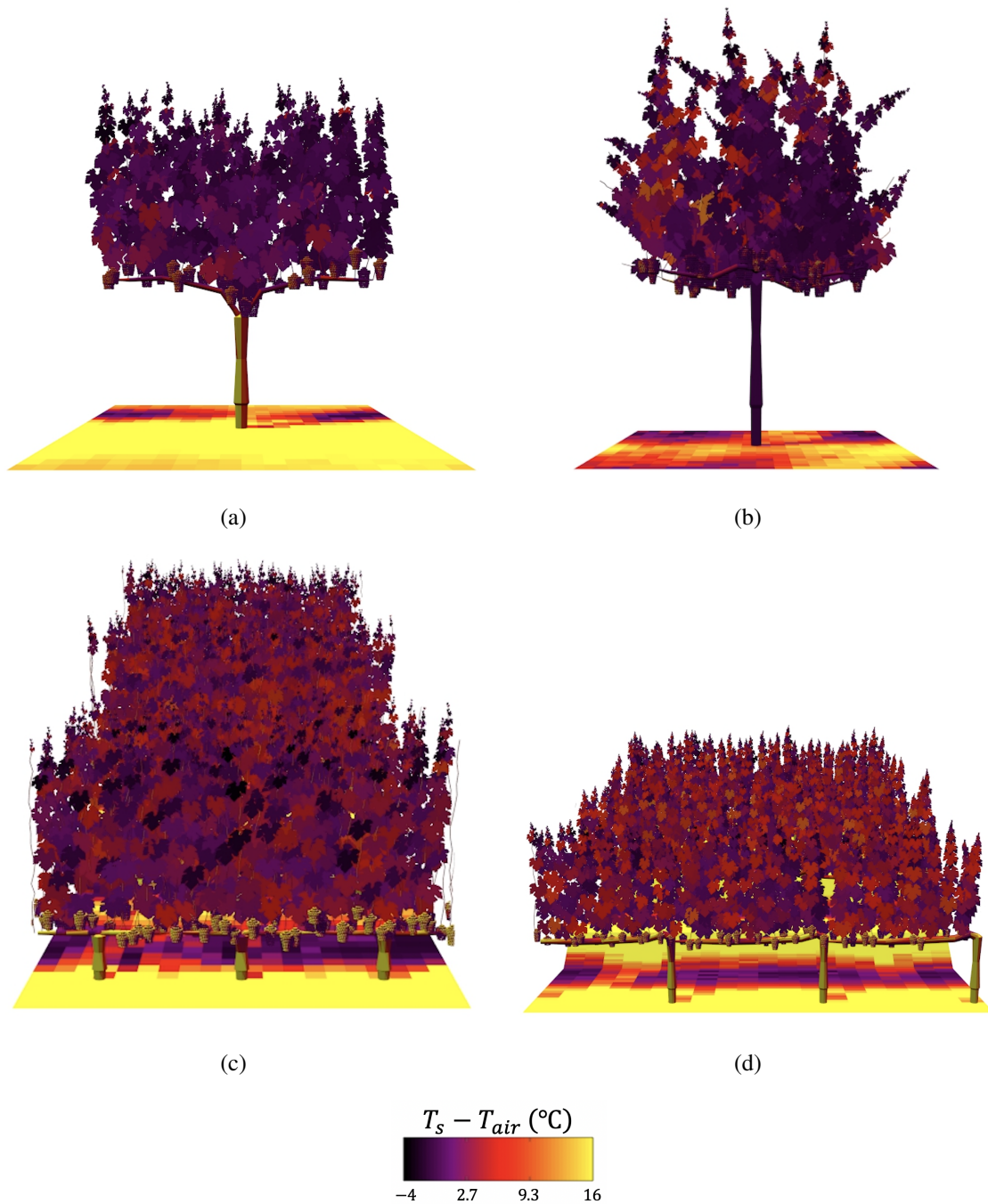


Figure 3.1. 3D Visualization of the vine and air temperature difference ($^\circ\text{C}$) in the East side of the vine at 11:00 hours on Sept 19th from: (a) VSP-2018, (b) Wye-2019, (c) Goblet-2019, (d) Unilateral-2019. Simulations depicted in (a) and (b) utilized periodic horizontal boundary conditions, whereas (c) and (d) utilized periodic conditions only in the row-parallel direction.

each site. It was assumed that partitioning of incoming solar radiation between PAR and NIR bands was 47% and 53%, respectively, and that all incoming solar radiation was collimated. The

incoming diffuse longwave radiation flux from the sky was estimated using the model of Prata [85].

Ambient values of T_{air} and RH were supplied directly from sensor measurements, as described in Sect. 3.3. Values of ε , h , g_w , C_p , and ρ_A were specified differently depending on the surface type, which is described in detail in the following sections. Calculation of R_n^\downarrow also implicitly requires specification of radiation reflectivity and transmissivity for each radiative band and surface element, which is also described below.

The above model was implemented within the “energy balance” model plug-in of Helios. The latest Helios source code can be downloaded at <https://www.github.com/PlantSimulationLab/Helios>.

3.2.3 Berry model parameters

For triangular elements corresponding to grape berries, it was assumed that, since the density of lenticels after véraison is low, the latent heat flux was negligible [111]. In terms of Eq. 3.1, this assumption was implemented by setting $g_w = 0$ for berry elements. It was also assumed that heat released from metabolic activity within the fruit is negligible, and thus no metabolic heat source term was included in Eq. 3.1.

The formulation given by Eq. 3.1 also inherently assumes that the surface temperature at any point is representative of the entire temperature of the object (i.e., the “lumped capacitance” approach). Furthermore, since the surface of the berry is discretized into many triangular elements that could have different temperatures, it was effectively assumed that each triangle corresponds to a “slice” of berry volume subtended by the triangle, which is at the same temperature of that triangular surface element, and responds to ambient changes with a time constant equal to that of the entire berry (i.e., based on $C_p\rho_A$).

Average berry element radiative properties for PAR and NIR bands are given in Table 3.1, which were measured for 3 replicates in the field (see Sect. 3.3). The emissivity ε was assumed to be 0.9 for the berries [115].

The convective heat transfer coefficient h for berries was calculated using the following relationships under turbulent conditions [75]:

$$h = \frac{k_a}{\delta} + 2\frac{k_a}{D}, \quad (3.2)$$

$$\delta = \left(\frac{0.0028D}{U} \right)^{1/2} + \frac{0.0025}{U}, \quad (3.3)$$

where D is the diameter of the sphere, U (m s^{-1}) is the velocity of air immediately outside of the berry boundary-layer, and $k_a = 0.024 \text{ W m}^{-1} \text{ K}^{-1}$ is the thermal conductivity of air. The average berry diameter was taken to be $D = 0.012 \text{ m}$. The berry heat capacity C_p and area density ρ_A were determined by assuming the berry was completely made of water, which gave $\rho_A = 332(r_{\text{berry}})$ kg m^{-2} (r_{berry} is berry radius) and $C_p = 4190 \text{ J kg}^{-1} \text{ K}^{-1}$.

3.2.4 Leaf model parameters

For transparency-masked rectangular elements corresponding to leaves, Eq. 3.1 was applied without the heat storage term (i.e., $\rho_A = 0$), operating under the assumption that the thin nature of leaves allows them to acclimate to changes in the ambient environment quickly compared to other elements in the simulated domain. This assumption means that Eq. 3.1 becomes quasi-steady for leaves, as the future state does not depend on the current temperature.

The moisture conductance g_w represents a serial pathway for water vapor diffusion comprised of conductances corresponding to stomatal and boundary-layer effects on the rate of transfer. The total conductance to water vapor can be written as

$$g_w = \frac{0.97g_H g_s}{0.97g_H + g_s}, \quad (3.4)$$

where g_H is the boundary-layer conductance to heat, and g_s is the stomatal conductance. The stomatal conductance was modeled following Buckley et al. [12] as described in Bailey [3]. Model coefficients were arbitrarily chosen to be equal to the values given in Bailey [3]. The leaf boundary-layer conductance was calculated using the standard Polhausen equation [99].

Average leaf radiative properties for PAR and NIR bands are given in Table 3.1, which were measured for 10 replicates in the field (see Sect. 3.3). The emissivity ε of leaves was assumed to be 0.96 [61].

3.2.5 Ground model parameters

For rectangular elements comprising the ground surface, Eq. 3.1 was applied without the latent heat term (i.e., $g_w = 0$), thus assuming that latent cooling due to water evaporation from the soil was minimal. The heat storage term in Eq. 3.1 was retained and used an assumed value of $C_p\rho_A$ of $30 \text{ kJ K}^{-1} \text{ m}^{-2}$. Clearly, the assumption of uniform temperature in the soil column when calculating the heat storage term is incorrect. However, the chosen value of $C_p\rho_A$ provided a reasonable temperature response time scale for the soil on the order of an hour and gave midday storage values between 20 and 30% of the net radiation flux, which is generally consistent with observations [18]. Furthermore, since the focus of this work was on modeling the temperature of the berries and not the ground specifically, this approximation was deemed acceptable given that the ground temperature only has a secondary effect on modeled berry temperature in terms of long-wave emission. Note also that convective heat transfer between the ground and berries was not modeled directly, but rather was specified using measured temperature and humidity near the berries.

The ground convective heat transfer coefficient was modeled using the following relationship [54]:

$$h = 4.861 + 14.587U. \quad (3.5)$$

Average ground radiative properties for PAR and NIR bands are given in Table 3.1, which were measured for 7 replicates in the field (see Sect. 3.3). The ground emissivity was assumed to be 0.95 [94].

3.2.6 Numerical solution

Equation 3.1 was discretized at time intervals of Δt using a backward-Euler scheme

$$R_n^\downarrow - \epsilon\sigma(T_s^{n+1})^4 = h(T_s^{n+1} - T_{air}) + \lambda g_w \frac{e_s(T_s^{n+1}) - e_a RH}{P_{atm}} + C_p\rho_A \frac{T_s^{n+1} - T_s^n}{\Delta t}, \quad (3.6)$$

where superscripts n and $n + 1$ respectively correspond to the current and future time steps. Given that T_s^n is known either from an initial condition or from the previous time step, the only remaining unknown is T_s^{n+1} , which was determined numerically at each time step using the

secant method [86]. The energy balance for each element was solved in parallel on the graphics processing unit (GPU) using NVIDIA CUDA [cf. 3]. A time step of $\Delta t = 5$ min. was chosen, which was much smaller than the expected temperature response timescale of grape berries (A.1). It was verified that further reducing the time step did not affect results.

3.3 Field experiment materials and methods

To validate the 3D model, field experiments were conducted in four *Vitis vinifera* L. cv. Cabernet Sauvignon vineyards from Sept 19th to Oct 10th (post-véraison to harvest) during the 2018 and 2019 seasons. Two study vineyards were located in Davis, CA (38.53194 N, 121.7528 W) and two others were located in Napa, CA (38.41694 N, 122.4071 W), with each vineyard having a different trellis type. At the research site in Davis, the vines were on a flat terrain, and in Napa the vines were terraced along an east facing slope of approximately 30 degrees. The grapevines sampled in Davis were trained to the vertical shoot position (VSP) trellis system (2018) and the Wye trellis system (2019), while the Napa grapevines were trained to a Unilateral cordon (2019) and a Goblet system (2019). The Unilateral vineyard was configured with one vine in each terrace level, while for Goblet there were two per level. The sampled vine in Goblet was adjacent to the terrace slope leading upward to the next row. The Napa Unilateral and Goblet grapevines were on the same slope at approximately the same elevation and row orientation. Thus it can be reasonably assumed that these two systems experienced nearly the same ambient conditions, making possible a comparison of the effects of canopy architecture. While the Davis VSP and Wye grapevines were in adjacent blocks with the same orientation, a direct comparison is not possible because measurements were collected in different years, and thus ambient weather conditions were different.

For the four experiments, berry temperature was measured using 0.076 mm diameter type ‘E’ thermocouples (OMEGA Engineering, Stamford, CT, USA). The thermocouples were inserted into the center of the berries in exposed clusters facing the east and west side of the vine, and at each side of the vine 4 thermocouples were placed in different berries within the cluster. Because berries could develop necrosis from being punctured by the thermocouple, thermocouples were relocated to adjacent exposed berries at least every 12 days to maintain relatively fresh conditions.

In order to remove the effects of canopy-scale energy and momentum transfer and focus only on berry-scale transfer, ambient measurements were made near the clusters and used to force the model. A weather station was installed at each study site immediately adjacent to the grapevines chosen for temperature measurements. The environmental variable inputs that were measured included incoming above-canopy photosynthetically active solar radiation (SQ 110; Apogee Instruments, Inc., Logan, UT, USA), wind speed (ATMOS 22; METEK group, Inc., Pullman, WA, USA), relative humidity and air temperature (HMP60 with radiation shield; Campbell Scientific, Logan, UT, USA). The incoming solar radiation was measured at a height of 3 m and was used to calibrate the incoming solar flux model in Helios as mentioned previously. The wind speed, relative humidity and air temperature were measured directly adjacent to the vine at the cluster height in order to estimate microclimatic conditions just outside of the berry boundary-layer. The sampling period for all weather data was 5 min. Specific humidity was estimated using the measured air temperature and relative humidity data, and since atmospheric pressure was not measured at the site, hourly average air pressure data from the National Oceanic and Atmospheric Administration (NOAA) local weather stations in Davis and Napa. Specific humidity was calculated as

$$q = \frac{0.622e_a}{P_{atm} - 0.378e_a}, \quad (3.7)$$

and

$$e_a = e_s(T_{air})RH, \quad (3.8)$$

where q is the specific humidity (kg kg^{-1}). Spectral radiative properties of berries, leaves and the ground were measured using a portable spectroradiometer (PSR+ 3500; Spectral Evolution, Inc., Lawrence, MA, USA).

In order to verify that the 3D vineyard geometries generated by the procedural model were reasonable, the 3D models were overlaid onto LiDAR point clouds collected at each site using a RIEGL VZ-1000 laser scanner (RIEGL Laser Measurement Systems GmbH; Horn, Austria). Additional geometric parameters describing the vineyard were extracted from the LiDAR scans, which are listed in Table [3.2](#).

Table 3.1. Averaged measured surface radiative properties used for model inputs

Berry reflectivity-PAR	0.0883
Berry transmissivity-PAR	0
Berry reflectivity-NIR	0.2543
Berry transmissivity-NIR	0
Leaf reflectivity-PAR	0.0855
Leaf transmissivity-PAR	0.0428
Leaf reflectivity-NIR	0.4455
Leaf transmissivity-NIR	0.4041
Ground reflectivity-PAR	0.1801
Ground transmissivity-PAR	0
Ground reflectivity-NIR	0.3998
Ground transmissivity-NIR	0

Table 3.2. Parameters used to quantify the structure of the virtually-generated vineyards.

Vineyard system	Aspect	Slope (°)	Row orientation	Row spacing (m)	Vine spacing (m)	Vine height (m)	Cordon height (m)	Avg. cluster height (m)	Crossarm length (m)
VSP	Flat	0	NW-SE	3.0	2.0	2.0	0.9	0.9	-
Wye	Flat	0	NW-SE	3.0	2.0	2.7	1.2	1.2	1.0
Goblet	East	30	N-S	1.5	0.9	1.7	0.3	0.3	-
Unilateral	East	30	N-S	2.0	1.5	1.8	0.7	0.6	-

3.3.1 Evaluation of model performance

To evaluate the model’s ability to simulate spatial and temporal fluctuations in grape berry temperature, experimental data measured on clear-sky days was used to drive the model and generate predicted berry temperatures. These temperatures were then separately averaged over east-facing and west-facing clusters and compared to average experimental values for the same exposure. The accuracy of the model was evaluated using the statistical error indices of normalized root mean square error (NRMSE), the coefficient of determination (R^2), and the

index of agreement [IA; 124].

3.4 Results

3.4.1 Ambient berry microclimate

An average characterization of weather conditions during the roughly 3-week period in which the weather stations were deployed is provided in Table 3.3. A more detailed graphical depiction of the measured air temperature, air relative humidity, wind speed, and of the calculated specific humidity time series data for the different experimental vineyard designs over the chosen validation period is shown in Fig. 3.2.

During the 3-week period, the daily average air temperature was similar in VSP and Wye, with a wider average daily range of temperature in VSP (18.9°C) compared to Wye (16.2°C). The daily average and average of maximum and minimum relative humidity were significantly higher in VSP compared to Wye, while the maximum wind speed measured in VSP was similar to Wye. Architectural differences between Wye and VSP were characterized by higher berry height, wider row spacing, and increased self-shading in Wye relative to VSP. Recalling that air temperature, humidity, and wind speed measurements were made at the height of the berry clusters, the higher berry height in Wye likely created daytime conditions of lower convective and radiative heat transfer from the warm ground to the fruiting zone, and overall greater turbulent mixing of warm, moist air out of the canopy. Specifically, during the validation day, the greater wind speed measured in Wye was likely responsible for the reduced air temperature and humidity at the measurement height compared to VSP (Fig. 3.2a-b,e-f,i-j,m-n).

For Goblet and Unilateral, during the 3-week period, the daily average and average range of temperature were similar. However, the average maximum relative humidity in Goblet was greater compared to Unilateral and the maximum wind speed was significantly higher in Unilateral compared to Goblet (Table 3.3). The architectural differences between Goblet and Unilateral were dominated by the higher berry height and wider row spacing in Unilateral relative to Goblet. Additionally, the close proximity of the Goblet vines to the adjacent terrace slope created an even larger ground view factor. During the validation day, similar to that observed in VSP relative to Wye, the proximity of the clusters to the ground and low wind speeds due to

the tight row spacing in Goblet likely contributed to the increased air temperature and humidity fluctuations compared to Unilateral (Fig. 3.2c-d,g-h,k-l,o-p).

Table 3.3. Measured daily average, average of the daily maximum and minimum air temperature and air relative humidity, and maximum wind speed data for the different experimental vineyard designs from Sept 19th to Oct 10th of 2018 and 2019.

Vineyard system	T_{air} ($^{\circ}C$)			RH (%)			U ($m\ s^{-1}$)
	Avg.	Max. avg.	Min. avg.	Avg	Max. avg.	Min. avg.	Max.
VSP	19.9	29.7	10.8	58.4	89.9	27.9	9.0
Wye	19.2	27.3	11.1	50.1	82.5	22.9	9.4
Goblet	19.3	30.1	10.4	51.1	79.9	20.2	4.5
Unilateral	19.8	29.7	10.9	47.3	76.1	17.2	13.4

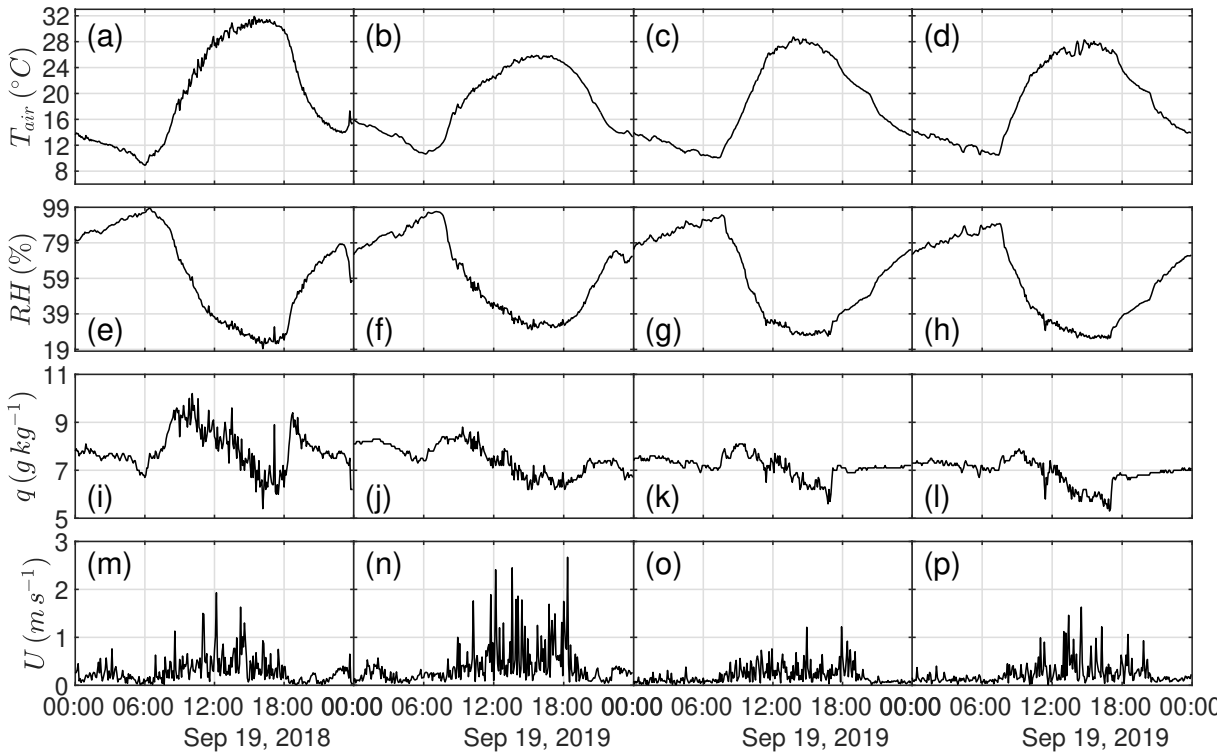


Figure 3.2. Measured ambient meteorological values used for model inputs: air temperature (T_{air}), relative humidity (RH), specific humidity (q) and wind speed (U) for VSP (a,e,i,m), Wye (b,f,j,n), Goblet (c,g,k,o) and Unilateral (d,h,l,p).

3.4.2 Spatial and temporal variation in berry temperature

Spatial and temporal variation in measured and simulated berry temperature is depicted graphically in Figs. 3.3 and 3.4, respectively. A sample visualization of the 3D distribution of the surface-air temperature difference for each vineyard is shown in Fig. 3.1.

During the night, all berry temperatures were near the ambient air temperature, and thus the spatial variability in berry temperature was small and did not vary noticeably among the vineyard designs. During daytime hours, berries in the shade tended to closely match the ambient air temperature, and could reach over 10°C above ambient when in direct sunlight. The maximum berry temperature increase over air temperature measured in the field was 12.4°C for VSP, 11.3°C for Wye, 12.2°C for Goblet and 14.0°C for Unilateral (Fig. 3.3). Besides, the closed canopy in Wye that limited berry sun exposure compared to VSP, it is likely that the greater wind speeds in Wye contributed to the enhanced sensible heat flux exchange and thus the reduced temperature as compared with VSP. For the Goblet and Unilateral vineyards, the east-facing slope and the ratio between plant height and plant spacing mainly determined the hours of berry exposure at the different positions, and therefore, the spatial berry temperature fluctuations. High berry temperatures tended to occur in berries in the west side of the vine during the afternoon when air temperature was warmer and there was exposure to direct sunlight (Figs. 3.2, 3.3 and 3.4). Measurements taken on berries of the west-facing clusters showed that the warmer afternoon temperature increased berry temperature up to 10°C more than that of a similar east-facing cluster. As shown in Fig. 3.3 the highest temperatures on the west side occurred between 15:00 and 17:00 for VSP and Wye (flat terrain), and between 14:00 and 16:00 for Unilateral and Goblet (east-facing slope). It is possible that in Goblet the lower wind speeds, along with proximity of berries to the slope, resulted in less canopy-scale turbulent mixing and a subsequent heating of within-canopy air near the berries compared to Unilateral.

3.4.3 Modeled berry energy balance

Modeled berry temperatures fluctuated rapidly with changes in absorbed radiation, sensible heat, and heat storage. Maximum values of simulated cluster absorbed radiation for the NW-SE orientations in VSP and Wye occurred about 3 hours before noon in the east side of the vine and 4 hours after noon in the west side (Fig. 3.5). Horizontal canopy division in Wye increased

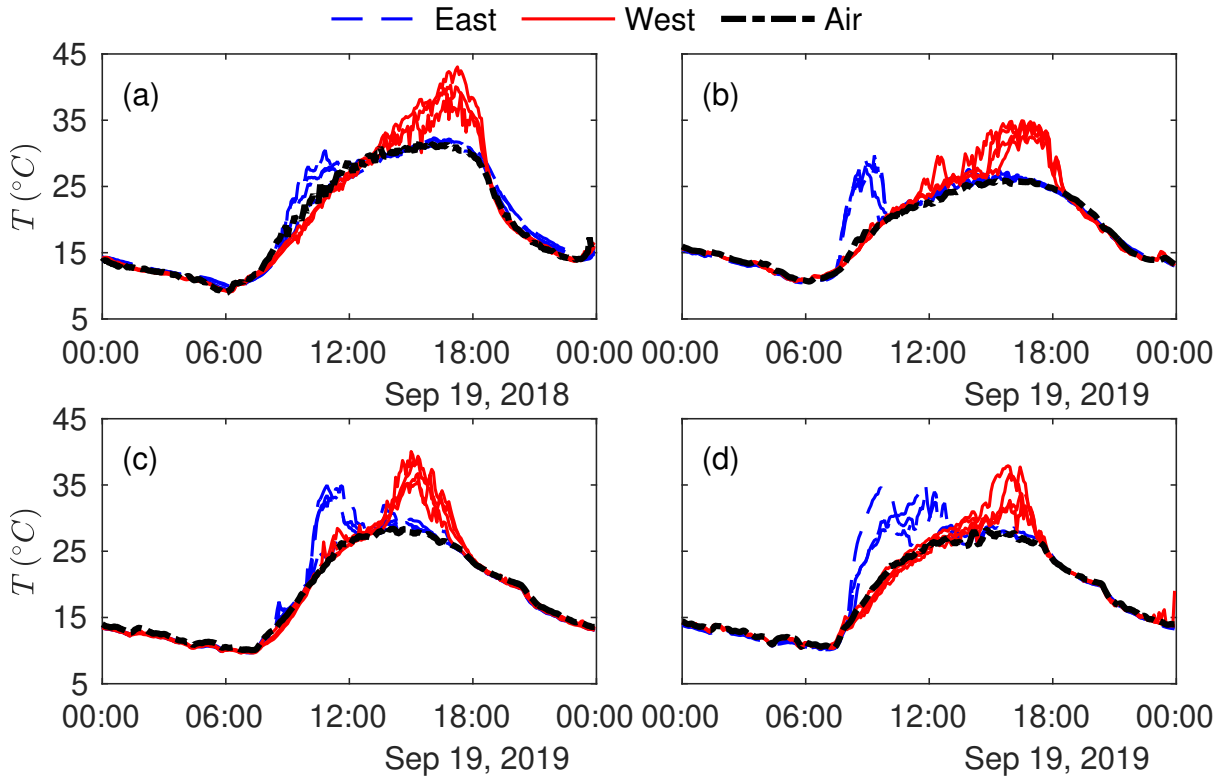


Figure 3.3. Daily course of each measured grape berry temperature in the east and west side of the vine for (a) VSP, (b) Wye, (c) Goblet and (d) Unilateral. Each line corresponds to a different berry measurement. The ambient air temperature is denoted by the black dotted line for reference.

self shading early and late in the day compared to VSP, which minimized exposure to direct sunlight. The widely spaced vines and high berry height in Unilateral favored greater berry light interception early in the morning compared to Goblet. In Goblet and Unilateral vineyard systems, the large difference in bunch exposure between the east and west side of the vines appeared to be dominated by the east-facing slope, which reduced the absorbed radiation in the west side of the vines compared to the east side. Vineyard geometry had a significant impact on the timing of cluster shading, primarily because of variation in row spacing relative to the plant height.

While the absorbed radiation fluxes were positive during the day, the sensible heat fluxes tended to be negative during the day because the berries were warmer than the ambient air. Overall, the sensible heat losses were greater in the afternoon due to the greater difference between berry and air temperature during these hours. Increased wind speed resulted in higher sensible heat losses and, therefore, berry temperatures closer to air temperature, specifically in

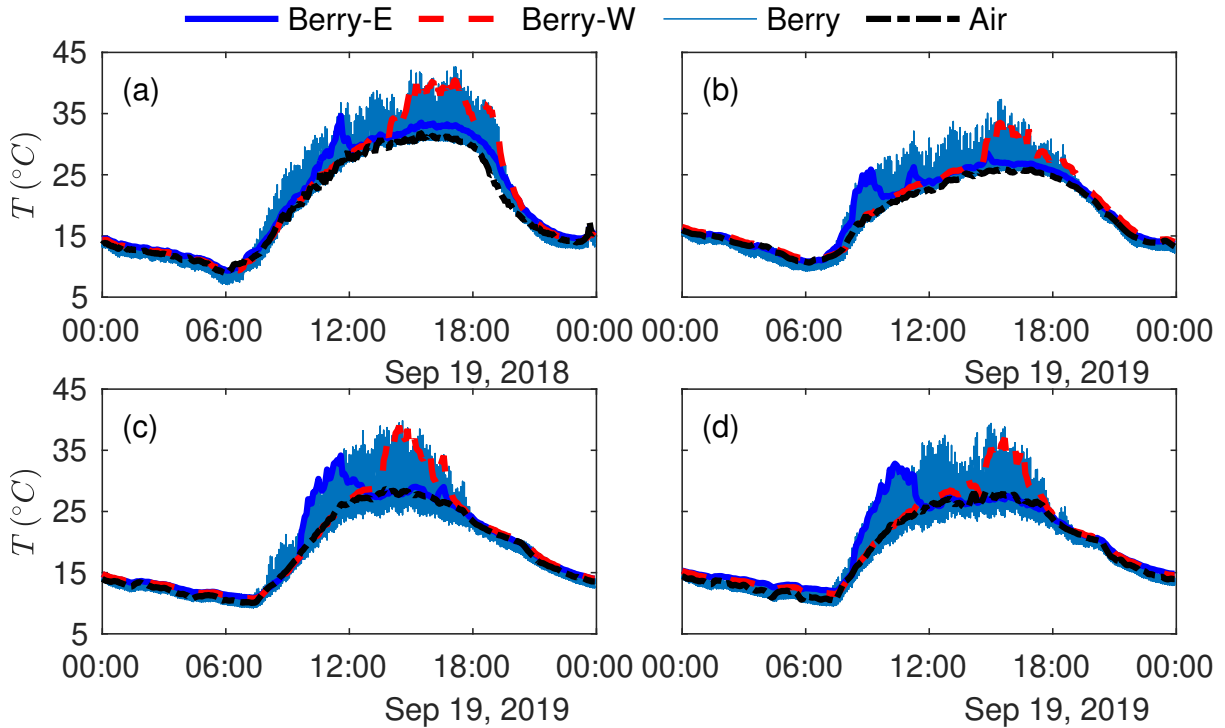


Figure 3.4. Simulated berry temperatures of (a) VSP, (b) Wye, (c) Goblet and (d) Unilateral. The dark blue line shows temperatures of an east-facing berry, the red dashed line of a west-facing berry, the light blue lines of all berry temperatures, and the black dashed line of air temperature.

sparse canopies (Figs. 3.2 and 3.5). The wider row spacing in open canopies (VSP), besides providing less wind resistance, also allowed more heating of the ground and air which resulted in higher sensible heat transfer. The greater sensible heat losses in Unilateral compared to Goblet could be explained by the proximity of the Goblet clusters to the adjacent terrace slope, which has the potential for very large temperature variation that greatly affected the sensible heat fluxes. As expected, the cluster heat storage tended to be negative in the morning as the berries began to rapidly warm, and positive in the afternoon while generally cooling and releasing heat (Fig. 3.5).

3.4.4 Validation of modeled berry temperature

The time series of measured and simulated berry temperature were compared graphically for east- and west-facing clusters in order to qualitatively assess model performance (Fig. 3.6). Graphical results indicated good qualitative agreement between measured and modeled diurnal berry temperature variation at each site. At night time or when berries were in the shade, modeled and measured temperatures closely matched the air temperature. During intermittent periods of

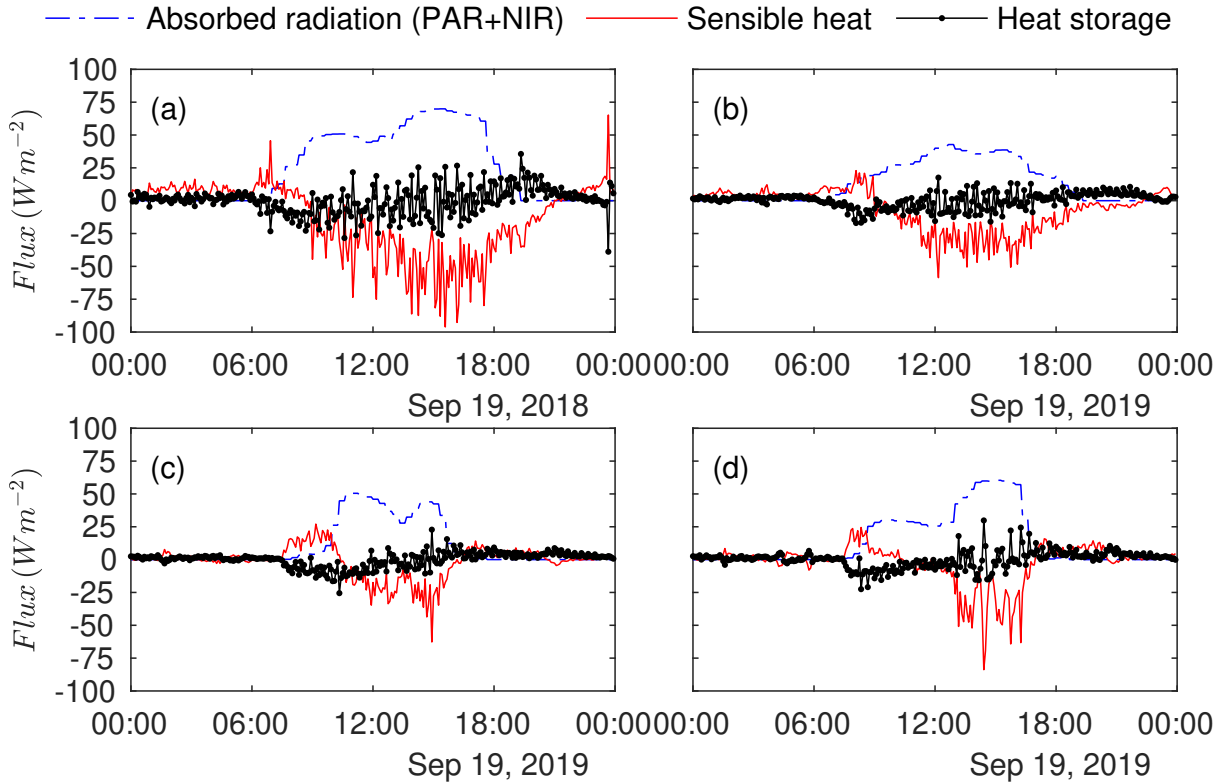


Figure 3.5. Simulated average berry surface heat fluxes for the four different vineyard designs: (a) VSP, (b) Wye (c) Goblet and (d) Unilateral. The adopted sign convention is that fluxes are positive for energy transfer into the berry surface.

solar exposure, the model was able to accurately replicate both the magnitude and duration of temperature increases over ambient. There were a few brief periods, such as in the Unilateral vineyard, in which the timing between the measured and modeled transition from sunlit to shaded conditions lagged by about an hour. It is likely that the observed discrepancies could be explained by slight inaccuracies in the exact position of each berry and leaf. Small errors in the geometric model can translate into large errors in absorbed radiation and berry temperature during periods of sun-shade transition.

The statistical error measures describing agreement between measured and modeled time series shown in Fig. 3.6 are summarized in Table 3.4. Quantitative agreement between measured and modeled berry temperature was excellent, with R^2 between 0.94 and 0.97, index of agreement between 0.98 and 0.99, and NRMSE between 4.6% and 8.5%. The Goblet vineyard showed the overall best agreement. Thus, while there could be brief periods of large error in predicted temperature at any instant when there were rapid transitions between sun and shade, their effect

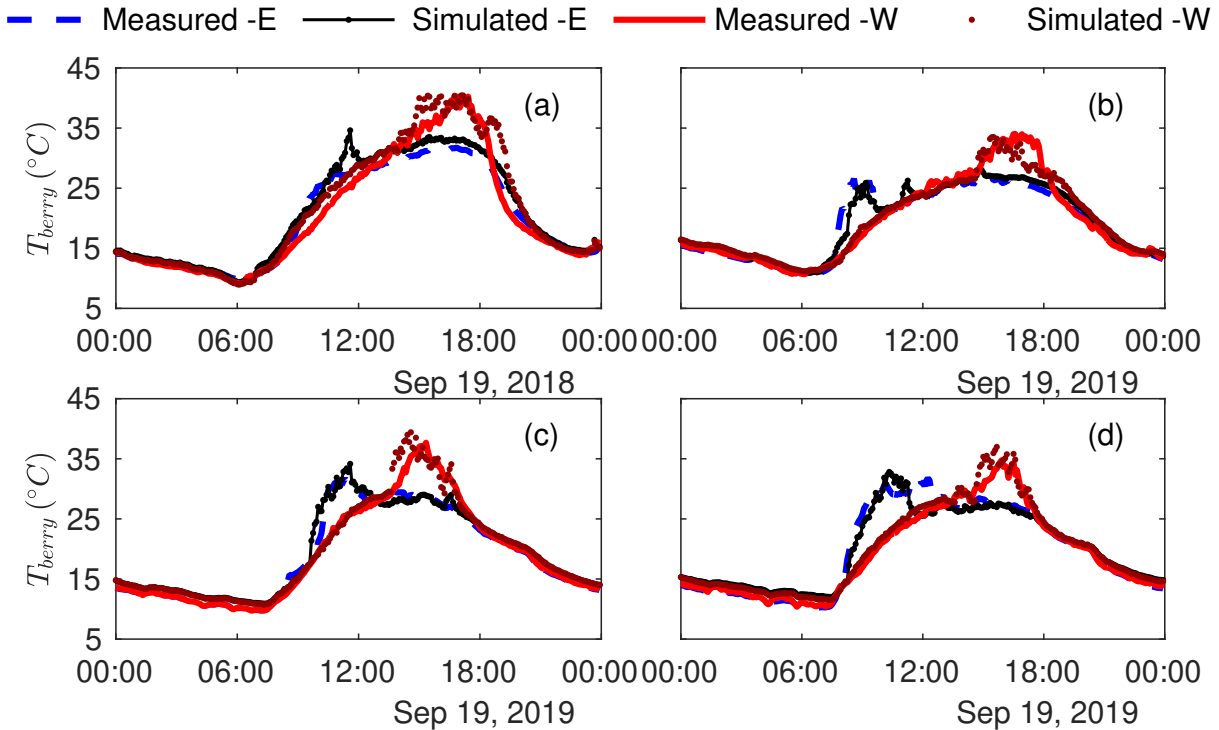


Figure 3.6. Daily course of the simulated and average measured grape berry temperature in the east and west side of the vine for (a) VSP, (b) Wye, (c) Goblet and (d) Unilateral.

on daily averaged errors were relatively small.

3.4.4.1 Effect of berry heat storage

The different plant geometries and row spacing also influenced the berry heat storage and, therefore, the variability in berry temperature (Fig. 3.7). Overall, including the heat storage term in the energy balance equation reduced the error of the temperature fluctuations. With no heat storage, the temperature increased or decreased too quickly, typically leading to over- or under-shooting of the berry temperature, which tended to increase model errors (Table 3.4).

3.5 Discussion

3.5.1 Canopy architecture and berry microclimate

The experimental data collected in this study corresponded to four field sites with different climatic and geographic conditions, and vineyard designs. The average within-canopy ambient microclimate is driven both by the local weather/climate at the site and by the canopy architecture.

Table 3.4. Model performance measures for the four different vineyard designs comparing modeled with measured berry temperature for 288 data points from exposed berries in the east and west side of the vine. Berry temperature data was calculated with and without the heat storage term. Berry temperature data calculated including the heat storage term is plotted in Fig. 3.6.

Vineyard system	Heat storage					
	East			West		
	R ²	IA	NRMSE	R ²	IA	NRMSE
VSP	0.9645	0.9918	0.0585	0.9363	0.9851	0.0758
Wye	0.951	0.9876	0.0707	0.9567	0.9882	0.0643
Goblet	0.9721	0.9927	0.0519	0.9732	0.9932	0.0456
Unilateral	0.9414	0.9827	0.0848	0.9718	0.9931	0.0464
Vineyard system	No heat storage					
	East			West		
	R ²	IA	NRMSE	R ²	IA	NRMSE
VSP	0.9584	0.9904	0.0587	0.9339	0.9847	0.0695
Wye	0.9577	0.9898	0.0603	0.9596	0.9897	0.0552
Goblet	0.9598	0.9897	0.0568	0.9587	0.9897	0.0516
Unilateral	0.9398	0.9826	0.0764	0.9613	0.9906	0.0532

While it is difficult to directly compare the two Davis experiments (VSP and Wye) because they were conducted during different years, the two Napa plots (Goblet and Unilateral) experienced virtually the same weather conditions and thus differences are likely to be dominated by canopy architecture. The primary architectural differences between the Goblet and Unilateral plots were that the row spacing in Goblet was much smaller, and berries were in general much closer to the ground. This tighter row spacing and overall denser canopy led to an expected trend of lower wind speeds, more humid air, and cooler air temperatures on average [102].

The ambient microclimate conditions have important implications for average berry temperatures because when there is minimal or no solar heating, such as at night or when the berries are in the shade, the berry temperature is nearly equal to the air temperature. Since berries spend the majority of their time with temperature near the air temperature, this period will dominate the overall average temperature of the berry. Accordingly, prior work measuring apple

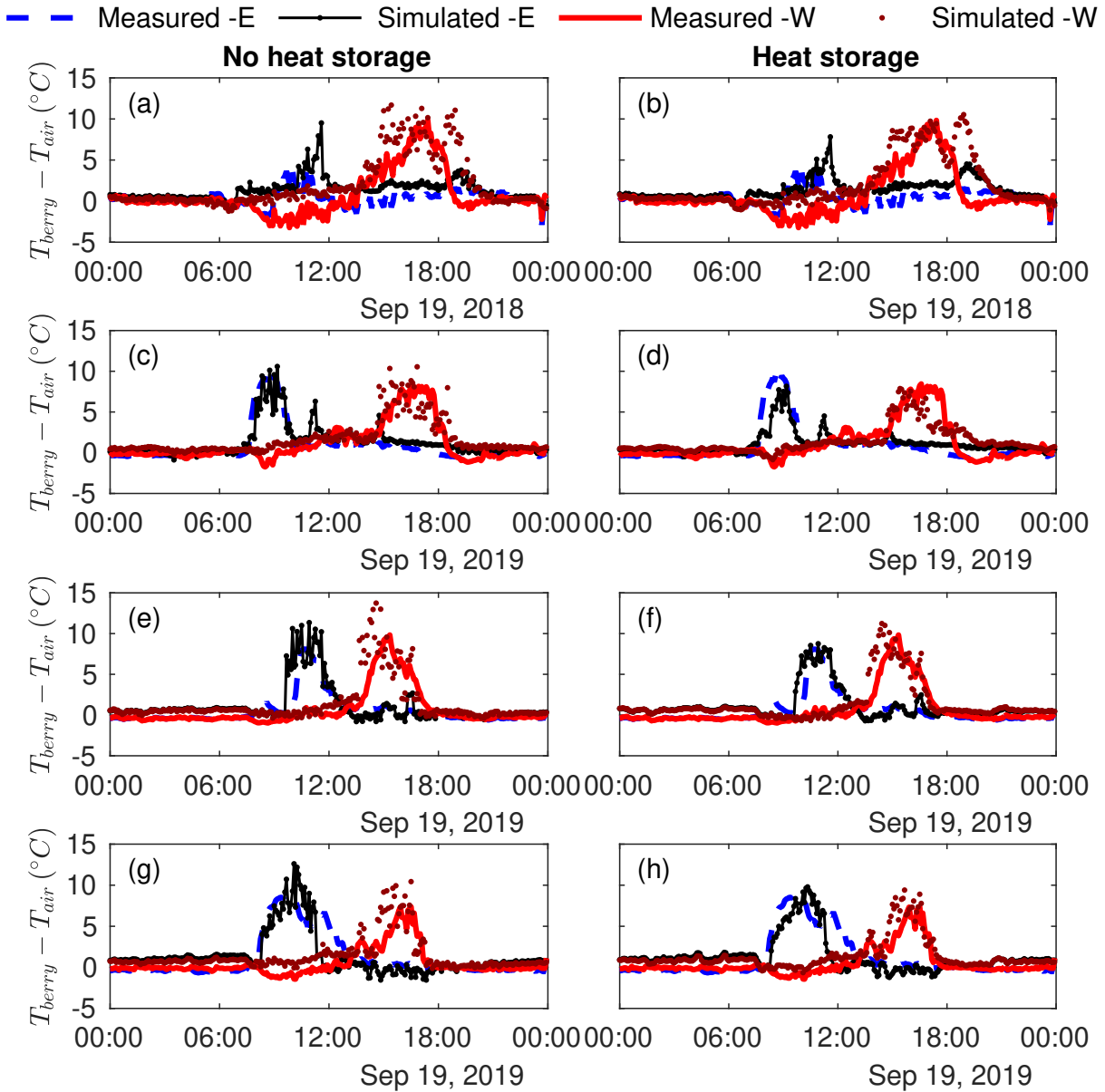


Figure 3.7. Effect of heat storage on average modeled temperature of a berry in the east and west side of the vine for (a-b) VSP, (c-d) Wye, (e-f) Goblet and (g-h) Unilateral.

fruit temperature found that the long-term average fruit temperature was very close to the air temperature, although there could be large deviations from the air temperature at any instant [97].

The differences in vineyard design not only created variability in ambient microclimate, but also introduced considerable temporal and spatial variability in berry temperature. Due to the predominantly north-south row orientation, there were often large differences between the

exposed east- and west-facing clusters at any instant in time. Exposure for west-facing clusters coincided with warmer ambient afternoon temperatures, which meant that the average and maximum temperatures of west-facing clusters was typically higher than for east-facing clusters. The substantial asymmetry in temperature accumulation in north-south oriented vineyards is well-known, and has given rise to strategies based on oblique row angles aimed at achieving more even heating between both sides of the row [e.g., 113].

Of the different variables explored, the berry temperature was also likely to be influenced by differences in wind speed created by the different vineyard geometries. The wider row spacing in open canopies provided less wind resistance and higher wind speeds that increased sensible heat losses. As observed in Unilateral compared to Goblet, the higher sensible heat losses resulted in fully-exposed berry temperatures closer to air temperature. The proximity of the clusters to the adjacent terrace slope in Goblet may have also increased berry temperatures since the ground has the potential to have high deviations in surface temperature relative to air temperature.

The duration and temporal pattern of berry exposure could vary considerably depending on specifics of the berry position. Except for in the Wye vineyard, there were rarely periods in which all berries on a given side of the vine were at a similar temperature (Fig. 3.3). Thus, depending on the horizontal or vertical position of the berry, and random positioning of neighboring leaves, there could be significant variability in berry temperature even on the same side of the vine.

3.5.2 Implications for modeling of berry temperature

Helios simulates complex interactions between the environment and different parts of the vine from ambient weather variables that are not particularly difficult to measure, thereby making it possible to evaluate the applicability of the model at other spatial and temporal scales. Because of the spatially-explicit nature of the plant microclimate model used in this work, it was possible to resolve average differences in berry temperature due to vineyard geometry. Previous models have assumed that the berry temperature is equal to the air temperature [e.g., 9, 27, 116, 122], or used simple heuristic rules to represent the mean effect of the vines [21]. The ability to represent berry temperature deviations from the ambient air temperature is likely important for processes that are sensitive to intermittent periods of high temperature, such as chemical composition [89] or berry burn [41, 51, 119]. Simple heuristic models are unlikely to be useful in evaluating the

effects of different trellis systems, particularly systems with complex geometries such as Wye. The results of the present study showed significant differences in spatial and temporal patterns in berry temperature between trellis systems, which were well-replicated by the spatially explicit model used for prediction.

The model formulation used in this work explicitly represented berry heat storage, and also compared the modeled result when berry heat storage was completely removed. As expected, removing berry heat storage resulted in much larger temporal fluctuations in response to high variability in ambient microclimate. Although inclusion of berry heat storage had a modest impact on average error metrics (which include the entire day), it did provide a noticeable reduction in temperature variability when berries were exposed to the sun. The stabilizing effect of berry heat storage also decreased maximum berry temperatures significantly.

3.5.3 Limitations and future work

A limitation of the proposed model is that it does not include the effect of rainfall or a wet canopy on berry temperature. However, most quality wines are produced in regions with little average rainfall during the period of berry development. The model also did not explicitly represent the 3D variation of temperature and associated heat within the fruit as has been done in the model developed by Saudreau et al. [98] and Saudreau et al. [97] for apple. However, validation results indicated that such detail was not necessary to achieve excellent agreement with measured temperatures, but rather an average exponential dampening of temperature fluctuations with appropriate time constant was sufficient. Another limitation of this study was that currently the model does not predict 3D spatial variations in wind speed, air temperature, or relative humidity, rather, these quantities were measured near the fruit clusters and used to drive the model. If within-canopy microclimate was not available, it could be necessary to implement a canopy-scale energy and momentum transport model.

Previous studies have shown that grape berry metabolism is sensitive to changes in both daily average temperatures and the magnitude of diurnal temperature fluctuations [19, 89], therefore, advances in our understanding of the berry temperature fluctuations might help develop novel strategies to obtain the desired grape quality. The validation exercise in this work focused specifically on berry temperature from post-véraison to harvest. In future studies, the model

could be modified to include latent heat fluxes and be validated to estimate berry temperature during ripening when berry evaporation may be significant and radiative properties of the berries likely differs.

In addition to evaluating strategies for mitigating excessive berry temperatures, the model developed in this work could be used on the macro-scale to predict daily berry temperature fluctuations in different regions, such as hilly or mountainous areas and/or areas with arid continental weather subject to dramatic temperature fluctuations [36]. The model could also be coupled with epidemiological and physiological models to study the effect of the spatial and temporal temperature variations on disease incidence or on physiological processes that determine grape yield and quality.

3.6 Conclusion

During periods in which berries are in the shade or during the night time, it is appropriate to assume that the berry temperature is equal to the ambient air temperature. Accurate prediction of large, intermittent increases in berry temperature during periods of solar exposure not only requires a correct application of the berry energy balance, but also accurate representation of the 3D vine structure which determines the transition between sunlit and shaded conditions. Applying the energy balance equation within a spatially-explicit 3D model allowed for robust predictions of berry temperature dynamics. Representing berry heat storage in the model helped to damp out rapid, non-physical temperature fluctuations, and ultimately improved model accuracy.

Acknowledgements

Financial support of this work was provided by the USDA National Institute of Food and Agriculture Hatch project 1013396. The authors wish to acknowledge Harlan Estate for their gracious collaborative and financial support of the Napa field site experiments.

Chapter 4

Fruit Zone Shading to Control Grape Berry Temperature: A Modeling Study

▮

Recent increases in average air temperatures and heat wave intensity can present challenges in maintaining grape productivity and quality. As a result, growers are exploring approaches to protect berries from excessive temperatures, however, they can be costly and time-consuming to evaluate experimentally and results may not be generalizable. In this work, we developed and evaluated a new 3D model that can predict metrics related to berry temperature and light interception in response to varying vineyard architecture, topography, and shade cloth density. The resulting modeling tool was applied to better understand and evaluate a range of potential vineyard design and management practices for mitigation of elevated berry temperatures in vertically-trained grapevines. Model validation showed close agreement between predicted and measured temperature dynamics, which responded appropriately to the application of shade cloth. In a simulation experiment, row spacing, row orientation, slope grade and aspect, and shade cloth density were varied in order to evaluate their effect on berry and canopy light interception, berry temperature spikes, and integrated berry heat accumulation. On flat terrain, NE-SW row orientation provided the best compromise of berry light and temperature balance between opposing vine faces while avoiding excessive berry temperatures, while N-S rows provided good

The material contained in this chapter has been submitted for publication to the journal: American Journal of Enology and Viticulture, with authorship: Ponce de León, M. A. and Bailey, B. N.

daily symmetry but had risk of high afternoon berry temperatures. The efficacy of shade cloth in mitigating excessive temperatures depended strongly on all variables considered. Slopes with southern or western exposure increased imbalance and risk of high berry temperatures, which in some cases could not be well-managed by shade cloth. Overall, the modeling tool appears capable of providing quantitative guidance for vineyard design and management where excessive berry temperatures are a concern.

4.1 Introduction

Climate models predict that greenhouse gases will increase global average ambient temperatures by approximately 1 and 3°C by 2030 and 2100, respectively [107], in addition to an increase in the frequency, duration and severity of heat waves, particularly in many wine grape growing regions [47, 81, 117, 123]. Elevated temperatures differentially affect rates of grape berry sugar accumulation and phenolic compound development, which can lead to trade-offs in harvest timing that can ultimately result in a reduction in overall grape quality [30, 32, 79, 95]. In Oakville, CA, Martínez-Lüscher et al. [64] reported that elevated temperatures for grape clusters result in unbalanced wines with higher pH and lower levels of anthocyanins. Other research conducted in Murrumbidgee, Australia reported that temperatures exceeding 40°C resulted in delayed ripening and caused berry sunburn [33]. High ambient air temperatures can exacerbate problems created by excessive berry solar exposure due to the reduction of convective cooling. These high temperatures due to direct sunlight can result in berry cellular damage within a few minutes, while moderately high temperatures can result in injuries or death after long exposure [119].

Grape growers have started to implement practices that modify vineyard microclimate in the short and long term to cope with elevated temperatures. These practices include use of vegetative shoots to shade the fruit [e.g., 67, 70], using shade cloths to reduce berry radiative heating [16, 33, 64, 65, 78, 88], spraying berries with a natural “sunscreen” such as a clay compound [11], water misting with sprinklers [15] and, when slope permits, changing the row orientation to reduce or balance solar radiation exposure [113]. Shade cloths, which are the focus of this work, reduce temperature by controlling the transmission of incoming radiation to the fruit zone,

without completely blocking all incident radiation, which could lead to a reduction in grape quality and an increase in disease risk [8]. Shade cloths can be used to cover the entire canopy and thus affect a large-scale change in vineyard microclimate, or they can be applied directly to the fruiting zone to localize their impacts to berry microclimate. Previous studies have reported that shade cloths are effective in reducing maximum berry temperatures, though they have used different methods for quantifying these effects. Martínez-Lüscher et al. [64] reported that 40% black shade cloths covering the fruiting zone of the canopy reduced cluster temperature by 3.7°C during the warmest time of the day, while Greer [33] found that 70% shade cloths covering the grapevines reduced canopy temperature by an average of 4.6°C throughout the day. Similarly, thin shade cloths and plastic films covering the grapevines were shown by Rana et al. [88] to reduce midday berry temperatures by $\sim 2^{\circ}\text{C}$ and $\sim 6^{\circ}\text{C}$ below air temperature, respectively.

While it is clear that shade cloth can be effective in reducing overall berry temperature, a higher degree of control of berry temperature may be desired. In certain instances, it may be beneficial to reduce berry temperature by a defined margin to avoid negative trade-offs, while also balancing temperatures between opposing sides of the vine. However, many interacting variables are likely to influence the efficacy of shade cloth, such as row orientation, row spacing, trellis type, and topography. Due to the large number of important variables affecting berry temperature, it can be difficult to generalize the relatively small number of experimental results that are only able to explore a few variable combinations in order to predict the effect of shade cloth for a given vineyard system.

Crop models provide the potential for generalizing the results of field experiments to predict the outcomes of proposed management strategies for a specific site or climate scenario. Such models could allow for optimization of the design or management of vineyards to mitigate elevated berry temperatures under current or future climates, given that a large number of simulations can be efficiently performed to cover a wide parameter space. Previous work has developed models of spherical fruit temperature [20, 97, 98, 103, 115], including one study that simulated the effect of hail nets on apple temperature [66]. In a recent study, a 3D model was developed and validated that accurately simulated the spatial and temporal temperature fluctuations of grape berries in vineyards with different climates, topographies, and trellises [58].

However, the current version of this model is not able to represent the effects of shade cloth on canopy and berry temperature.

The overall goal of this work was to enable model-based evaluation and optimization of strategies for grape berry temperature control using fruit zone shade cloth. With this goal in mind, specific objectives of this study were to: 1) develop a physically-based 3D model of grape berry temperature that incorporates the effect of shade cloth, 2) generate an experimental data set against which the model can be validated, and 3) quantify the interacting effects of different strategies for excessive berry temperature mitigation such as altered row orientation, row spacing, topography, and shade cloth density.

4.2 Materials and methods

4.2.1 3D model of grape berry temperature

The model of grape berry temperature was based on the 3D model described in Ponce de León and Bailey [58], and modified to include the effects of shade cloth. A brief description of the overall model is provided below, with a focus on novel additions associated with shade cloth.

The model was developed within the Helios modeling framework [3] and has been validated based on field measurements of berry temperature between véraison to harvest [58]. The computational domain consists of 3D geometric elements that fully resolve the spatial structure of the plants, berries, and shade cloth (Fig. 4.1). The berries were represented by 3D tessellated spheres composed of triangular elements, the ground surface by a planar grid of rectangular elements, the woody tissues by a cylindrical mesh of triangular elements, and the leaves by planar rectangles masked to the shape of leaves using the transparency channel of a PNG image [cf. 3]. The shade cloth was formed by rectangles masked to the shape of a grid using the transparency channel of a PNG image, where “holes” in the shade cloth were created based on a grid of transparent pixels.

For all elements in the computational domain, the model calculates the temperature (T_s) that balances the energy budget equation, which is a balance between energy fluxes of radiation, sensible heat, latent heat, and heat storage:

$$\underbrace{R_n^\downarrow - \epsilon \sigma T_s^4}_{\text{Radiation}} = \underbrace{h(T_s - T_{air})}_{\text{Sensible heat}} + \underbrace{\lambda g_w \frac{e_s(T_s) - e_s(T_{air}) * RH}{P_{atm}}}_{\text{Latent heat}} + \underbrace{C_p \rho_A \frac{dT_s}{dt}}_{\text{Heat storage}}. \quad (4.1)$$

The definitions and values for each variable used in the model are given in Table 4.1. Each term of the energy balance is also described in detail in Ponce de León and Bailey [58].

Radiation transfer was simulated using a backward-ray-tracing approach that ensures each geometric element is adequately sampled for both short-wave and long-wave radiation [2]. The model launches a large number of rays from each geometric element to simulate the various modes of radiation transfer, including emission, reflection and transmission based on the radiative properties of each element. When a ray encounters a transparent pixel on an element masked by a PNG image, the ray continues with no interaction. This allows for an efficient fully-resolved representation of shade cloth with a large number of holes. To eliminate domain edge effects, periodic lateral boundaries can be enabled that effectively creates an infinitely repeating vine geometry in the horizontal.

For berries, the latent flux term was assumed to be zero since latent cooling is typically considered negligible after véraison [111]. For this study, heat released from metabolic activity within the fruit was assumed to be low enough to be neglected. The heat transfer coefficient from fruit, ground, and leaf surfaces to the atmosphere, h , are specified as described in Ponce de León and Bailey [58]. Previous field tests suggested an important role of berry heat storage in accurately representing temperature dynamics, and laboratory and field tests have shown that the chosen values for C_p and ρ_A (Table 4.1) result in berry dynamic temperature responses in close agreement with measurements [58].

For the shade cloths, the latent cooling term is not included because the cloths were assumed to be dry, and the heat storage was also neglected because the cloths are thin. The heat transfer coefficient h was calculated using the following relationships for a cylinder in cross flow under turbulent conditions [7]:

$$h = \frac{Nu k_a}{L}, \quad (4.2)$$

where

$$Nu = CRe^m Pr^{0.33}, \quad (4.3)$$

is the Nusselt number,

$$Re = \frac{LU}{\nu}, \quad (4.4)$$

is the Reynolds number, $k_a = 0.024 \text{ W m}^{-1} \text{ K}^{-1}$ is the thermal conductivity of air, L (m) is the vertical dimension of the shade cloth, $C = 0.037$ and $m = 0.8$ are empirical coefficients [80], U (m s^{-1}) is the velocity of air immediately outside of the berry boundary-layer, $\nu = 1.5 \times 10^{-5} \text{ m}^2 \text{ s}^{-1}$ is the kinematic viscosity of air, and $Pr = 0.709$ is the Prandtl number of air. Although heat transfer from the porous shade cloth is clearly not equivalent to that of a cylinder, the correlation for a cylinder was used as an approximation. The shade cloth heat transfer coefficient influences the temperature of the shade cloth, which ultimately has a secondary effect on berry temperature. The effective “diameter” of the shade cloth, L , was taken to be the vertical distance traversed by the shade cloth arc.

The shade cloth fibers (i.e., solid portion of simulated shade cloth mesh) was assumed to be opaque to solar radiation, and assumed to have a reflectivity of 0.3 in both the PAR and NIR bands. Thus, the overall transmissivity of the cloth was determined by the specified shade cloth density only. The shade cloth fiber emissivity was assumed to be equal to 0.96.

Equation 3.1 was discretized in time using an implicit backward Euler scheme, and solved at each time step using the secant method. This numerical solution was parallelized across each primitive using NVIDIA CUDA and GPU computing. Further details on the numerical solution of Eq. 3.1 can be found in Ponce de León and Bailey [58]. A 5 min time step was used in the numerical integration scheme. The 3D model software and documentation is available through the public GitHub repository (<https://www.github.com/PlantSimulationLab/Helios>).

4.2.2 Validation and simulation experiments

The model of grape berry temperature was first validated by comparing predicted berry temperatures against direct measurements of berry temperatures collected in three different vineyards (described below). To account for the error generated by the model at a larger time step, we

Table 4.1. Parameter description and source of the values associated with the energy budget equation in the 3D model for the different vineyard designs.

Symbol	Variable description	Value/Source	Units
T_s	Surface temperature	Calculated for each element in the simulated domain	K
R_n^\downarrow	Net absorbed all-wave radiation flux	Sum of short-wave and long-wave components. Calculated according to the model of Bailey [2]	W m^{-2}
τ	Transmissivity for each element in the PAR and NIR bands	Berries: 0; leaves: 0.0428 (PAR) and 0.4041 (NIR); ground: 0 [58] Shade cloth fibers: 0.	Unitless
ρ	Reflectivity for each element in the PAR and NIR bands	Berries: 0.0883 (PAR) and 0.2543 (NIR); leaves: 0.0855 (PAR) and 0.4455 (NIR); ground: 0.1801 (PAR) and 0.3998 (NIR) [58]; shade cloth fibers: 0.3 (PAR and NIR)	Unitless
ε	Emissivity	Berries: 0.9 [115], leaves: 0.96 [61]; ground: 0.95 [94]; shade cloth fibers: 0.96.	Unitless
σ	Stefan–Boltzmann constant	5.67×10^{-8}	$\text{W m}^{-2} \text{K}^{-4}$
T_{air}	Air temperature immediately outside of the element boundary-layer	Forced based on measurements near the fruit zone	K
h	Heat transfer coefficient calculated between the surface and ambient air	Equations for berries, leaves, and ground are described in Ponce de León and Bailey [58]	$\text{W m}^{-2} \text{K}^{-1}$
λ	Latent heat of vaporization for water	44,000	J mol^{-1}
g_w	Moisture conductance to water vapor diffusion between the inter-surface air spaces and ambient air	Modeled only for the leaves following Buckley et al. [12] and using the model coefficients in Bailey [3]	$\text{mol m}^{-2} \text{s}^{-1}$
e_s	Saturated water vapor pressure	Calculated from Tetens equation [14]	kPa
RH	Relative humidity immediately outside of the element boundary-layer	Forced based on measurements near the fruit zone	Unitless
k_a	Thermal conductivity of air	0.024	$\text{W m}^{-1} \text{K}^{-1}$
U	Wind speed immediately outside of the berry boundary-layer	Measured near the fruit zone from the field experiments and calculated for the simulated VSP cases with 1 m and 2 m row spacings according to Eq. 4.5	m s^{-1}
P_{atm}	Ambient air pressure	101.0	kPa
C_p	Heat capacity of object.	Berries: 4190; ground: 2000	$\text{J kg}^{-1} \text{K}^{-1}$
r_{berry}	Berry radius	0.006 (measured average)	m
ρ_A	Object area density	Berries: $332(r_{berry}) = 2.0$; ground: 15	kg m^{-2}
L	Shade cloth vertical distance	Goblet: 0.33; Unilateral: 0.41; VSP: 0.41	m

validated the model for three days with different ranges in air temperature. Data from these field experiments was then used to provide necessary inputs for a simulation experiment in which the model was used to examine the effects of shade cloth and vineyard configuration for a range of hypothetical vineyards.

4.2.2.1 Field validation experiments

To validate model predictions of berry temperature augmentation by shade cloths, a field experiment was carried out in *Vitis vinifera* L. cv. Cabernet Sauvignon vines in Napa, CA (38° 25' 0.98" N, 122° 24' 25.56" W) from 19 Sept. to 10 Oct. 2019. During this period, three days with different ranges in temperature were selected for intensive examination: a day with average ambient temperatures (19 Sept. 2019), the day with the highest ambient temperatures (25 Sept. 2019), and the day with the lowest ambient temperature (30 Sept. 2019). The vines at this site were planted on an east facing slope (30°) with a N-S row orientation. Vines in adjacent N-S blocks were trained to Goblet and Unilateral trellis systems. The Unilateral vineyard was configured with one vine in each terrace level, while Goblet with two vines per terrace level. The sampled vine in Goblet was in the interior of the terrace level, adjacent to the terrace slope. For both systems, 40% green shade cloths were installed after véraison and remained in place until harvest. The shade cloths were draped vertically across the clusters at approximately 0.2 m above the vineyard floor for Goblet and 0.4 m for Unilateral. The shade cloth width was 0.5 m in Goblet and 0.6 m in Unilateral. The shade cloth vertical distance traversed by the shade cloth arc was 0.33 m for Goblet and 0.41 m for Unilateral and VSP.

To simulate berry temperature under different shade cloth densities and positions, input data from another field experiment carried out in a vertical shoot position (VSP) trellis system in Davis, CA (38° 31' 54.98" N, 121° 45' 10.08" W) was used. This experiment was carried out from 19 Sept. to 10 Oct. 2018. The vines were oriented NW-SE and were on flat terrain.

At all sites, berry temperatures were measured using 0.076 mm diameter type 'E' thermocouples (OMEGA Engineering, Stamford, CT, USA). Four thermocouples were inserted into exposed berries on the east side of the vine and another 4 in berries on the west side of the vines (Control). Additionally, for Goblet and Unilateral, 4 thermocouples were inserted into the berries under the shade cloths on the west side of the vines. Additional details of experimental

measurements can be found in Ponce de León and Bailey [58], including spectral radiative properties of berries, leaves and the ground, the geometric parameters describing the vineyard extracted from LiDAR scans, and additional microclimate measurements.

4.2.2.2 Meteorological inputs

To calculate R_n , the model requires specification of the incoming radiation flux, which was generated following the REST2 model of Gueymard [35], which itself requires site longitude, latitude, offset from UTC, atmospheric pressure, air temperature, atmospheric turbidity coefficient, relative humidity, and Julian day of the year. The incoming radiation was split into short-wave radiation (PAR and NIR) and long-wave radiation. The short-wave radiation was assumed to be partitioned between PAR (<700 nm) and NIR (>700 nm) bands, 47% and 53%, respectively. The incoming diffuse long-wave radiation flux from the sky was estimated using the model of Prata [85]. The input parameters to calculate R_n are the surface reflectivity and transmissivity for PAR and NIR bands, and the surface emissivity (ϵ) for long-wave radiation for each element in the domain. The measured values for berries, leaves and ground are reported in Ponce de León and Bailey [58] and listed in Table 4.1. For all simulations, ambient diffuse solar radiation was neglected and all solar energy was collimated in the direction of the sun. The number of direct rays sampled on each element was set to 500 rays. The radiation scattering depth was chosen to be 3, and it was verified that using larger values would have a negligible impact on results.

To calculate the sensible heat flux, the model requires input of wind speed, U , adjacent to the berries, which was directly measured in the validation experiments. As row spacing changes, U is likely to change, and thus cannot be directly specified based on data for the hypothetical vineyards with variable row spacing. For the VSP simulation experiments with 1 m and 2 m row spacing, we calculated the wind speed based on the reference wind speed measurement at 3 m row spacing (U_{ref}) obtained from the VSP field experiment assuming an exponential wind velocity profile

$$U = U_{ref} \exp \left[-(a - a_{ref}) \left(1 - \frac{z}{h_c} \right) \right], \quad (4.5)$$

where $h_c = 2$ m is the vine height, $z = 0.9$ m is the cluster elevation above the ground, and a is

the attenuation coefficient calculated as [29]

$$a = \frac{0.2LAIh_c}{l_m} \quad (4.6)$$

where LAI is the leaf area index, and l_m is the mean distance between leaves in the VSP canopy, which was estimated as

$$l_m = \frac{4wh_c}{\pi LAI} \quad (4.7)$$

where $w = 0.07$ m is the average leaf width.

The reference attenuation coefficient, $a_{ref} = 0.76$, was calculated using Eqs. 4.6 and 4.7 with the calculated LAI for the VSP vine geometry with 3 m row spacing.

To calculate the latent heat flux, the model requires input of T_{air} , RH , and P_{atm} (see Table 4.1). For all the VSP simulation experiments, we used the measured T_{air} and RH data from the field experiment in the VSP system.

To calculate the heat storage, the model requires input of heat capacity and object density. For the case of berries, the density was calculated assuming the berry was completely made of water. For the ground, we assumed a value of $C_p\rho_A$ of $30 \text{ kJ K}^{-1} \text{ m}^{-2}$ [58].

4.2.2.3 Simulation experiment cases

The 3D geometries of Goblet, Unilateral and VSP trellis systems were generated based on LiDAR measured canopy parameters as described in Ponce de León and Bailey [58] using the procedural plant model generator in Helios. The primary architectural differences between the Goblet and Unilateral systems were that the row spacing in Goblet was smaller (1.5 m vs. 2.0 m) and berries were closer to the ground (height of 0.3 m vs. 0.6 m). Compared to Goblet and Unilateral, VSP had a wider row spacing (3.0 m) and the berries were farther from the ground (0.9 m).

Different simulation cases were set up to evaluate the effect of shade cloth on berry temperature in vineyards with different row orientations, row spacing, and topography using the VSP trellis system (see Table 4.2). Among the range of simulated hypothetical vineyards, the cases with 3 m row spacing had the lowest overall LAI ($0.72 \text{ m}^2 \text{ m}^{-2}$) compared to the cases with 2 m ($1.08 \text{ m}^2 \text{ m}^{-2}$) and 1 m ($2.15 \text{ m}^2 \text{ m}^{-2}$) row spacing. Note that the vegetation density of

individual plants was the same in each case, and canopy-level LAI varied due to row spacing (i.e., planting density) only. Vineyard configurations simulated on a slope utilized periodic conditions only in the row-parallel direction, while those on flat terrain utilized periodic horizontal boundary conditions.

The shade cloths in the simulated domain had 30%, 50%, and 70% density. The shade cloth percentage corresponds to the fraction of the grid that is solid (i.e., 100% has no transmission). An additional control treatment with no shade cloth was also simulated (see Table 4.2). The modeled shade cloths for VSP had a width of 0.6 m and were positioned 0.65 m above the ground in the east and west side of the vine. The dimensions and position of the shade cloth modeled for Goblet and Unilateral are described in Sect. 4.2.2.1. Based on the chosen shade cloth geometry, berries were always shaded regardless of sun position or slope. Sample visualizations of the 3D distribution of surface temperature for the vine canopy cases under 40% shade cloth is shown in Fig. 4.1.

The meteorological inputs for the simulation experiment were specified based on measurements from the VSP vineyard in Davis, CA as introduced above. In order to make presentation of the large number of simulation results tractable, we chose a single representative day of meteorological data to force the simulations, and focused on relative differences between cases. The chosen day was Sept. 19, 2018, the meteorological data for which is provided in Ponce de León and Bailey [58]. This day could be loosely classified as “average” for the post-véraison time period at the site.

The direction of the slope faces was varied and included N, NE, E, SE, S, SW, W, and NW. For all cases, the overall slope inclination was 30°. The slope was terraced such that 90% of each 1 m row interval and 50% of each 2 m and 3 m row intervals were flat.

4.2.2.4 Analysis of simulation results

To evaluate the model accuracy, the time series of experimental measurements and simulated temperatures for berries furthest west were compared. Model agreement with field measurements was quantified using the error metrics normalized root mean squared error (NRMSE)-normalized by the difference between maximum and minimum measured data, the coefficient of determination (R^2), and the index of agreement [IA; 124]. To analyze the modeled berry

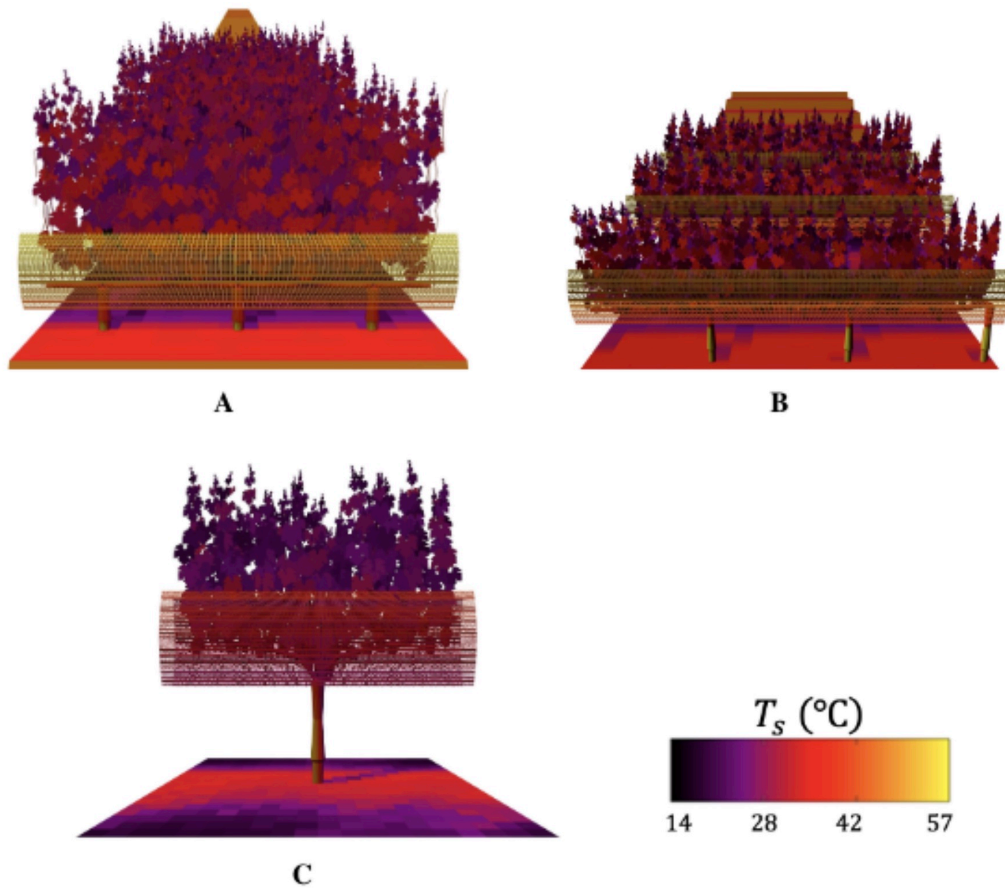


Figure 4.1. 3D Visualization of the surface temperature ($^{\circ}\text{C}$) in the east side of the vine at 10:00 on 19 Sept. 2019 for (A) Goblet, (B) Unilateral and (C) VSP trellises.

Table 4.2. Variables assessed in simulations that included vineyard designs with different shade cloth density, row spacing, row orientation, and topography.

Variable	Values
Shade cloth densities (%)	Control (no shade cloth), 30, 50, 70
Row spacing (m)	1, 2, 3
Row orientation	N-S, NE-SW, E-W, NW-SE
Topography	Flat terrain, and 30° slope facing: N, NE, E, SE, S, SW, W, NW

temperature results in the “simulation experiment”, we took the average temperature of five berries in each of five exterior clusters on both sides of the vine. The selected number of berries and clusters represent a typical experimental sampling strategy [e.g., 105]. For comparison

purposes, the total canopy and cluster daily light interception was calculated by integrating the light interception fluxes over the day. The daily light interception was calculated per vine area for the canopy and per berry surface area for the clusters. To compare the effect of shade cloth density on berry temperatures in the simulated vineyard designs, we used indices based on the duration of elevated temperature (cumulative hours berry temperature exceeds a threshold of 32°C and 35°C) and the intensity (growing degree hours, GDH, calculated based on the sum of daily thermal units above a base temperature of 10°C). The 35°C temperature threshold was chosen because it has been reported to correspond to the approximate onset of unfavorable effects of elevated temperature on grape composition [31].

Furthermore, to identify conditions that effectively balance berry temperature between opposing sides of the vine, we constructed a conditional inference tree with the variables listed in Table 4.2. The conditional inference tree was constructed using the “party” package of R statistical software [R Development Core Team 2013 39]. The conditional inference tree is a tree-based classification algorithm that performs binary recursive partitioning of data into groups containing observations with similar values [109]. Conditional inference trees are similar to decision trees, the main difference being that each node in the conditional inference trees uses a significance test of independence to select a predictor variable rather than selecting the predictor variable that maximizes the information measure [40]. In the conditional inference tree, predictor variables are circled and ranked and the ones at the top have the highest correlation with the response variable. The algorithm stops if the null hypothesis of independence is not rejected, however, for visualization purposes, the maximum depth of the decision tree was set to 4.

4.3 Results

4.3.1 Ambient berry microclimate

Figures 4.2A-C and 4.3A-C show meteorological measurements at the Napa experimental site for three days characterized by different air temperatures: a day with average ambient temperatures (19 Sept. 2019), the day with the highest ambient temperatures (25 Sept. 2019), and the day with the lowest ambient temperatures (30 Sept. 2019). While the ranges in air temperature were different across the sampling period, Goblet and Unilateral exhibited similar daily average and

range of ambient temperature.

The magnitude of the wind speed varied across the sampling period, but overall Unilateral tended to have greater wind speeds compared to Goblet (Figs. 4.2D-F and 4.3D-F). During the day, the wind in the fruiting zone tended to come from the east while at night the wind tended to come from the west for both trellis systems (Figs. 4.2G-H and 4.3G-H). Since the row orientation of Goblet and Unilateral was N-S and the vines were on an east-facing slope, the wind coming from the east tended to be of greater magnitude.

For both Goblet and Unilateral, the relative humidity significantly decreased on 25 Sept. 2019, likely due to the increase in air temperature. Overall, during the sampling period, Unilateral tended to be slightly less humid compared to Goblet. This can be explained by the wider row spacing in Unilateral that enhanced mixing of the canopy air compared to Goblet (Figs. 4.4J-L and 4.4J-L).

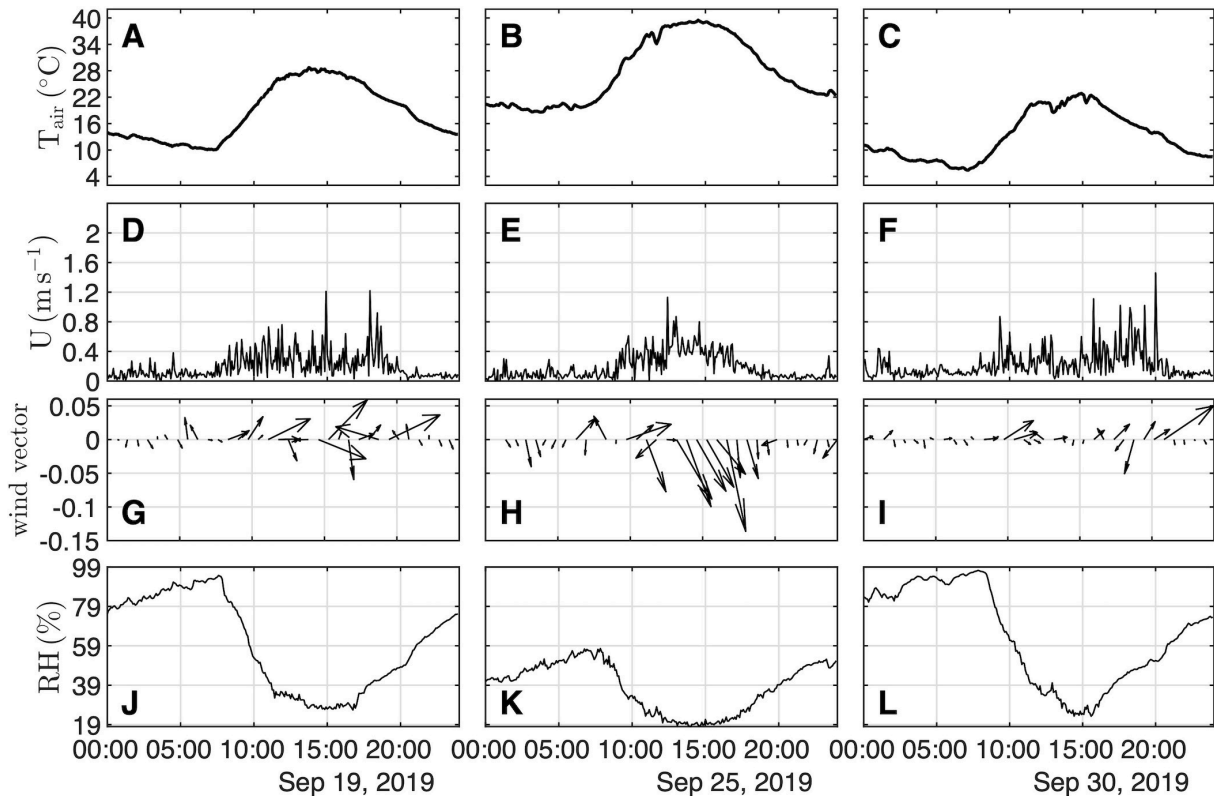


Figure 4.2. Meteorological data for Goblet vineyard. Daily course of measured air temperature (A,B,C), wind speed (D,E,F), wind direction (G,H,I) and relative humidity (J,K,L) data during three different days (columns). Data is plotted every 5 min., except for wind direction which was plotted every 40 min.

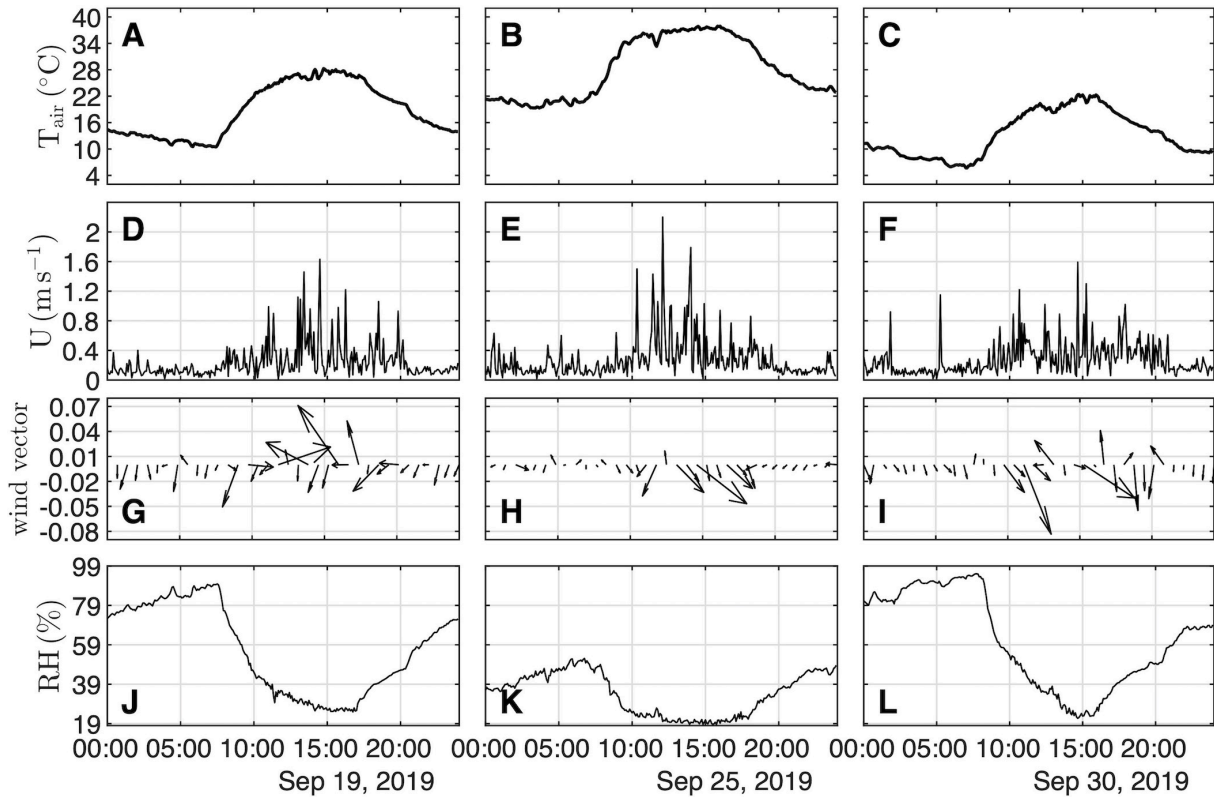


Figure 4.3. Same as Fig. 4.2 except for Unilateral vineyard.

4.3.2 Effect of shade cloth on grape berry temperature

During the sampling period, average daily maximum temperatures of the west-facing berries under the shade cloths were 1.6°C and 2.7°C higher than the daily maximum air temperature in Goblet and Unilateral, respectively. The control west-facing berries with no shade cloth were up to 8.2°C and 5.9°C above the daily maximum air temperature in Goblet and Unilateral, respectively (Table 4.3). The relative reduction in maximum berry temperatures due to the shade cloth in Goblet and Unilateral was consistent across the sampling period, which included a wide range of ambient air temperatures (Fig. 4.4). Pulp temperatures of more than 40°C were measured on 25 Sept. 2019 for unshaded berries in both trellis systems. For both Goblet and Unilateral, the berry temperature under the shade cloth was close to the air temperature in the morning, while air temperature differences between berries under the shade cloths increased in the afternoon. The peak in measured elevated temperatures happened at different times in Goblet (~ 15:00) and Unilateral (~ 16:00), primarily due to the influence of the ratio between plant height and row spacing on berry exposure. In the evening, under low-light conditions, the

berry temperatures were similar to the air temperatures, while at night, radiative cooling likely caused the pulp temperature to fall below the air temperatures. Under low light and at night, the temperature differences among treatments were small (Table 4.3).

Table 4.3. Characterization of differences in average microclimate between treatments for the entire experimental period spanning 19 Sep to 10 Oct 2019: Daily average of berry temperature; average of daily maximum and minimum temperature of berries in the west side of the vine; average of the daily maximum and minimum temperature difference between the berries and air temperature.

Vineyard system	T_{berry} ($^{\circ}C$)			$T_{berry} - T_{air}$ ($^{\circ}C$)	
	Avg.	Max. avg.	Min. avg.	Max. avg.	Min. avg.
Goblet-Shade cloth	18.6	31.7	9.6	1.6	-0.8
Goblet-Control	19.0	38.3	9.5	8.2	-0.9
Unilateral-Shade cloth	19.4	32.4	10.2	2.7	-0.7
Unilateral-Control	19.4	35.6	10.0	5.9	-0.9

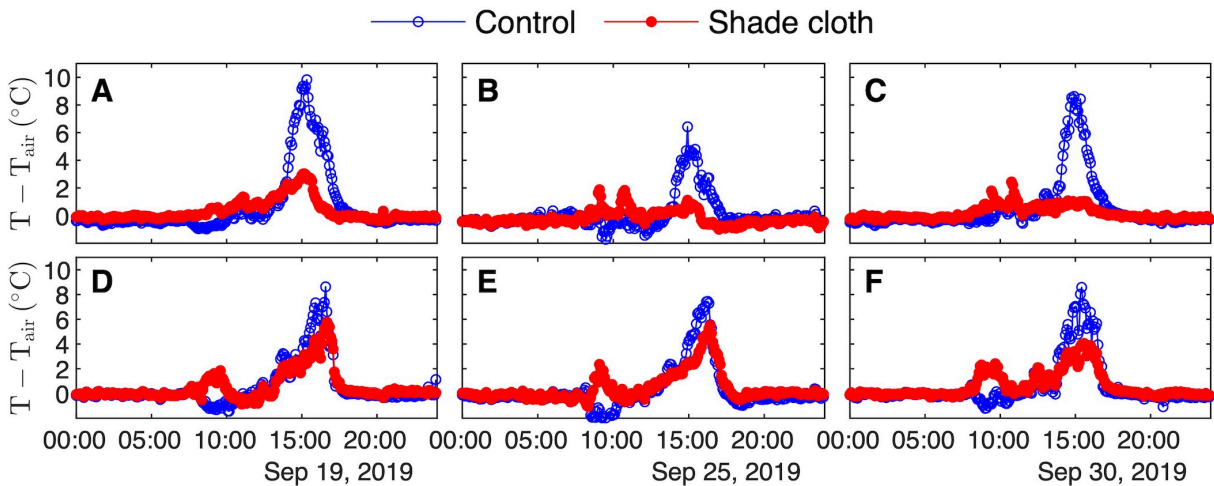


Figure 4.4. Measured berry temperature increase over air temperature for Goblet (A,B,C) and Unilateral (D,E,F) vineyard. Daily course of average measured grape berry temperature in the west side of the vine for three days with different ranges in air temperature. Data plotted every 5 min.

4.3.3 Model validation

The model was validated by using the experimental measurements to determine whether the modeled berry temperatures appropriately responded to the shade cloth relative to the control (Fig. 4.5). The model reproduced the magnitude of the berry temperature increase over air temperature reasonably well for both Goblet and Unilateral. The largest source of error appeared

to be due to the transition period when berry sun exposure began, where the time of the simulated maximum temperature increase tended to happen earlier than that of the measurement (Fig. 4.5). This mismatch could be due to slight inaccuracies in determining the position of each berry and leaf. Comparisons of the 5 min. daily course of simulated and measured berry temperature showed that the overall performance was excellent, with R^2 of 0.963 for Goblet and 0.978 for Unilateral, IA of 0.990 for Goblet and 0.995 for Unilateral, and NRMSE of 4.79% for Goblet and 3.60% for Unilateral (Table 4.4).

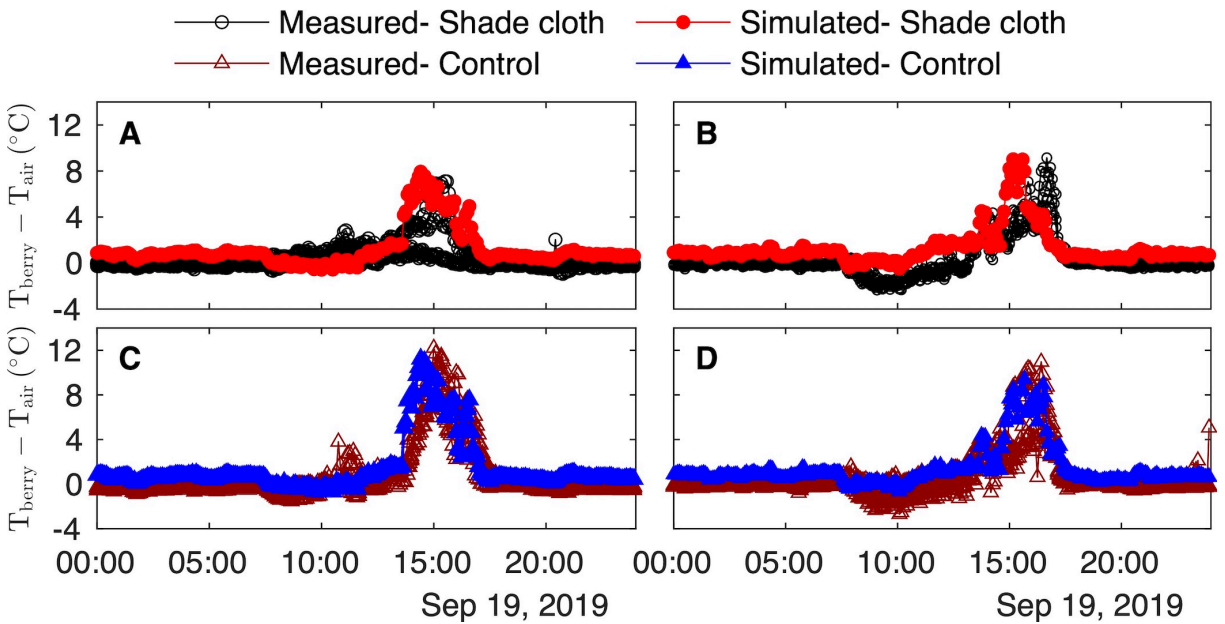


Figure 4.5. Daily course of measured and simulated grape berry temperature increase over air temperature for berries under 40% shade cloths in the west side of the vine for (A) Goblet and (B) Unilateral, and of exposed berries with no shade cloth (control) for (C) Goblet and (D) Unilateral. Each black or brown line corresponds to a different berry measurement.

Table 4.4. Model performance metrics for Goblet and Unilateral comparing modeled and measured berry temperature under shade cloth in the west side of the vine for three days with different ranges in air temperature. A graphical comparison of the data on 19 Sept 2019 only is shown in Fig. 4.5.

Vineyard system	R^2	IA	NRMSE
Goblet	0.9628	0.9903	0.0479
Unilateral	0.9783	0.9947	0.0360

4.3.4 Simulation study

4.3.4.1 Flat terrain with no shade cloth

Figures 4.7, 4.8, and 4.6 summarize the results of the simulation experiment in which the effect of different row orientations, row spacing, and slope aspects on berry temperature were evaluated. Orienting vineyards N-S on a flat terrain allowed for uniform canopy and cluster exposure to solar radiation, since radiation is approximately symmetric about the N-S axis (Fig. S1). However, the berry temperature on the west side of the vine significantly increased in the afternoon compared to the east side because hysteresis in air temperature causes asymmetry about solar noon. On average, berry temperature on the west side of the vines was greater than 35°C for about 1-2.5 hours longer than the east side (depending on row spacing) (Table S1). Interestingly, although there was temporal asymmetry due to air temperature and temperature extremes, the net daily accumulation of berry growing degree hours was virtually identical between each side of the vine (Fig. 4.8).

On flat terrain, rows oriented NW-SE increased light interception and fruit overexposure in the afternoon and E-W reduced light interception and fruit overexposure in the afternoon (Figs. S1 and S2). The high exposure to direct sunlight in NW-SE oriented rows resulted in simulated berry temperatures up to 7.8°C higher on the SE side compared to the NW side (Figs. S3 and S4). Compared to rows oriented NE-SW, rows oriented NW-SE had an additional 3 hours of canopy light interception above 200 W m⁻² between 14:00 and 17:00 and berry temperatures greater than 35°C for 2 additional hours (Table S1).

Narrow spacing affected berry temperature by potentially reducing the duration of berry exposure due to shading from neighboring vines. Compared to the wider row spacing, the berries in narrow row spacing in N-S rows on a flat terrain intercepted up to 36% less sunlight (Fig. 4.6) and reduced elevated berry temperatures on the west-facing side (Table S1). In the E-W row orientation, the number of hours with berry temperatures greater than 35°C was also reduced with the narrow row spacing due to the shading from neighboring vines (Fig. 4.6 and Table S1). The most balanced sunlight exposure and growing degree hours between each side of the vine was achieved in the N-S row orientation, although notable hourly berry temperature differences were present for both narrow and wider row spacing. For example, west-facing berries exceeded

35°C for about 1 hour for the narrower row spacing and about 3.6 hours for the wider row spacing (whereas east-facing berries did not).

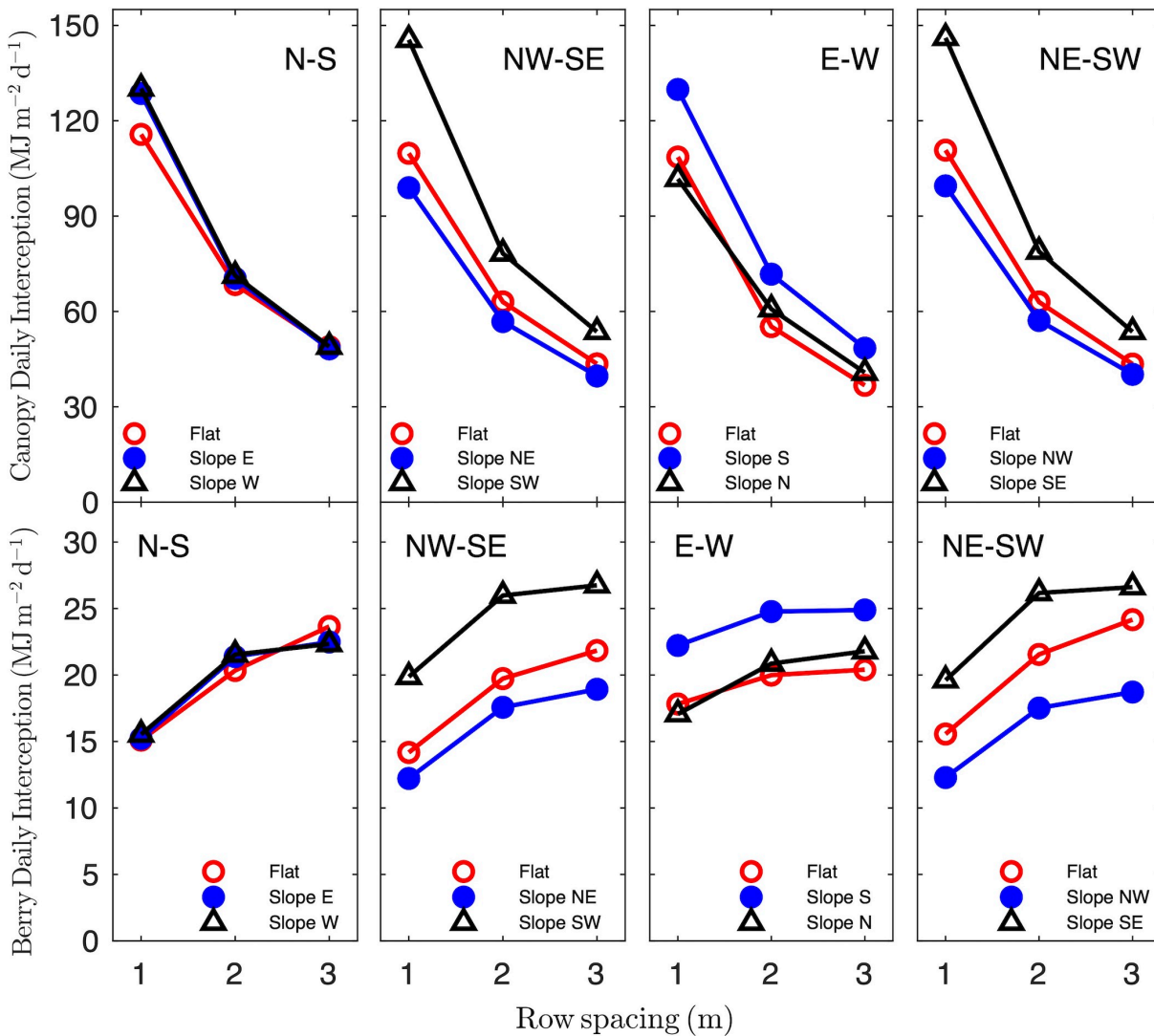


Figure 4.6. Simulated total canopy and berry daily light interception (PAR+NIR) in the VSP trellis system with different row spacing (1 m, 2 m, and 3 m), row orientation (N-S, NE-SW, E-W, NW-SE), and topography (flat and sloped vineyards facing N, NE, E, SE, S, SW, W, and NW). Each point represents a single value for each vineyard design.

4.3.4.2 Sloped terrain with no shade cloth

Adding a 30° slope to each of the simulations had a considerable effect on berry temperature, and could significantly change its behavior relative to flat terrain. Furthermore, the conditional inference tree results showed that the slope aspect had the strongest effect on the imbalance in temperature between different sides of the vines (Fig. 4.9). In general, sloping to the south or

west tended to increase light interception, berry temperatures, and berry temperature imbalance relative to north- or east-facing slopes. For example, compared to the vines oriented NW-SE on flat terrain, the vines oriented NW-SE on a southwest-facing slope increased the number of hours of $T_{berry} > 35^{\circ}\text{C}$ up to 1.25 h on the southwest side (Fig. 4.7; Table S1). In contrast, situating these vines on a northeast-facing slope decreased the number of hours of $T_{berry} > 35^{\circ}\text{C}$ up to 2 h on the northeast side (Table S1).

For N-S oriented vines, slope had a minimal effect on daily integrated quantities such as daily light interception and berry growing degree hours, but did significantly affect short-term increases in berry temperature. N-S rows on west-facing slope increased the number of hours of $T_{berry} > 35^{\circ}\text{C}$ for west-facing berries by over 2 h relative to flat terrain. However, these effects tended to be averaged out in N-S rows to maintain good symmetry over a daily period.

The NE-SW oriented vines maintained good protection from berry temperature spikes and relatively good symmetry between sides of the vine as slope was added. There were some non-intuitive effects of slope aspect that should be highlighted. For NE-SW oriented rows, the northwest-facing slope had more hours with $T_{berry} > 35^{\circ}\text{C}$ than for the southeast-facing slope, but the opposite was true for daily-integrated quantities. This illustrates that exposure due to partially western-facing slope was more effective at generating temperature extremes than a partially southern-facing slope, but the opposite is true for daily-integrated quantities.

4.3.4.3 Effect of shade cloth

The efficacy of shade cloth in reducing or equalizing berry temperature strongly depended on the row orientation and slope aspect (Fig. 4.7). In general, adding shade cloth to the side of the row with partial or full south or west exposure tended to produce a significant reduction in berry temperatures and heat accumulation, as is to be intuitively expected. Adding shade cloth to sides of the vine with partial or full north or east exposure typically had weaker effect, and could actually increase temperatures on north-facing berries due to trapping of energy transmitted from the south.

While avoiding fruit overexposure reduces fruit temperature, in some cases, controlling the amount of direct radiation received by berries with shade cloths consistently maintained the berry temperature below 35°C . For instance, in vines oriented N-S and NW-SE with wider rows, 50%

and 70% shade cloth significantly reduced the time berry temperature was above 35°C late in the afternoon in west facing berries (Table S1).

It was possible in several cases to achieve near-equal heat accumulation between sides of the vine while also minimizing berry temperature extremes by applying shade cloth to one side of the vine. For example, applying 70% shade cloth to the SE side of the vine in NE-SW oriented rows on flat terrain effectively balanced heat accumulation (Fig. 4.8) while also eliminating berry temperatures above 35°C. E-W oriented rows always had high imbalance in heat accumulation regardless of shade cloth density or slope aspect.

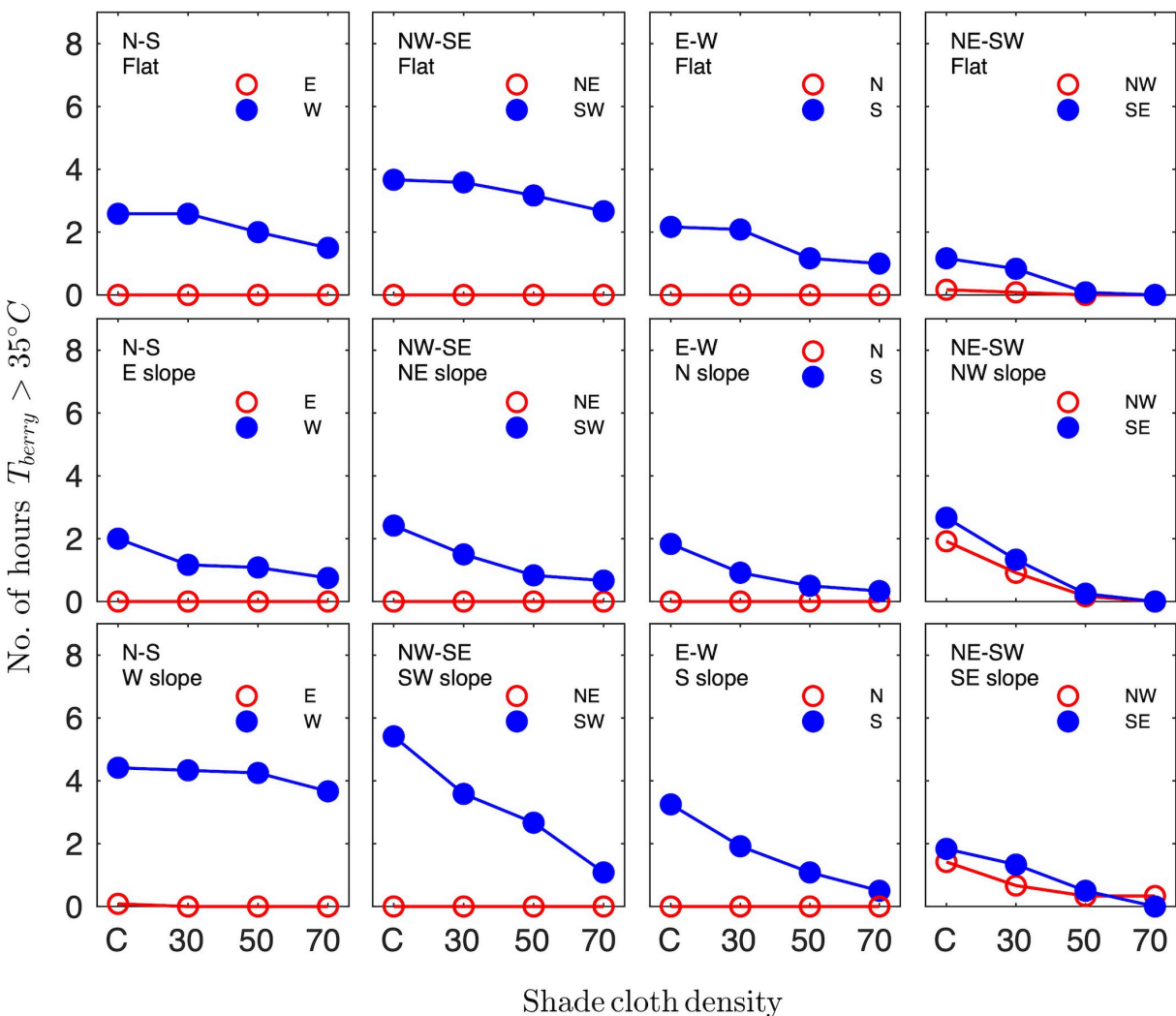


Figure 4.7. Number of hours with berry temperatures >35°C in the VSP trellis system with 3 m row spacing with different shade cloth densities (control, 30%, 50% and 70%), row orientation (N-S, NE-SW, E-W, NW-SE) and topography (flat and sloped vineyards facing N, NE, E, SE, S, SW, W, and NW). Maximum air temperature was 31.9 °C.

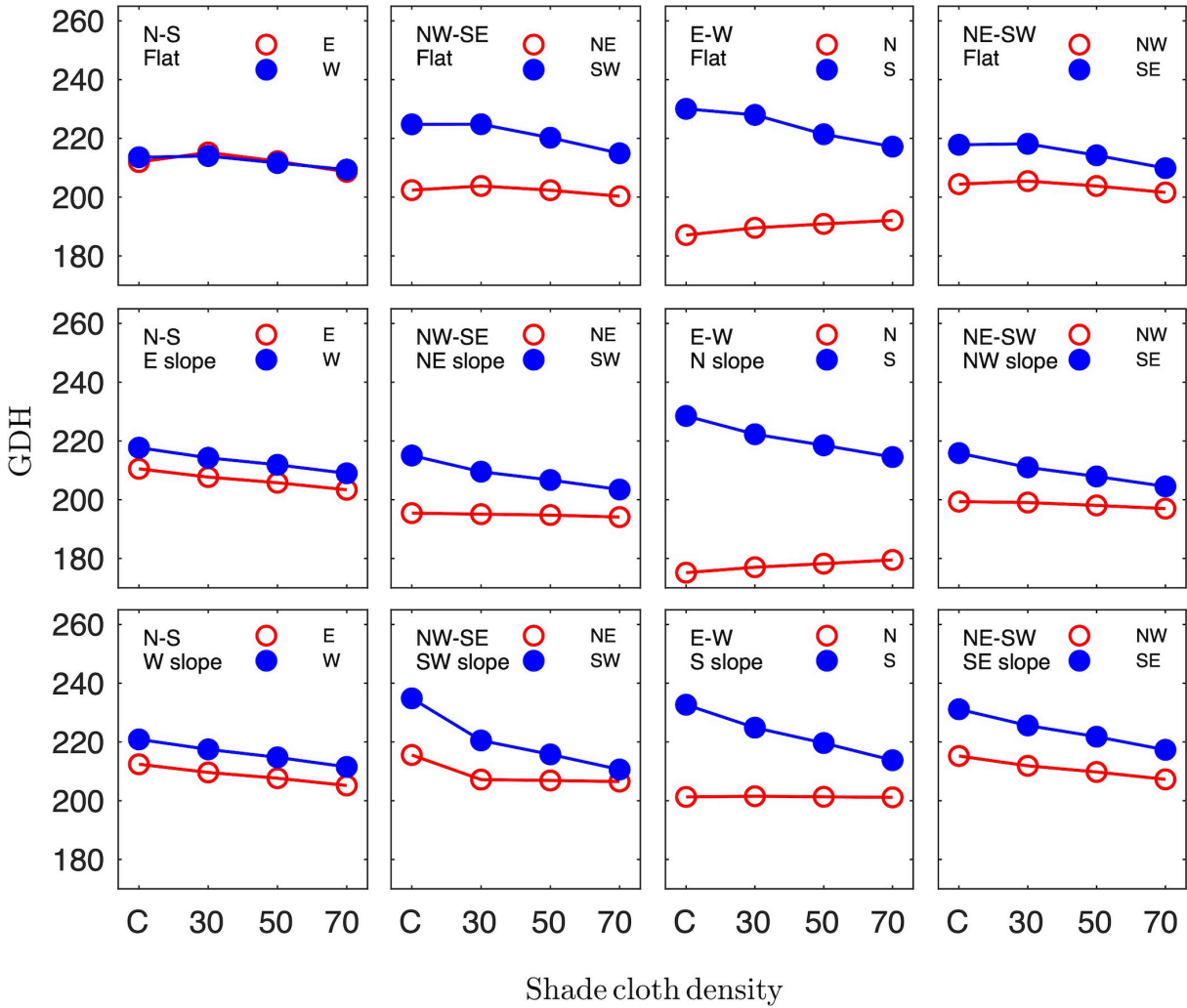


Figure 4.8. Growing degree hours from 7:00 to 19:00 hours in the VSP trellis system with 3 m row spacing with different shade cloth densities (control, 30%, 50% and 70%), row orientation (N-S, NE-SW, E-W, NW-SE) and topography (flat and sloped vineyards facing N, NE, E, SE, S, SW, W, and NW).

4.4 Discussion

4.4.1 Model performance

Comparisons between measured and modeled berry temperature indicated that the model is able to reproduce general spatial and temporal patterns of temperature, and can capture the additional effects of shade cloth. This is in addition to prior validation efforts demonstrating excellent model performance in the absence of shade cloth [58]. Experimental validation of 3D, spatially explicit models is complicated by high sensitivity of localized model predictions to specifics of the canopy geometry. However, overall close agreement between measurements and

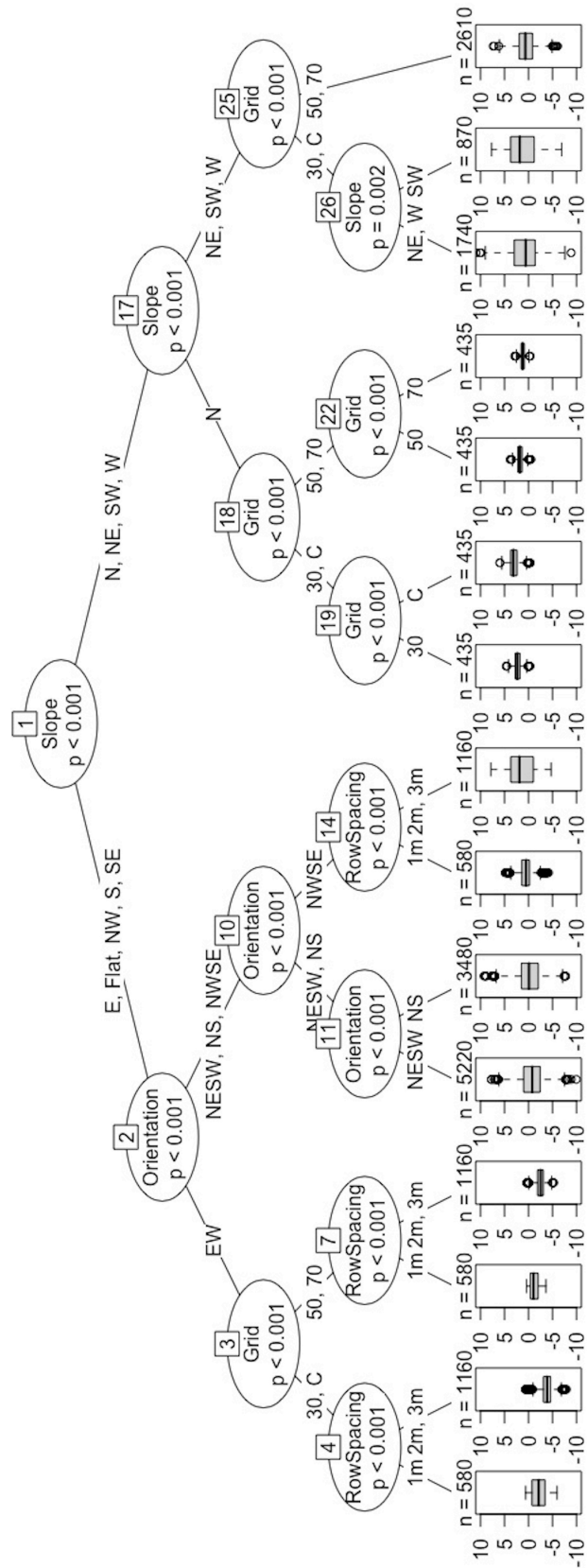


Figure 4.9. Conditional inference tree for berry temperature difference between both sides of the vine from 7:00 to 19:00 hours. Categories for each split are shown below the variable name box. For instance, for node 1 (Slope) the split was into berry temperature data in the Flat, E, NW, S and SE facing slopes vs those in the N, NE, SW and W slopes. The p-value in the nodes denotes the significance level used for a split to take place. Box plots include the medians (solid black line), upper and lower quartiles (grey box) and 1.5x the inner quartiles (error bars). Sample sizes at each terminal node show number of values in that boxplot. The complete data set is plotted in Fig. S1.

model predictions in an average sense suggested that the model is robust to variation in vineyard architecture, topography, and the addition of shade cloth.

For model validation purposes, local measurements of ambient berry microclimate were used to drive simulations. Effects of large-scale microclimatic variation was not included within this model, which could affect the predictive ability of the model as large-scale features are varied such as topography [23, 108]. Variation in topography could induce changes in wind speed or sensible heating of the air independent of vineyard structure, which was not represented in the model. However, radiation exposure is the primary driver of berry temperature deviations from ambient, and other microclimatic effects due to large-scale topography are likely to be secondary and establish the baseline temperature state similar to changing weather.

4.4.2 Vineyard design on flat terrain

The results of this study for flat terrain largely confirmed conclusions of previous work regarding design of vertically-trained vineyards for berry temperature management, but revealed some additional trade-offs for consideration. Similar to previous findings, the NE-SW row orientation (northern hemisphere) on flat terrain is likely to be the best compromise between canopy and berry light interception, reduction of elevated berry temperatures, and balancing of heating between opposing sides of the vine, which was also argued by Tarara et al. [113]. A trade-off of this vineyard design is that it modestly reduces overall vine light interception relative to the more common N-S row orientation. Additionally, there are still significant differences in berry heat accumulation and exposure between sides of the vine in a NE-SW row orientation. However, for VSP vineyards on flat terrain with no shade cloth, the NE-SW row orientation appeared to be the best overall at equalizing exposure between sides of the vine and reducing berry temperature extremes.

For N-S oriented rows on flat terrain, previously well-documented imbalances in berry temperature between sides of the vine were also observed [43]. It is intuitive to understand that the higher air temperatures and lower humidity that occur in the afternoon, when combined with berry exposure to the west sun, creates higher berry temperature than in the morning when ambient conditions are cooler. There is strong evidence that the accumulation of berry anthocyanin is a function of temperature and light Buttrose et al. [13], Downey et al. [26], Hunter

et al. [43], Spayd et al. [105] and that the temperature difference between sides of the vine can create imbalance in the mass of the berries, as well as on titratable acidity, pH and phenolic compounds [8, 25, 43, 64, 105, 114]. If row access by mechanical equipment is not a concern, decreasing row spacing could offer some protection against berry temperature extremes, although this is not effective at balancing opposing sides of the vine. Interestingly, results indicated that although there was high berry temperature imbalance localized to the afternoon, daily integrated metrics such as daily growing degree hours and daily berry light interception were almost perfectly balanced between sides of the vine in N-S rows. However, it is possible this was coincidental, or that abnormal diurnal temperature fluctuations such as that caused by clouds could break this symmetry.

The NW-SE row orientation on flat terrain resulted in the most elevated berry temperatures. Berries on the southwest side of the vine spent nearly 4 hours above 35°C, and shade cloth did little to mitigate these temperatures because the sun was nearly perpendicular to the shade cloth at the hottest time of day.

Most previous work examining the effects of shade cloth does so for a single site and vineyard design [e.g., 16, 64, 78, 88], but results indicated that details of topography and vineyard architecture can have a significant effect on shade cloth performance. In N-S oriented rows on flat terrain, smaller row spacing relative to canopy height significantly reduced the hours of berry exposure to direct sunlight in the east and west side of the vine due to shading from neighboring vines. There are negative trade-offs to consider when reducing row spacing. While berry temperatures were reduced in vineyards with narrower row spacing, grape and wine quality could decline at some point when row spacing is reduced due to excessive berry shading [42]. Mechanical equipment access may be impeded below some threshold row spacing. Full-size equipment generally requires a minimum row spacing of around 3 m for single canopy systems [53]. Thus, depending on the availability of equipment for mechanization and the vineyard design, shade cloth appeared to be a viable option for mitigation of berry overexposure in widely spaced rows.

This study considered only VSP trellis systems at a single fruiting height, which resulted in the potential for high fruit exposure. Other trellis systems that reduce berry exposure are

becoming more popular in warm climate regions [37, 71]. However, since it is usually undesirable to completely shade clusters because of its negative effect on berry quality, it is still necessary to understand the interaction effects between canopy architecture and berry exposure. While the results of this work can provide some initial guidance in this regard, future work analyzing different trellis types is still needed. Because of the spatially explicit nature of the model presented in this work, it is likely that only minimal adjustments to the model are needed to accommodate different trellis types.

4.4.3 Vineyard design on sloped terrain

For most cases, it was observed that planting on a slope fully or partially facing south or west increased berry exposure and elevated temperatures relative to north- or east-facing slopes or flat terrain (northern hemisphere). Furthermore, a west-facing slope tended to increase temperatures more relative to a south-facing slope. This is intuitive given that the sun spends most of the day to the south, and the sun is to the west during the warmest time of a typical day.

In several cases, slope had the negative effect of increasing the imbalance in heat accumulation between sides of the vine. This was especially true for the E-W row orientation, which caused very large imbalance that could not be effectively mitigated by shade cloth. For N-S and NE-SW oriented rows, the impact of slope on the berry temperature metrics was generally small.

Shade cloth was able to mitigate the negative effects of slope in many cases. Applying 70% shade cloth in the sloped cases achieved excellent balance in heat accumulation between sides of the vine with N-S, NW-SE, and NE-SW orientations. The 70% shade cloth was also able to reduce the time above 35°C to 1 hour or lower in all but the case with N-S rows on a west-facing slope, and NW-SE rows on flat terrain.

4.5 Conclusion

The 3D model developed in this work was able to represent the effects of shade cloth on berry temperature and, thus, provided a viable tool for quantification of interactions between hypothetical vineyard designs and shade cloth on metrics related to berry temperature. The tool could also be effective in performing model-based vineyard designs in which the optimal design is determined under a set of constraints such as slope aspect or minimum row spacing. Although

this means that the optimal design is likely to be case-specific, the tool was used to examine general trade-offs in various designs, which are summarized below.

While the N-S row orientation on flat terrain was effective in balancing daily berry light interception and heat accumulation between opposing sides of the vine, it is also susceptible to temporally localized berry temperature spikes on the west side that could be managed by applying dense shade cloth. For cases with no shade cloth, the NE-SW orientation was likely the best compromise between berry temperature reduction and balance between opposing sides of the vine, although it still had significant imbalance in heat accumulation and extreme berry temperatures. Addition of sloped terrain tended to exacerbate berry temperature extremes and imbalance when the slope was facing south or west, which in several cases could not be well-managed using shade cloth. The shade cloths were more effective in reducing berry temperatures in cases with greater row spacing relative to plant height because adjacent rows could potentially provide their own shade.

The simulation experiment in this work used the new modeling tool to examine general trends in berry temperature and light interception as vineyard architecture and shade cloth density were varied. Because of the challenge in concisely presenting results of a very large number of simulated cases, results are limited to a limited number of architectures, a narrow time period, a single latitude, and site-specific weather conditions. As such, care should be taken in direct application of the simulated values for vineyard design, as they may change for a certain site or design. However, the model itself provides a tool that could be used to provide quantitative guidance for vineyard design or management at a specific site.

Acknowledgements

Financial support of this work was provided by the American Vineyard Foundation, USDA National Institute of Food and Agriculture Hatch project 1013396, and a graduate stipend was provided to María A. Ponce de León by the American Society for Enology and Viticulture. The authors wish to acknowledge Harlan Estate for their gracious collaborative and financial support of the Napa field site experiments.

Chapter 5

Conclusion

Together, Chapters 2-4 motivated and carried out the development of a modeling tool that can be used to identify strategies for mitigating the effect of excess sunlight and unfavorable temperatures on grape berries. The tool was then used to study how vineyard design and management strategies related to berry shading interacted to influence berry temperature and light interception.

Chapter 2 evaluated widely used assumptions when modeling solar radiation interception in plant canopies, namely assumptions of vegetation homogeneity and isotropy. Because of their simple, tractable form, one-dimensional (1D) turbid medium models of radiation interception that assume homogeneity or isotropy are used across a broad range of disciplines. However, it is relatively well-known that with varying levels of vegetation sparseness and preferential leaf orientations (such as that characteristic of grapevines), the implicit assumptions of vegetation homogeneity and isotropy in this simple class of 1D models are frequently violated. Yet it is not well-known how this assumption violation translates into model errors in a given situation. Results of this work provided quantitative guidance for when a simple 1D model can be appropriately used to estimate light interception. For complex canopies like grapevines, the results highlighted the need to use a 3D radiation model because these models can represent the vertical and horizontal variability in the canopy and their effect on light interception accurately.

Chapter 3 developed and validated a three-dimensional (3D) model for grape berry temperature to understand whether the effect of excess sunlight on grape production can be mitigated by designing and managing vineyards in a way that effectively creates a favorable berry microcli-

mate. For the first time, a 3D vine-resolving structural model was coupled with a high-resolution energy balance model for providing accurate and spatially-explicit predictions of berry temperature dynamics. The developed 3D model accurately simulated the spatial and temporal temperature fluctuations of grape berries in vineyards with different climate, topographies, and trellises.

Chapter 4 explored different scenarios to mitigate the effect of excess sunlight and temperature. Previously developed models for grape temperature have not been used to evaluate the interacting effects of different management strategies to reduce grape berry temperature. This chapter measured the effect of vineyard design and shade cloth on berry temperature and quantified trade-offs between the different management strategies to maintain optimal berry heat balance and reduce the elevated berry temperatures. Altering light interception by using shade cloths affected the reduction of elevated berry temperatures depending on the vineyard design. A great effect of the shade cloths was found in clusters exposed to direct sunlight for prolonged hours, which tended to be in cases where the vines had greater plant spacing relative to plant height, and where rows were oriented NS and NW-SE in either a flat or sloped terrain facing W or SW, respectively. While changing the row orientation to NE-SW can be an effective long-term practice to reduce the effect of elevated temperature, for cases where changing the vineyard design is not possible, the shade cloths presented an alternative to reduce unfavorable berry temperatures in many cases. The variables that determine cluster exposure to direct sunlight, such as topography, trellis systems, row orientation, and shade cloths should be considered carefully to develop management strategies for optimizing grape quality.

The primary novel outcome of this dissertation that advances the current state-of-the-art is the development of a new tool that could be used to address the role of agricultural management in climate adaptation. Technologies that increase the rate of adaptation to climate change are of great value to farmers, the wine industry, policymakers, and the scientific community. In future studies, the 3D model could be used to evaluate the effect of vineyard designs on berry temperature under changing environmental conditions, to assess the effect of different irrigation strategies on grape production, and to relate the spatial and temporal variability in berry temperature to variations in berry quality traits.

Appendix A

Appendix

A.1 Berry thermal time constant

A laboratory experiment was conducted to determine the approximate thermal time constant of grape berries, and whether the energy balance formulation and parameters used in the 3D model provided a similar time constant. In the lab, thermocouples were placed just under the skin and in the center of an isolated grape berry with approximate radius of 6 mm. The berry initially at a nearly uniform temperature T_0 of 23.85°C was heated at time t_0 by turning on a heat lamp located above the berry. The temperature of both thermocouples were sampled every 5 s, yielding the temperature response curve shown in Fig. [A.1a](#).

The following exponential function was fitted to the temperature responses:

$$T(t) = T_0 + (T_{final} - T_0) \left(1 - \exp\left(-\frac{t - t_0}{\tau}\right) \right), \quad (\text{A.1})$$

where $T(t)$ is the berry skin or pulp temperature at time t , T_{final} is the steady-state temperature, and τ is the time constant which is the time it takes to reach 63% of the steady-state temperature.

In order to replicate the laboratory conditions in the model, an isolated berry was placed in the domain. All ambient environmental conditions were set to constant values including wind speed $U = 0$. The modeled berry temperature was allowed to equilibrate to these constant environmental conditions, and subsequently at time $t_0 = 4.5$ min the solar flux was instantaneously increased to yield an exponential temperature response as shown in Fig. [A.1a](#). Equation [A.1](#) was fitted to the modeled temperature response curves, which yielded a time constant value of 16.1 min (Table

A.1). This value was very similar to the time constants determined from experimental data of 15.4 min for the skin temperature and 17.5 min for the center temperature. It was thus concluded that the modeled dynamical response of berry temperature was reasonable.

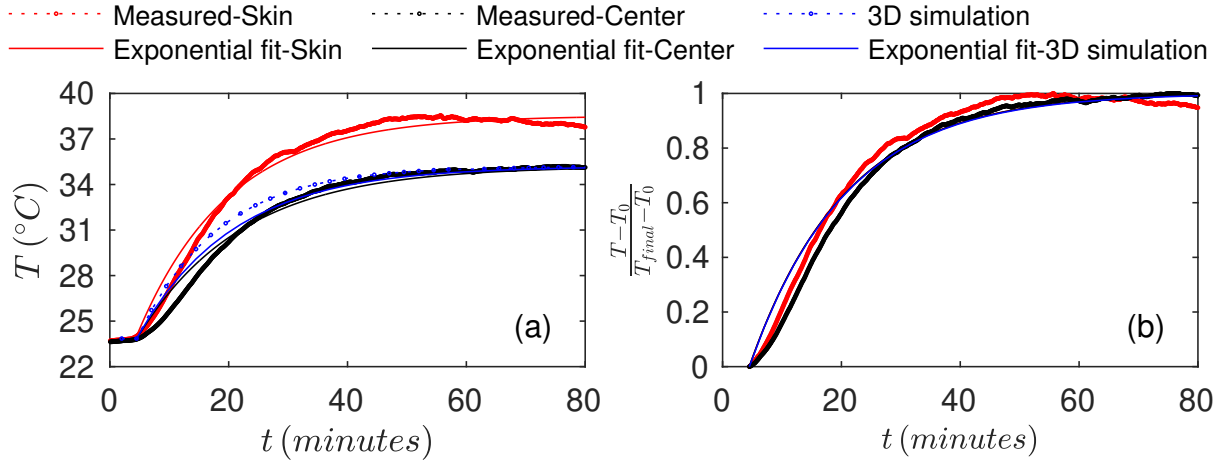


Figure A.1. (a) Measured, 3D simulated and fitted (Eq. **A.1**) temperature response of an isolated berry. (b) Normalized temperature response for data shown in (a).

Table A.1. Time constant τ determined from fitting of Eq. **A.1** to measured and simulated data, and associated error metrics.

	τ (min)	R^2	IA	NRMSE
Measured - Skin	15.4	0.9732	0.9928	0.0414
Measured - Center	17.5	0.9811	0.9947	0.0376
3D simulation	16.1	0.9459	0.9845	0.0669

REFERENCES

- [1] Austin, C.N., Grove, G.G., Meyers, J.M., Wilcox, W.F., 2011. Powdery mildew severity as a function of canopy density: Associated impacts on sunlight penetration and spray coverage. *American journal of enology and viticulture* 62, 23–31.
- [2] Bailey, B.N., 2018. A reverse ray-tracing method for modelling the net radiative flux in leaf-resolving plant canopy simulations. *Ecol. Model.* 368, 233–245.
- [3] Bailey, B.N., 2019. Helios: A scalable 3D plant and environmental biophysical modeling framework. *Front. Plant Sci.* 10, 1185.
- [4] Bailey, B.N., Mahaffee, W.F., 2017a. Rapid, high-resolution measurement of leaf area and leaf orientation using terrestrial LiDAR scanning data. *Meas. Sci. Technol.* 28, 064006.
- [5] Bailey, B.N., Mahaffee, W.F., 2017b. Rapid measurement of the three-dimensional distribution of leaf orientation and the leaf angle probability density function using terrestrial lidar scanning. *Remote Sens. Environ.* 193, 63–76.
- [6] Bailey, B.N., Overby, M., Willemsen, P., Pardyjak, E.R., Mahaffee, W.F., Stoll, R., 2014. A scalable plant-resolving radiative transfer model based on optimized GPU ray tracing. *Agric. For. Meteorol.* 198-199, 192–208.
- [7] Bergman, T.L., Incropera, F.P., DeWitt, D.P., Lavine, A.S., 2011. *Fundamentals of heat and mass transfer.* John Wiley & Sons.
- [8] Bergqvist, J., Dokoozlian, N., Ebisuda, N., 2001. Sunlight exposure and temperature effects on berry growth and composition of Cabernet Sauvignon and Grenache in the Central San Joaquin Valley of California. *Am. J. Enol. Vitic.* 52, 1–7.
- [9] Bindi, M., Miglietta, F., Gozzini, B., Orlandini, S., Seghi, L., 1997. A simple model for simulation of growth and development in grapevine (*vitis vinifera*L.). ii. model validation. *VITIS-GEILWEILERHOF-* 36, 73–76.

- [10] Boote, K., Pickering, N., 1994. Modeling photosynthesis of row crop canopies. *HortScience* 29, 1423–1434.
- [11] Brillante, L., Belfiore, N., Gaiotti, F., Lovat, L., Sansone, L., Poni, S., Tomasi, D., 2016. Comparing kaolin and pinolene to improve sustainable grapevine production during drought. *PLoS One* 11, e0156631.
- [12] Buckley, T.N., Turnbull, T.L., Adams, M.A., 2012. Simple models for stomatal conductance derived from a process model: cross-validation against sap flux data. *Plant Cell Environ.* 35, 1647–1662.
- [13] Buttrose, M., Hale, C., Kliewer, W.M., 1971. Effect of temperature on the composition of 'Cabernet Sauvignon' berries. *Am. J. Enol. Vitic.* 22, 71–75.
- [14] Campbell, G.S., Norman, J., 2012. An introduction to environmental biophysics. Springer Science & Business Media.
- [15] Caravia, L., Pagay, V., Collins, C., Tyerman, S., 2017. Application of sprinkler cooling within the bunch zone during ripening of Cabernet Sauvignon berries to reduce the impact of high temperature. *Aust. J. Grape Wine R.* 23, 48–57.
- [16] Cartechini, A., Palliotti, A., 1995. Effect of shading on vine morphology and productivity and leaf gas exchange characteristics in grapevines in the field. *Am. J. Enol. Vitic.* 46, 227–234.
- [17] Chen, Q., Baldocchi, D., Gong, P., Dawson, T., 2008. Modeling radiation and photosynthesis of a heterogeneous savanna woodland landscape with a hierarchy of model complexities. *Agric. For. Meteorol.* 148, 1005 – 1020.
- [18] Choudhury, B., Idso, S., Reginato, R., 1987. Analysis of an empirical model for soil heat flux under a growing wheat crop for estimating evaporation by an infrared-temperature based energy balance equation. *Agric. For. Meteorol.* 39, 283–297.
- [19] Cohen, S.D., Tarara, J.M., Kennedy, J.A., 2008. Assessing the impact of temperature on grape phenolic metabolism. *Anal. Chim. Acta* 621, 57–67.

- [20] Cola, G., Failla, O., Mariani, L., 2009a. Berrytone—a simulation model for the daily course of grape berry temperature. *Agricultural and forest meteorology* 149, 1215–1228.
- [21] Cola, G., Failla, O., Mariani, L., 2009b. Berrytone—A simulation model for the daily course of grape berry temperature. *Agric. For. Meteorol.* 149, 1215–1228.
- [22] Connor, D.J., 2006. Towards optimal designs for hedgerow olive orchards. *Aust. J. Agric. Res.* 57, 1067–1072.
- [23] De Rességuier, L., Mary, S., Le Roux, R., Petitjean, T., Quénot, H., van Leeuwen, C., 2020. Temperature variability at local scale in the bordeaux area. relations with environmental factors and impact on vine phenology. *Front. Plant Sci.* 11, 515.
- [24] Dokoozlian, N., 2009. Integrated canopy management: a twenty year evolution in california. *Recent advances in grapevine canopy management* , 43–52.
- [25] Downey, M.O., Dokoozlian, N.K., Krstic, M.P., 2006. Cultural practice and environmental impacts on the flavonoid composition of grapes and wine: a review of recent research. *Am. J. Enol. Vitic.* 57, 257–268.
- [26] Downey, M.O., Harvey, J.S., Robinson, S.P., 2004. The effect of bunch shading on berry development and flavonoid accumulation in shiraz grapes. *Aust. J. Grape Wine R.* 10, 55–73.
- [27] Due, G., Morris, M., Pattison, S., Coombe, B., 1993. Modelling grapevine phenology against weather: Considerations based on a large data set. *Agric. For. Meteorol.* 65, 91–106.
- [28] Esprey, L., Sands, P., Smith, C., 2004. Understanding 3-PG using a sensitivity analysis. *Forest Ecol. Manag.* 193, 235 – 250.
- [29] Goudriaan, J., 1977. Crop micrometeorology: a simulation study. Ph.D. thesis. Pudoc.
- [30] Gouot, J.C., Smith, J.P., Holzapfel, B.P., Barril, C., 2019. Impact of short temperature exposure of *Vitis vinifera* L. cv. Shiraz grapevine bunches on berry development, primary metabolism and tannin accumulation. *Environ. Exp. Bot.* 168, 103866.

- [31] Gouot, J.C., Smith, J.P., Holzapfel, B.P., Walker, A.R., Barril, C., 2018. Grape berry flavonoids: a review of their biochemical responses to high and extreme high temperatures. *J. Exp. Bot.* 70, 397–423.
- [32] Greer, D., Weedon, M., 2014. Temperature-dependent responses of the berry developmental processes of three grapevine (*Vitis vinifera*) cultivars. *N. Z. J. Crop Hortic. Sci.* 42, 233–246.
- [33] Greer, D.H., 2013. The impact of high temperatures on *Vitis vinifera* cv. Semillon grapevine performance and berry ripening. *Front. Plant Sci.* 4, 491.
- [34] Greer, D.H., Weston, C., Weedon, M., 2010. Shoot architecture, growth and development dynamics of *Vitis vinifera* cv. Semillon vines grown in an irrigated vineyard with and without shade covering. *Funct. Plant Biol.* 37, 1061–1070.
- [35] Gueymard, C.A., 2008. REST2: High-performance solar radiation model for cloudless-sky irradiance, illuminance, and photosynthetically active radiation - Validation with a benchmark dataset. *Sol. Energy* 82, 272–285.
- [36] Hamman, R., Dami, I.E., Walsh, T., Stushnoff, C., 1996. Seasonal carbohydrate changes and cold hardiness of chardonnay and riesling grapevines. *Am. J. Enol. Vitic.* 47, 31–36.
- [37] Hayman, P., Longbottom, M., McCarthy, M., Thomas, D., 2012. Managing grapevines during heatwaves. Grape and wine research and development corporation .
- [38] Hosoi, F., Omasa, K., 2009. Estimating vertical plant area density profile and growth parameters of a wheat canopy at different growth stages using three-dimensional portable lidar imaging. *ISPRS J. Photogramm. Remote Sens.* 64, 151 – 158.
- [39] Hothorn, T., Hornik, K., Strobl, C., Zeileis, A., 2010. Party: A laboratory for recursive partytioning.
- [40] Hothorn, T., Hornik, K., Zeileis, A., 2006. Unbiased recursive partitioning: A conditional inference framework. *J. Comput. Graph. Stat.* 15, 651–674.

- [41] Hulands, S., Greer, D., Harper, J., et al., 2014. The interactive effects of temperature and light intensity on *Vitis vinifera* cv.'Semillon' grapevines. II. Berry ripening and susceptibility to sunburn at harvest. *Eur. J. Hortic. Sci* 79, 1–7.
- [42] Hunter, J., 1998. Plant spacing implications for grafted grapevine ii soil water, plant water relations, canopy physiology, vegetative and reproductive characteristics, grape composition, wine quality and labour requirements. *South African Journal of Enology and Viticulture* 19, 35–51.
- [43] Hunter, J., Volschenk, C., Mania, E., Castro, A.V., Booyse, M., Guidoni, S., Pisciotta, A., Di Lorenzo, R., Novello, V., Zorer, R., 2021. Grapevine row orientation mediated temporal and cumulative microclimatic effects on grape berry temperature and composition. *Agricultural and Forest Meteorology* 310, 108660.
- [44] Iandolino, A., Pearcy, R., Williams, L.E., 2013. Simulating three-dimensional grapevine canopies and modelling their light interception characteristics. *Aust. J. Grape Wine R.* 19, 388–400.
- [45] Iqbal, M., 1983. *An Introduction to Solar Radiation*. Academic Press, Burlington. 408 pp.
- [46] Johnson, I., Thornley, J., 1984. A model of instantaneous and daily canopy photosynthesis. *J. Theor. Biol.* 107, 531 – 545.
- [47] Jones, G.V., 2007. *Climate change: Observations, projections, and general implications for viticulture and wine production*. Econ. Depart. Working paper 7, 14.
- [48] Jones, J., Hoogenboom, G., Porter, C., Boote, K., Batchelor, W., Hunt, L., Wilkens, P., Singh, U., Gijsman, A., Ritchie, J., 2003. The DSSAT cropping system model. *Eur. J. Agron.* 18, 235 – 265.
- [49] Jones, J.W., Antle, J.M., Basso, B., Boote, K.J., Conant, R.T., Foster, I., Godfray, H.C.J., Herrero, M., Howitt, R.E., Janssen, S., Keating, B.A., Munoz-Carpena, R., Porter, C.H., Rosenzweig, C., Wheeler, T.R., 2017. Brief history of agricultural systems modeling. *Agric. Syst.* 155, 240 – 254.

- [50] Kliewer, W.M., Wolpert, J.A., Benz, M., 2000. Trellis and vine spacing effects on growth, canopy microclimate, yield and fruit composition of Cabernet Sauvignon. *Acta Hortic.* 526, 21–32.
- [51] Krasnow, M., Matthews, M., Smith, R., Benz, J., Weber, E., Shackel, K., 2010. Distinctive symptoms differentiate four common types of berry shrivel disorder in grape. *Calif. Agric.* 64, 155–159.
- [52] Kucharik, C.J., Norman, J.M., Gower, S.T., 1999. Characterization of radiation regimes in nonrandom forest canopies: theory, measurements, and a simplified modeling approach. *Tree Physiol.* 19, 695–706.
- [53] Kurtural, S.K., Fidelibus, M.W., 2021. Mechanization of pruning, canopy management, and harvest in winegrape vineyards. *Catalyst: Discovery into Practice* 5, 29–44.
- [54] Kustas, W.P., Norman, J.M., 1999. Evaluation of soil and vegetation heat flux predictions using a simple two-source model with radiometric temperatures for partial canopy cover. *Agric. For. Meteorol.* 94, 13–29.
- [55] Larsen, D.R., Kershaw Jr, J.A., 1996. Influence of canopy structure assumptions on predictions from Beer's law. A comparison of deterministic and stochastic simulations. *Agric. For. Meteorol.* 81, 61–77.
- [56] Lauri, P.E., 2009. Developing a new paradigm for apple training. *The Compact Fruit Tree* 42, 17–19.
- [57] Lemeur, R., Blad, B.L., 1975. A critical review of light models for estimating the shortwave radiation regime of plant canopies, in: *Developments in Agricultural and Managed Forest Ecology*. Elsevier. volume 1, pp. 255–286.
- [58] Ponce de León, M.A., Bailey, B.N., 2021. A 3D model for simulating spatial and temporal fluctuations in grape berry temperature. *Agric. For. Meteorol.* 306, 108431.

- [59] Levick, S.R., Asner, G.P., Kennedy-Bowdoin, T., Knapp, D.E., 2009. The relative influence of fire and herbivory on savanna three-dimensional vegetation structure. *Biol. Cons.* 142, 1693 – 1700.
- [60] Liu, T., Gu, L., Dong, S., Zhang, J., Liu, P., Zhao, B., 2015. Optimum leaf removal increases canopy apparent photosynthesis, ¹³C-photosynthate distribution and grain yield of maize crops grown at high density. *Field Crops Res.* 170, 32–39.
- [61] López, A., Molina-Aiz, F., Valera, D., Peña, A., 2012. Determining the emissivity of the leaves of nine horticultural crops by means of infrared thermography. *Sci. Hortic.* 137, 49–58.
- [62] Louarn, G., Lecoeur, J., Lebon, E., 2008. A three-dimensional statistical reconstruction model of grapevine (*Vitis vinifera*) simulating canopy structure variability within and between cultivar/training system pairs. *Ann. Bot.* 101, 1167–1184.
- [63] Lunagaria, M., Shekh, A., 2006. Radiation interception, light extinction coefficient and leaf area index of wheat (*Triticum aestivum* L.) crop as influenced by row orientation and row spacing. *J. Agric. Sci.* 2, 43–54.
- [64] Martínez-Lüscher, J., Chen, C.C.L., Brillante, L., Kurtural, S.K., 2017. Partial solar radiation exclusion with color shade nets reduces the degradation of organic acids and flavonoids of grape berry (*Vitis vinifera* L.). *J. Agric. Food Chem.* 65, 10693–10702.
- [65] Martínez-Lüscher, J., Chen, C.C.L., Brillante, L., Kurtural, S.K., 2020. Mitigating heat wave and exposure damage to ‘Cabernet Sauvignon’ wine grape with partial shading under two irrigation amounts. *Front. Plant Sci.* 11, 1760.
- [66] McCaskill, M.R., McClymont, L., Goodwin, I., Green, S., Partington, D.L., 2016. How hail netting reduces apple fruit surface temperature: A microclimate and modelling study. *Agric. For. Meteorol.* 226, 148–160.
- [67] Millar, A., 1972. Thermal regime of grapevines. *Am. J. Enol. Vitic.* 23, 173–176.
- [68] Modest, M.F., 2013. Radiative heat transfer. Academic press.

- [69] Monsi, M., Saeki, T., 1953. The light factor in plant communities and its significance for dry matter production. *Jpn. J. Bot.* 14, 22–52.
- [70] Morrison, J.C., Noble, A.C., 1990. The effects of leaf and cluster shading on the composition of cabernet sauvignon grapes and on fruit and wine sensory properties. *Am. J. Enol. Vitic.* 41, 193–200.
- [71] Nicholas, K.A., Durham, W.H., 2012. Farm-scale adaptation and vulnerability to environmental stresses: Insights from winegrowing in northern california. *Glob. Environ. Change* 22, 483–494.
- [72] Niinemets, Ü., 1998. Adjustment of foliage structure and function to a canopy light gradient in two co-existing deciduous trees. Variability in leaf inclination angles in relation to petiole morphology. *Trees* 12, 446–451.
- [73] Niinemets, Ü., 2010. A review of light interception in plant stands from leaf to canopy in different plant functional types and in species with varying shade tolerance. *Ecol. Res.* 25, 693–714.
- [74] Nilson, T., 1971. A theoretical analysis of the frequency of gaps in plant stands. *Agric. Meteorol.* 8, 25–38.
- [75] Nobel, P., 1975. Effective thickness and resistance of the air boundary layer adjacent to spherical plant parts. *J. Exp. Bot.* 26, 120–130.
- [76] Norman, J., Welles, J., 1983. Radiative transfer in an array of canopies 1. *Agron. J.* 75, 481–488.
- [77] North, P.R., 1996. Three-dimensional forest light interaction model using a Monte Carlo method. *IEEE Trans. Geosci. Remote Sens.* 34, 946–956.
- [78] Oliveira, M., Teles, J., Barbosa, P., Olazabal, F., Queiroz, J., 2014. Shading of the fruit zone to reduce grape yield and quality losses caused by sunburn. *OENO One* 48, 179–187.

- [79] Mira de Orduña, R., 2010. Climate change associated effects on grape and wine quality and production. *Food Res. Int.* 43, 1844–1855.
- [80] Papadakis, G., Frangoudakis, A., Kyritsis, S., 1992. Mixed, forced and free convection heat transfer at the greenhouse cover. *J. Agric. Eng. Res.* 51, 191–205.
- [81] Pathak, T.B., Maskey, M.L., Dahlberg, J.A., Kearns, F., Bali, K.M., Zaccaria, D., 2018. Climate Change Trends and Impacts on California Agriculture: A Detailed Review. *Agronomy* 8, 25.
- [82] Percival, D., Fisher, K., Sullivan, J., 1994. Use of fruit zone leaf removal with vitis vinifera l. cv. riesling grapevines. ii. effect on fruit composition, yield, and occurrence of bunch rot (*botrytis cinerea* pers.: Fr.). *American journal of enology and viticulture* 45, 133–140.
- [83] Pieri, P., 2010. Modelling radiative balance in a row-crop canopy: cross-row distribution of net radiation at the soil surface and energy available to clusters in a vineyard. *Ecol. Model.* 221, 802–811.
- [84] Porter, J., Jamieson, P., Wilson, D., 1993. Comparison of the wheat simulation models AFRCWHEAT2, CERES-Wheat and SWHEAT for non-limiting conditions of crop growth. *Field Crops Res.* 33, 131–157.
- [85] Prata, A., 1996. A new long-wave formula for estimating downward clear-sky radiation at the surface. *Q.J.R. Meteorol. Soc* 122, 1127–1151.
- [86] Press, W.H., Teukolsky, S.A., Vetterling, W.T., Flannery, B.P., 2007. Numerical recipes 3rd edition: The art of scientific computing. Cambridge university press.
- [87] Raabe, K., Pisek, J., Sonnentag, O., Annuk, K., 2015. Variations of leaf inclination angle distribution with height over the growing season and light exposure for eight broadleaf tree species. *Agric. For. Meteorol.* 214-215, 2–11.

- [88] Rana, G., Katerji, N., Introna, M., Hammami, A., 2004. Microclimate and plant water relationship of the “overhead” table grape vineyard managed with three different covering techniques. *Sci. Hortic.* 102, 105–120.
- [89] Reshef, N., Fait, A., Agam, N., 2019. Grape berry position affects the diurnal dynamics of its metabolic profile. *Plant Cell Environ.* 42, 1897–1912.
- [90] Reynolds, A.G., Heuvel, J.E.V., 2009. Influence of grapevine training systems on vine growth and fruit composition: A review. *Am. J. Enol. Vitic.* 60, 251–268.
- [91] Reynolds, A.G., Wardle, D.A., Naylor, A.P., 1996. Impact of training system, vine spacing, and basal leaf removal on Riesling. vine performance, berry composition, canopy microclimate, and vineyard labor requirements. *Am. J. Enol. Vitic.* 47, 63–76.
- [92] Rosati, A., Badeck, F., DeJong, T., 2001. Estimating canopy light interception and absorption using leaf mass per unit leaf area in *Solanum melongena*. *Ann. Bot.* 88, 101–109.
- [93] Ross, J., 1981. *The Radiation Regime and Architecture of Plant Stands*. Dr. W. Junk Publishers, The Hague, The Netherlands. 424 pp.
- [94] Rubio, E., Caselles, V., Badenas, C., 1997. Emissivity measurements of several soils and vegetation types in the 8–14, μm wave band: Analysis of two field methods. *Remote Sens. Environ.* 59, 490–521.
- [95] Sadras, V.O., Petrie, P.R., 2011. Climate shifts in south-eastern Australia: early maturity of Chardonnay, Shiraz and Cabernet Sauvignon is associated with early onset rather than faster ripening. *Aust. J. Grape Wine R.* 17, 199–205.
- [96] Sampson, D.A., Smith, F., 1993. Influence of canopy architecture on light penetration in lodgepole pine (*Pinus contorta* var. *latifolia*) forests. *Agric. For. Meteorol.* 64, 63–79.
- [97] Saudreau, M., Marquier, A., Adam, B., Sinoquet, H., 2011. Modelling fruit-temperature dynamics within apple tree crowns using virtual plants. *Ann. Bot.* 108, 1111–1120.

- [98] Saudreau, M., Sinoquet, H., Santin, O., Marquier, A., Adam, B., Longuenesse, J.J., Guillioni, L., Chelle, M., 2007. A 3D model for simulating the spatial and temporal distribution of temperature within ellipsoidal fruit. *Agric. For. Meteorol.* 147, 1–15.
- [99] Schuepp, P., 1993. Tansley Review No. 59. Leaf boundary layers. *New Phytol.* 125, 477–507.
- [100] Sitch, S., Smith, B., Prentice, I., Arneth, A., Bondeau, A., Cramer, W., Kaplan, J., Levis, S., Lucht, W., Sykes, M., Thonicke, K., Venevsky, S., 2003. Evaluation of ecosystem dynamics, plant geography and terrestrial carbon cycling in the LPJ dynamic global vegetation model. *Global Change Biol.* 9, 161–185.
- [101] Smart, R., Dick, J.K., Gravett, I.M., Fisher, B., 2017. Canopy management to improve grape yield and wine quality-principles and practices. *South African Journal of Enology and Viticulture* 11, 3–17.
- [102] Smart, R.E., 1985. Principles of grapevine canopy microclimate manipulation with implications for yield and quality. A review. *Am. J. Enol. Vitic.* 36, 230–239.
- [103] Smart, R.E., Sinclair, T.R., 1976. Solar heating of grape berries and other spherical fruits. *Agric. Meteorol.* 17, 241–259.
- [104] Smith, N., Chen, J., Black, T., 1993. Effects of clumping on estimates of stand leaf area index using the LI-COR LAI-2000. *Can. J. For. Res.* 23, 1940–1943.
- [105] Spayd, S.E., Tarara, J.M., Mee, D.L., Ferguson, J., 2002. Separation of sunlight and temperature effects on the composition of *Vitis vinifera* cv. Merlot berries. *Am. J. Enol. Vitic.* 53, 171–182.
- [106] Stenberg, P., 2006. A note on the G-function for needle leaf canopies. *Agric. For. Meteorol.* 136, 76 – 79.
- [107] Stocker, T., 2014. *Climate change 2013: the physical science basis: Working Group I contribution to the Fifth assessment report of the Intergovernmental Panel on Climate Change.* Cambridge University Press.

- [108] Strack, T., Schmidt, D., Stoll, M., 2021. Impact of steep slope management system and row orientation on canopy microclimate. comparing terraces to downslope vineyards. *Agric. For. Meteorol.* 307, 108515.
- [109] Strobl, C., Malley, J., Tutz, G., 2009. An introduction to recursive partitioning: rationale, application, and characteristics of classification and regression trees, bagging, and random forests. *Psychol. Methods* 14, 323.
- [110] Suffern, K.G., 2007. *Ray Tracing from the Ground Up*. A K Peters/CRC Press, Boca Raton, FL. 784 pp.
- [111] Swift, J., Buttrose, M., Possingham, J., 1973. Stomata and starch in grape berries. *Vitis* 12, 38–45.
- [112] Taiz, L., Zeiger, E., 2014. *Plant Physiology and Development*. Sinauer. 761 pp.
- [113] Tarara, J., Ferguson, J., Hoheisel, G.A., Peña, J.P., 2005. Asymmetrical canopy architecture due to prevailing wind direction and row orientation creates an imbalance in irradiance at the fruiting zone of grapevines. *Agric. For. Meteorol.* 135, 144–155.
- [114] Tarara, J.M., Lee, J., Spayd, S.E., Scagel, C.F., 2008. Berry temperature and solar radiation alter acylation, proportion, and concentration of anthocyanin in merlot grapes. *Am. J. Enol. Vitic.* 59, 235–247.
- [115] Thorpe, M., 1974. Radiant heating of apples. *J. Appl. Ecol.* , 755–760.
- [116] Valdés-Gómez, H., Celette, F., de Cortázar-Atauri, I.G., Jara-Rojas, F., Ortega-Farías, S., Gary, C., 2009. Modelling soil water content and grapevine growth and development with the STICS crop-soil model under two different water management strategies. *OENO One* 43, 13–28.
- [117] Van Leeuwen, C., Darriet, P., 2016. The impact of climate change on viticulture and wine quality. *J. Wine Econ.* 11, 150–167.

- [118] Viswanadham, Y., 1981. The relationship between total precipitable water and surface dew point. *J. Appl. Meteorol.* 20, 3–8.
- [119] Wahid, A., Gelani, S., Ashraf, M., Foolad, M.R., 2007. Heat tolerance in plants: an overview. *Environ. Exp. Bot.* 61, 199–223.
- [120] Warren Wilson, J., 1960. Inclined point quadrats. *New Phytol.* 59, 1–7.
- [121] Weber, J., Penn, J., 1995. Creation and rendering of realistic trees, in: *Proceedings of the 22Nd Annual Conference on Computer Graphics and Interactive Techniques*, ACM. pp. 119–128.
- [122] Wermelinger, B., Baumgärtner, J., Gutierrez, A., 1991. A demographic model of assimilation and allocation of carbon and nitrogen in grapevines. *Ecol. Model.* 53, 1–26.
- [123] White, M.A., Diffenbaugh, N., Jones, G.V., Pal, J., Giorgi, F., 2006. Extreme heat reduces and shifts United States premium wine production in the 21st century. *Proc. Natl. Acad. Sci. U.S.A* 103, 11217–11222.
- [124] Willmott, C.J., 1981. On the validation of models. *Phys. Geogr.* 2, 184–194.
- [125] Zorer, R., Moffat, T., Strever, A., Hunter, J., 2013. Hourly simulation of grape bunch light microclimate using hemispherical photography, in: *18th International Symposium of the Group of International Experts of vitivinicultural Systems for CoOperation (GiESCO 2013)*, pp. 748–752.